Doctoral Dissertation

Numerical and Experimental Study of Tsunami Triggered Oil Spill from Oil Storage Tanks in Industrial Complexes of Osaka Bay

Wai Phyo Kyaw

July 2017

Division of Global Architecture

Department of Naval Architecture and Ocean Engineering

Graduate School of Engineering,

Osaka University

Doctoral Dissertation

Numerical and Experimental Study of Tsunami Triggered Oil Spill from Oil Storage Tanks in Industrial Complexes of Osaka Bay

Wai Phyo Kyaw

July 2017

Graduate School of Engineering
Osaka University

The Dissertation Committee for Wai Phyo Kyaw Certifies that this is the approved version of following dissertation:

Numerical and Experimental Study of Tsunami Triggered Oil Spill from Oil Storage Tanks in Industrial Complexes of Osaka Bay

Committee:

Prof. Yasuyuki Toda

Prof. Shinichi Aoki

Associate Professor Hiroyoshi Suzuki

ABSTRACT

Oil storage tanks in industrial zones along the coastal lines have a high risk of major oil spill when tsunamis attack. The 2011 Great East Japan Earthquake induced a major tsunami, resulting tremendous devastation along the Pacific coastline of Japan's northern islands. At the entrance of the Kesennuma Bay, Miyagi Prefecture, there were heavy oil and gasoline fuel tanks to fuel fishing boats, which were broken and drifted into the bay along with tsunami wave resulting oil spill. The oil spill strengthened tsunami induced fire in Kessenuma City, and also it was found that mud samples in the bay had a high level of oil contamination after the disaster, showing that the tsunami triggered high turbid water mixed with spill oil and deposited on the sea bottom. Likewise, considerably dense industrial parks are distributed along the coastal line of Osaka Bay. Especially Osaka North Port and Sakai Senboku Industiral Parks consist of a large number of oil storage tanks and oil refineries.

The cabinet Office, government of Japan addresses earthquakes originating in the Nankai Trough, which can unleash a tsunami with an approximated maximum wave height of 6 meters along the coastal line of Osaka Bay. For reviewing the risk management of Osaka Bay Area, estimating the scenario of tsunami triggered oil spill from these industrial parks is urgently needed for planning the ship evacuating routes from the bay, and the evacuation of residences nearby.

In order to achieve this scenario, firstly, experiments and simulations were carried out to get deep insight of oil diffusion and movement when subjected to an incoming wave. Simple experiments and visualizations at a laboratory scale were carried out. Then, a numerical method, OpenFOAM which is an open source computational fluid dynamic technique, was used to simulate the whole scenario of these experiments. The simulation code includes multiphase (oil-water-air), convection-diffusion effect, and up most three dimensionalities. After validating the simulation code with the experiments, the code was used to simulate the full scale oil spill scenario of potential tsunami triggered oil spill from industrial parks along the coastline of Osaka Bay.

Then, the possible maximum strength of potential tsunami around the industrial parks in the Osaka Bay was estimated by using the Storm surge and Tsunami Simulator in Oceans and Coastal Areas (STOC) developed by the port and airport research institute of Japan (PARI). By combination these two simulation methods, the results could build a scenario of a tsunami-triggered oil spill from Sakai Senboku Industrial park. Also, STOC-OIL, an oil transport model

developed by PARI using Lagragian method was used to estimate the distribution of oil spill after the tsunami. The results could help to add the oil spill effect in reviewing the risk management of industrial zones around the coastal line.

In addition, the occurrence of major oil spill depends on the possibility of oil storage tanks drifting with the tsunami run up. Previously, the amount of the oil spill from these tanks was estimated by safety factors based on theoretical assumption according to the guideline of Fire and Disaster management Agency (FDMA) of Japan. Hence, experiments and numerical simulations were carried out to check the behavior of the tank movement due to incoming wave and to estimate the possible amount of oil spill. However, the result of experiments and numerical simulations showed that the guidelines overestimated the amount of oil spill. Therefore, a new modification was proposed to the guideline of FDMA.

ACKNOWLEDGEMENTS

Firstly, I would like to express my sincere gratitude my advisor Prof. Dr. Naomi Kato. With a great inspiration on him and his kind guidance, I became a graduate student in the Department of Naval Architecture and Ocean Engineering, Osaka University. Also, he also supported me greatly throughout the entire study of my PhD and related research. His patience, motivation, enthusiasm and immense knowledge helped me a lot for overcoming the challenges of the research. I have learnt how to conduct a research from the very basics from identifying the research, executing research idea, organizing experiments, conducting simulation to writing research proposals during both my master and doctoral candidate life. He gave me a great motivation to go on whenever I face challenges. Without his kind guidance and support, this dissertation would not have been completed

I would like to show my sincere gratitude to Associate Prof. Dr. Hiroyoshi Suzuki for guiding and helping me after the retirement of Prof. Naomi Kato. With his always smiling and warm personality, I felt easy and safe in conducting my experiments. Also, his great knowledge in numerical simulation, I could overcome difficulties in research. I am also thankful for his guidance and support throughout my writing my dissertation.

I would like to thank Associate Prof. Dr. Youhei Takagi for his contribution in the code and my coding in the research. He helped greatly and taught me how to handle the numerical coding and developing the coding process.

I also want to show my great thank to Assistant Prof. Dr. Hidetaka Senga for his warm and kind help for me. From his delicate and gentle nature, I could communicate and learn a lot from him during my research.

I would like to express my sincere gratitude to Prof. Dr. Shinichi Aoki and Prof. Dr. Yasuyuki Toda for accepting to be my doctoral thesis committee member. It was very helpful with their great help and thorough review on my dissertation manuscript.

I would like to acknowledge and thank for the technical support and training of the Port and Airport Research Institute of Japan for contributing to the Storm Surge and Tsunami Simulator in Oceans and Coastal Areas (STOC), OpenCFD Ltd for OpenFOAM® CFD package and and IH Cantabria for IHFOAM code. I would like to show my gratitude to 内閣府公表の津波及び地震

動解析 (Tsunami and Earthquake Analysis Cabinet Office, Japan) and 大阪府石油コンビナート等防災本部 (Osaka Prefecture Petrochemical Disaster Prevention Cabinet. The Department of Civil Engineering, Osaka University provided the tsunami tank for conducting experiments. He would also like to show their gratitude to Tsunami and Earthquake Analysis Cabinet Office, Japan and Osaka Prefecture Petrochemical Disaster Prevention Cabinet Headquarters for the geographic data and their publications.

I acknowledge Japan Ministry of Education, Culture, Sports, Science andTechnology (MEXT) for providing Japanese Government (Monbukagakusho) scholarship for both my master and doctoral course in the past five years.

I would like to show my great thank to my sincere, close friend and lab member Mr. Thaw Tar for his help in experiments and his advises in my numerical simulation. And, I am indebted to Prof. Daw Myint Myint Khine and Assistant Prof. Daw Khine Myo Thwin, who contributed the very first encouragement to me in following this path of advanced study.

I would like to thank Mr. Michiaki Sugiyama, Mr. Atsushi Yamada, Mr. Tatsuya Ochi, Mr. Liu Junling and all the other members in our research group for their contribution and useful advises. And, I am indebted to all the member in the laboratory for their help and encouragement during my research. I am also really appreciated to Ms. Kazuyo Hase, Mr. Yazuso Honda and Dr. Yan Naing Win, who help a lot and treat me like a family during my stay and study in Osaka University.

Finally, and most importantly, I am indebted to the love and support that I have received from my family members. Specially, I would like to show my gratitude to my father, who the background force for me to pursue the study and my mother who always encourage me with immense emotional support and warmth. And, I would like to thank my fiancé, Nan Aye Phyu Thin for being with me all these years with great understanding and love.

NORMENCLATURE

α_k : Phase fraction of each phase

ρ_k : Density for each phase

$\vec{u}_k$: Velocity for each phase

μ_k : Dynamic viscosity for each phase

$\vec{F}_{D,k}$: Interface momentum transfer or drag force

$\vec{F}_{S,k}$: Surface tension force

C_D: drag coefficient

Re: Reynolds number

$\vec{u}_c$: Artificial interface compression velocity

C_α : Coefficient for switching interface compression

Cr: Courant number

γ: Gradient of volume fraction

D : Total water depth [m]

f_o : Coriolis parameter [1/s] $= 2\Omega \sin\theta$)

g : Gravitational acceleration [m/s^2] (≈ -9.8)

h : Thickness ratio of water in a computational cell (hereinafter referred to as the “layer thickness ratio”)

H : Water depth [m]

p : Pressure [Pa]

p_{atm} : Atmospheric pressure [Pa]

R : Earth's radius [m] (assuming that the Earth is a sphere, not an ellipsoid)

u : x-component of flow velocity [m/s]

v : y-component of flow velocity [m/s]

w : z-component of flow velocity [m/s]

γ_v: Porous value (porosity) [-] ($0 \leq \gamma_v \leq 1$, defined in Fig. 4.4)

$\gamma_x, \gamma_y, \gamma_z$: Porous values (permeability in each direction) ($0 \leq \gamma_x, \gamma_y \leq 1, \gamma_z = 1$)

η : Water level [m]

v_H: Horizontal kinematic viscosity coefficient [m^2/s]

v_V : Vertical kinematic viscosity coefficient [m^2/s]

U_c : the velocity calculated by STOC

U_s : the dispersed velocities due the characteristic of the oil

U_d : the dispersed velocities due to turbulent flow eddies.

C_{w0} : binary switching coefficient for the wind effect (1, if the wind effect is calculated)

C_{w1} : coefficient of the wind (0.035~0.02), (function of particles density in each section)

C_{w2} : coefficient of turbulent wind (function of time)

C_{c1} : coefficient of the water current flow (=1)

C_{c2} : coefficient of turbulent water current flow (function of time)

C_{s1} : coefficient of dispersed flow (=1)

C_{s2} : coefficient of turbulent dispersed flow (function of time)

θ : the deflection due to Coriolis force.

ρ: Seawater density [kg/m^3]

F_{tV} : vertical uplifting force on the tank

F_{tH} : horizontal hydrodynamic force on the tank

ρ : density of seawater

α : coefficient for horizon hydrodynamic force

R : radius of the tank

β : coefficient for vertical uplifting force

η_{max} : maximum wave height

TABLE OF CONTENTS

LIST OF FIGURES

LIST OF TABLES

CHAPTER 1

INTRODUCTION

1.1 Background

On Friday 11 March 2011 at 05:46:23 UTC, the Great East Japan Earthquake with a magnitude of 9.0 Mw occurred approximately 70 km east of the Oshika Peninsula of Tohoku region, Japan. An approximately 180-km-wide seabed at 60 m offshore from the east coast of Tohoku was elevated by 10 meters. This seabed elevation triggered a major tsunami, which resulted in tremendous devastation along the Pacific coastline of Japan's northern islands. The recorded tsunami observations following the earthquake along the coastline stated that most severe cases, corresponding to wave heights of above 7 m, occurred in Iwate, Miyagi and Fukushima prefectures located in the northeast part of the Japan mainland.

Meanwhile, in the Kesennuma Bay in the Miyagi Prefecture, the waves were measured to have a height of 9 m followed by maximum tsunami outflow currents with a speed of 11 m/s less than 10 minutes after the wave head. Kesennuma City stated that 22 out of 23 oil storage tanks (with a capacity of 40 to 3000 kiloliters), were destroyed by the tsunami in the Mianmi Kesennuma District, and 11543 kiloliters of petroleum oil, mainly heavy oil as well as light oil and gasoline, was estimated to be spilled out.

1.2 Oil Spill from Oil Storage Tanks a nd Tsunami-Induced Fire

Among the damages, major oil spills from the oil storage tanks occurred in Kesenuma City, Miyagi Prefecture. The city stated that there was a major oil spill from oil storage tanks, which contain heavy oil and gasoline. During the disaster, those oil storage tanks were drifted and unleashed 11523 kiloliters of oil, mainly heavy oil as well as gasoline and light oil. The tanks, which were destroyed by the tsunami, were originally located at the entrance of the bay to fuel fishing boats. When the tsunami hit those oil tanks, most of them broke and drifted into the bay along with spilled oil. 22 out of 23 oil storage tanks were broken and drifted into the bay, and oil spill occurred through the way. After the tsunami, 18 tanks were found in different parts of the city, though 4 tanks went missing according to the fire department of Kessenuma city. The farthest drifted tank reached up to 2.4 km from the mouth of Bay.

Also in Sendai City, Miyagi Prefecture, the tsunami inundation led to drifting of small and empty storage tanks, and collapsed pipes. Since the emergency shutdown valves of pipelines did not work because of the blackout after the earthquake, large amount of oil spilled out into the dike (Zama et al., 2012). Fig. 1.1 shows the heavy oil spill in dike in Sendai area. The tank was empty when the tsunami struck and submerged into the sea water up to 3.5m high form the bottom plate. The tank did not uplift nor displace even though it was empty. However, the broken pipelines that crossed near the tanks, spilled out oil into the dike (Nishi, 2012).

The Kesennuma Bay area was changed into a sea of fire during the Great East Japan Earthquake. The major spillage of heavy oil strengthened the fire. When the seawater and oil mixture came in contact with some heat source (perhaps, short-circuiting of wrecked fishing boat or cables), there was a start of ignition, and the fire finally reached back to the city itself. In Kesennuma City, 13 cases of fire occurred after the tsunami during the Great East Japan Earthquake.

Fig. 1.1 Heavy oil spill out from conveying pipes in Sendai (FDMA)

Kesennuma city suffered from fire during the disaster due to tsunami triggered oil spill as shown in Fig. 1.2. Tsunami-induced fire is generally expanded due to the presence of petroleum facilities which has a potential of discharging combustible gases and liquids. Tsunami run up destroyed containers of any hazardous material and, consequently, unleashed combustibles which

could be easily ignited. According to the Fire and Disaster Management Agency (FDMA) of Japan, the fire was believed to be ignited from the sparks that were aroused when metal objects collided with each other in the tsunami run up or by short circuits of electrical appliances among the debris.

Based on the investigation carried out by the Japan Association of Fire Science and Engineering (Hokugo, 2013), there are three main tsunami-induced fire breakout patterns. One of the patterns is tsunami-induced fire related to leak from oil storage tanks, which is the case found in Kesennuma Bay.

Fig. 1.2 Tsunami induced fire in Kesennuma City (Daily mail, 2012)

Normally, the grade A heavy oil spilled out has relatively high flash point. However, the timber, wood and other material from the collapsed buildings might have soaked the oil to become good source for burning. When these oil soaked debris came in contact with fire from other sources during disaster, they were ignited into fire like wick combustion (Hokugo, 2013). Moreover, the small pieces of oil-soaked wood fire scattered around acted as candle wicks and kept the fire going for a long time. At the same time, they were dispersed by the wind and tsunami and created a great fire, which even spread to the isolated island of Oshima.

According to the publication of the analysis, research and information on accidents (ARIA) database operated by the French Ministry of Ecology, Sustainable Development and Energy (2013),

the fishing port was covered with 5 cm thick precipitation layer of oil. In addition, NHE (n-hexane extract) from the seabed with the thickness of 10 cm was measured, assuming that the distribution is uniform within the thickness (Arakawa and Nakamura, 2016). The time history of the amount of NHE in Kesennuma Bay was determined, and it revealed that the level of NHE reached 24% of total spilled oil in December 2012, with the level decreasing to 11% in December 2015.

After burning out a large extent of spilled out oil on the sea, some of the left-over oil seems to have been carried away by the tide and wind, but there are still chances of those drifting oil contaminations approaching nearby coast again. Moreover, it has been found that the mud sample in the Kesennuma bay has a high level of oil contamination. Usually, oil is considered to be lighter than seawater and the oil spill never sinks down to the sea bottom. However, in a tsunami-triggered oil spill, the tsunami triggered high turbid seawater mixed with the oil spill out. This mixture of mud and oil might have settled to the sea bottom.

Fig. 1.3 Mud sample with oil contamination in Kesennuma City (The Mainichi Newspaper, 2012)

Unlike ordinary oil spill, tsunami triggered oil spill comes together with the phenomena of mixing oil with sediment soil particles from the sea floor. Tsunami current has strong turbulence, which leads to the formation of high turbid sea water. When that water comes in contact with the oil spilled out from the fuel tanks along the coast subjected to the tsunami, there is a potential for

mixing of the oil and soil particles. As a consequence, the relatively heavier oil-soil particles mixture usually sinks down to the bottom of the sea rather than floating on the sea surface as in case of ordinary oil spill. This leads to severe environmental problems because it is hard to locate and collect the precipitated oil-soil particles mixture on seabed in a relatively wide area and this mixture has a potential for floating up to the surface again due to the consequence of other disasters like storms. The mud samples in Kesennuma Bay was found to contain high levels of oil contamination as shown in Fig. 1.3.

The Mainichi Newspaper (2012) reported that, from July 2011 to February 2012, surveys were carried out in 71 places of 30–40 m depth seabed, and all the mud sediment samples were observed to include oil deposits, which is difficult to decompose the mud sediment into mud itself and oil. Among them, 10 survey points close to the land have 1.9 to 1.1 times higher oil contamination level than the national environmental standards (1000 ppm). Though any further oil contamination has not been detected in the seawater of Kesennuma Bay, in the future, the effect of oil contamination in the mud on the aquaculture of seafood needs to be considered.

1.3 Analysis of the Disaster and Countermeasures at Coastal Industrial Zones

Before the Great East Japan Earthquake, the potential risk of destruction of oil storage tanks in coastal industrial zones by tsunami waves was identified, but any countermeasures were not taken for this case. There were certain tanks which proved to be resistant to that kind of disaster, comprising both earthquakes and tsunamis. During the Great East Japan Earthquake, tsunami waves of over 7 meters high hit the Sendai Harbour of Miyagino Ward in Sendai City. Two prestressed concrete (PC) structure water supply tanks were totally flooded, and one of them was collided with a container vessel. However, none of them had major damage to its main body.

Prestressed concrete (PC) structure refers to one with concrete wall stressed by piano wires to raise the structural strength as well as resistance, and promote durability. It is usually utilized in the construction of water supply tanks of high capacity to withstand relatively high water pressure. However, in case of fuel tanks, the structure is typically relied on steel plates.

With the adoption of the PC construction method, the fuel tanks destroyed by the tsunami will be reconstructed in Kesennuma City. Eight tanks with a total capacity of 7000 kiloliters will be built in the Minami Kesennuma District by fall 2016. Of course, the tanks with the PC

construction have the advantage of the potential resistance to be drifted away by the tsunami of the same scale of the Great East Japan Earthquake, and to allow them to withstand collision from floating debris. However, there exists a chance of bursting out for the pipe connections to cause the oil leakage.

Before the Great East Japan Earthquake, the potential risk of fuel tanks in coastal industrial zones being destroyed by tsunami waves was identified, but virtually, there was no countermeasure for this case. The Fire and Disaster Management Agency analyzed the relationship between depth of inundation and extent of damage at fuel tanks in both Iwate and Miyagi Prefectures after the disaster. And it had been found that if the height of the tsunami inundation is between 2.5 to 5 meters, the pipes start to burst, and when the inundation rises above 5 meters, the main body of the tank suffers damage as well.

The tsunami fire of Kesennuma Bay revealed the disaster risks that lay in the coastal industrial zones, where fuel tanks concentrate. Based on the data, they created a simulation model of tsunami damage, and instructed 33 prefectures with petrochemical complexes to review their disaster prevention plans. In this disaster, oil also spilled out even from damaged pipes. The Fire and Disaster Management Agency expanded the subject of their requirement to install emergency shutdown valves, which prevent fuel leakage from the pipes, for tanks with a capacity of over 10 thousand kiloliters to over 1000 kiloliters.

1.4 Risk Analysis in Osaka Bay

In Osaka Bay, there is an intensive distribution of industrial parks along the coastline. In particular, Osaka North Port and Sakai Senboku Industrial zones comprise a massive number of oil storage tanks. In addition, there is a potential Nankai Trough earthquake of an intensity of 6 or smaller. This earthquake can unleash a tsunami with a maximum wave height of 6 meters along the coastline of Osaka Bay. To review the risk assessment of the Osaka Bay Area, building the scenario of a tsunami-triggered oil spill from these industrial parks is urgently needed for planning the ship evacuating routes from the bay and the evacuation of nearby residences. Hence, this research proposes to estimate the distribution of potential oil spill in the Osaka Bay caused by a tsunami due to a Nankai Trough earthquake by numerical simulations. The simulation domains include the residential zones and bay area near the Sakai Senboku Industrial zone in order that the risk analysis of Osaka Bay Area can be revised by considering the effect of oil.

CHAPTER 2

LITERATURE REVIEW

Historically, many researcher have studied tsunami waves and developed various models to simulate tsunami numerically. Tsunami waves are generally developed by three mechanisms: seismic movement, underwater landslide and meteorite fall. Researchers found that the underwater landslides are the most dangerous mechanism for tsunami generation. And current research focuses on Osaka Bay area, which is directly facing to one of Japan largest fault zone: Nankai fault.

Most of the researchers studying tsunami waves used solitary waves. When a solitary wave propagates up a gradual slope, its shape changes, with the front face of the wave steepening and secondary waves emerging from the back face of the wave. Eventually, the waves separates into a series of solitary waves followed by a train of oscillatory waves (Madsen and Mei, 1969).

Iwasaki (1987) used two dimensional linear potential theory to simulate wave generation by moving the domain boundary. Then, the results were very close to the results of three dimensional experiments.

Titov and GonzaLez (1997) introduced the method of splitting tsunami (MOST). The MOST model can simulate three processes of tsunami evolution: generation by an earthquake, transoceanic propagation, and inundation in dry land.

Two dimensional horizontal coordinate tsunami model was presented by Kirby (1996) with several approximations, the model could make a more realistic effect like wave breaking and shoreline run up.

The basics of tsunami propagation and run-up for the simple geometry of a channel was discussed by Kowalik (2001) and modifications for numerical techniques were suggested for the long-distance propagation and for the nonlinear processes in tsunami waves.

Both two-dimensional and three-dimensional calculation using the full Navier-Stokes equations, of a hypothetical landslide were also conducted by Gisler et al. (2006). It was suggested that high-amplitude waves are dangerous to nearby communities, the wavelengths and periods of these waves are relatively short, and they would not propagate efficiently over long distances.

Nonlinear shallow-water equations for tsunami in Cartesian coordinates were solved. By Zhang et al. (2007). Their research was very helpful to better understand the fundamental physics and phenomenon of tsunami.

In Japan, storm surge and tsunami simulation considering three dimensional characteristic of flow have been described by Kakinuma and Tomita (2005). This model is now fully developed to simulate the tsunami generation and have validated. In this research this model is used to estimate potential tsunami around the Osaka Bay.

Also, the transport and fate processes of oil spills were studied and various oil spill models have been developed. Most of these models emphasize the movement of an oil slick on the water surface, and a relatively limited number of publications reveal the analysis of oil spill fate processes and concentration distribution in a vertical water column.

Oil spill simulation for a hypothetical oil spill in the Strait of Georgia was conducted with the oil spill contingency and response (OSCAR) model (Niu et al., 2016). This is a three-dimensional (3-D) particle-based model that simulates the evolution of oil on the water surface, along shorelines and dispersed and dissolved oil concentrations in the water column. The oil spill is modeled with a stochastic approach, and the fate and behavior were modeled by the transport of wind and hydrostatic model for the Strait of Georgia and the Salish Sea. In addition, simulations of the oil spill in the seas were conducted with a 3-D model, based on the particle approach.

A hybrid method of the Princeton Ocean Model (POM) and the third-generation wave model, simulating wave's nearshore (SWAN), was used to simulate the oil spill from a tanker in the Dalian coastal region as described by Guo and Wang (2009).

An oil spill from a ship collision accident in the Bohai Strait was also simulated using POM, and Stokes wave theory was used as demonstrated by Wang et al. (2008).

In addition, two- and 3-D oil spill models for coastal waters was introduced by Chao et al. (2001). In a two-dimensional (2-D) simulation, the initial oil slick is divided into a number of small grids, and a set of plane coordinates are assigned to each grid. In a 3-D simulation, based on the rate of vertical dispersion of the oil slick, the concentration distribution of oil particles in the water column was predicted. A 3 -D multilevel tidal hydrodynamics model is used in both simulations.

Also, a mathematical model that under the effect of ocean dynamic condition of tide, wind and wave, using a Monte Carlo method to simulate the movement of oil slick was established in Chen et al. (2007).

The National Oceanic and Atmospheric Administration (NOAA) has developed General NOAA Operational Modeling Environment (GNOME), Trajectory Analysis Planner (TAP) and Automated Data Inquiry for Oil Spills (ADIOS) for response and recovery from an oil spill in case of accidents. With the help of the online oceanographic data server, GNOME can be used to predict where the oil is most likely to travel and how quickly it may come ashore or threaten vulnerable coastal resources. TAP is used to predict which coastal area can be affected by a known oil spill source. ADIOS is an oil weathering model that predicts how different types of oil undergo physical changes in the marine environment.

However, most of the accidents resulting in oil spill occur due to the explosion or collision of tankers and failure in offshore structures. Hence, the source of oil spill turned out to be in the middle of the water body, and the transport of oil is due to gravity, inertia, viscosity and surface tension forces: the advection and turbulent diffusion due to the current and wind. In contrast, tsunami-triggered oil spill accidents have a different nature and phenomenon, as the mass inflow of water is dominant for the transport to oil spill, which is not initially in the water body itself, and the nonuniform flow due to the close existence of coastline and residential area, which reveals the more dangerous nature of fire breaking out. Previously, only tsunami damage level was estimated to depict the disaster maps for the coastline. However, apparently, these estimations did not consider the oil spill from industries situated along the coastline, like the case of the tsunami-triggered oil spill in Kesennuma city. The disaster caused by a tsunami-triggered oil spill from industrial parks will be largest in Osaka Bay among Tokyo Bay, Ise Bay and Osaka Bay, where large-scale industrial parks are located within metropolises because Osaka Bay area has the most vulnerability against a tsunami.

Hence, in this study, it is necessary to estimate the strength of the potential tsunami in the Osaka Bay area. Then, a new numerical method that includes both the mass inflow of water representing the tsunami wave and the transport of oil spill is needed to simulate the whole scenario of tsunami-triggered oil spill. It is also necessary to implement the overflow of water over the dry land, where the primary source of oil spill existed. Once the initial oil spill into the sea due to the

tsunami is estimated, an oil spill response model like GNOME, TAP and ADIOS can be applied to predict the likely movement and behavior of the oil spill under the influence of winds, tides and ocean currents.

In addition, oil storage tanks are typically designed as cylindrical thin shell elements to support the lateral pressure of the internal fluid. Under conventional loading the wall of the container is subjected to tensile stresses which are readily resisted by the thin shell and standard welds used to fabricate the cylinder. In regions of high seismicity and in areas where high wind loads are possible additional design requirements are prescribed. However, Seismic and wind design requirements do not provide adequate protection to oil storage tanks during tsunami events. Although the movement of oil storage tanks and oil spill in the tsunami inundation was prominent especially during the 2011 Great East Japan Earthquake as shown in Fig. 2.1, the phenomena had been already aware of since 2004 Indonesia Tsunami (Saatcioglu et al., 2006). Also, Goto., (2005) also analyzed the failure due to sliding, floating, and buckling of oil storage tank in Banda Aceh and Malahayati, Indonesia as shown in Fig. 2.2. However, the damaged and drifted oil storage tanks during the 2004 India Ocean tsunami only resulted non petrochemical oil spill, hence, only the damage to the oil storage tanks were reported rather than the oil spill.

Fig. 2.1 Oil storage tanks damaged in the Port of Kuji after the tsunami of 2011 Great East Japan Earthquake

(b)

Fig. 2.2 Relocated oil storage tanks in Malahayati, Indonesia during 2004 Indian Ocean tsunami

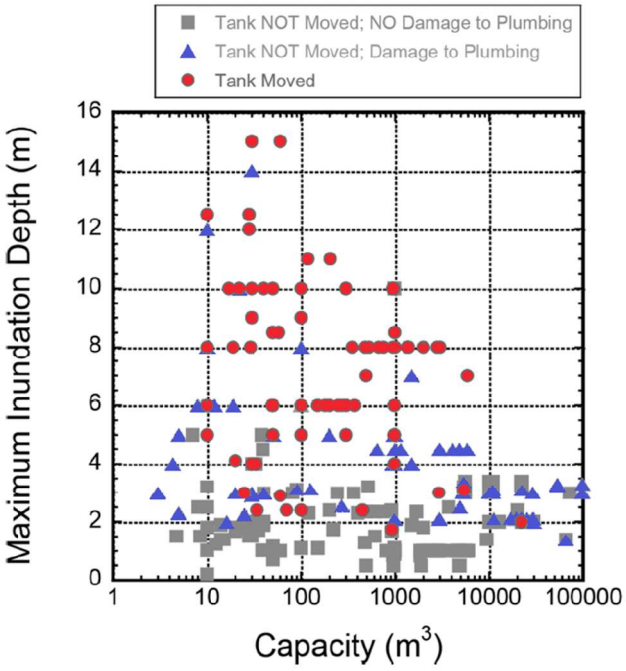

Fig. 2.2 Correlation between maximum inundation depth and severity of damage to oil storage tanks due to the 2011 Tohoku earthquake tsunami. The inundated tanks are indicated by different symbols representing the severity of damage. (Hatayama K., 2014)

In the 2011 Great East Japan Earthquake, 418 oil storage tanks were damaged and 157 of these tanks were drifted by the tsunami. Hatayama K., (2014) conducted surveys and on-site reconnaissance to assess the number of damaged and drifted tanks as shown in table 1 and table 2, and also proposed a rough but fact-based method, which hit an accuracy of 76%, to predict damage to a tank from a given maximum inundation depth.

Table 2.1 Number of oil storage tanks damaged by the 2011 Great East Japan Earthquake tsunami with respect to storage capacity (capacity class)

Capacity (C) Class (m^3)		$C <$ 500	500 $\leq C <$ 1,000	1,000 $\leq C <$ 10,000	10,000 $\leq C <$ 50,000	50,000 $\leq C$	Un-known	Sum
By Capacity Class		262	64	51	21	15	5	418
By Prefecture	Hokkaido	2	1	0	0	0	0	3
	Aomori	22	4	12	0	0	0	38
	Iwate	60	8	8	0	0	0	76
	Miyagi	125	38	28	19	15	4	229
	Fukushima	49	11	2	2	0	1	65
	Ibaraki	3	2	1	0	0	0	6
	Chiba	1	0	0	0	0	0	1

Table 2.2 Number of oil storage tanks drifted by the 2011 Great East Japan Earthquake tsunami with respect to storage capacity (capacity class)

Capacity (C) Class (m^3)		$C <$ 500	500 $\leq C <$ 1,000	1,000 $\leq C <$ 10,000	10,000 $\leq C <$ 50,000	50,000 $\leq C$	Un-known	Sum
By Capacity Class		110	30	16	1	0	0	157
By Prefecture	Aomori	3	0	0	0	0	0	3
	Iwate	40	4	0	0	0	0	44
	Miyagi	55	19	14	1	0	0	89
	Fukushima	12	7	2	0	0	0	21

On the other hand, tsunami forces to oil storage tanks was estimated by smoothed particle hydrodynamics (SPH) methods and the effects of tsunami water intrusion into the gap between tank bottom plate and foundation was studied for the drifting potentials of oil storage tanks (Ibata et al., 2016). Also, Monte Carlo simulations were used to calculate the probability of oil storage tank failure and tsunami height (Ahmed et al., 2016). FDMA also conducted experiments for analyzing the effect of oil containment dike around the oil storage tanks in tsunami waves. Also, the movement behavior of oil storage tanks of different internal amount in the inundation were tested. However, in these experiments, different weights were used instead of real liquid.

CHAPTER 3

PRELIMINARY ANALYSIS OF THE BEHAVIOR OF OIL MOVEMENT IN THE INCOMING WAVE

The analysis of the behavior of oil movement in the incoming wave was firstly conducted by experimental method. Then, numerical simulation methods were used to simulate the phenomenon to evaluate the applicability of the method for full scale oil spill scenario.

3.1 **Experimental Setup**

A model of oil reservoir which contains oil with the same level of ambient water was used. The oil reservoir, which was filled with heavy oil, was placed at the one end of a 1 m long tank, while the wave was created from the opposite end. In both experiment and simulations, the wave was created by dam break method to represent the wave close to the tsunami case.

Experiments in the laboratory scale for the oil response behavior after being hit by the wave was carried out in laboratory of Osaka University. With the help of high speed cameras, the movement of oil was recorded for every split second. The experimental setup is as shown in Fig. 3.1. When the movable slide wall (green) was lifted up, the water broke as the behavior of a dam breaking phenomenon. This would create a wave which heads towards the oil reservoir.

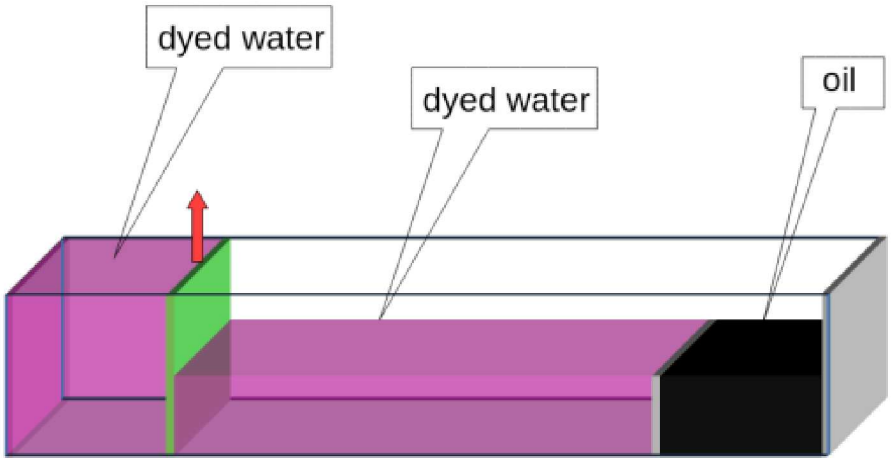

(a)

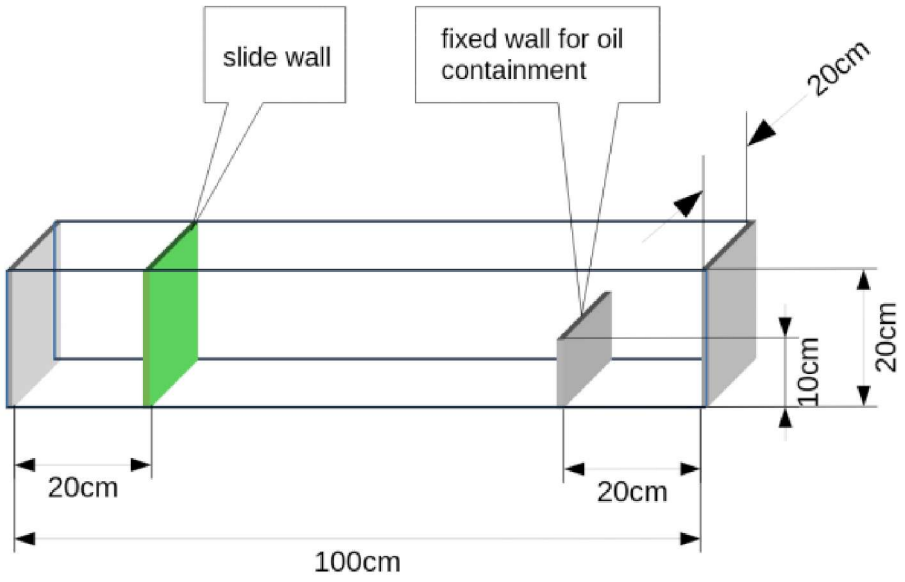

(b)

Fig. 3.1 (a) Sketch of experiment setup (b) Detail dimensions of the tank and wall positions

To achieve the precise time history of the movement of oil after removing the wall, the area closed to the oil reservoir was scaled finely with centimeter mesh as shown in Fig. 3.2. The total volume of water inside the tank was 10000cm^3, and 2000cm^3 of oil, representing the 20% of the volume of water, was kept in the reservoir.

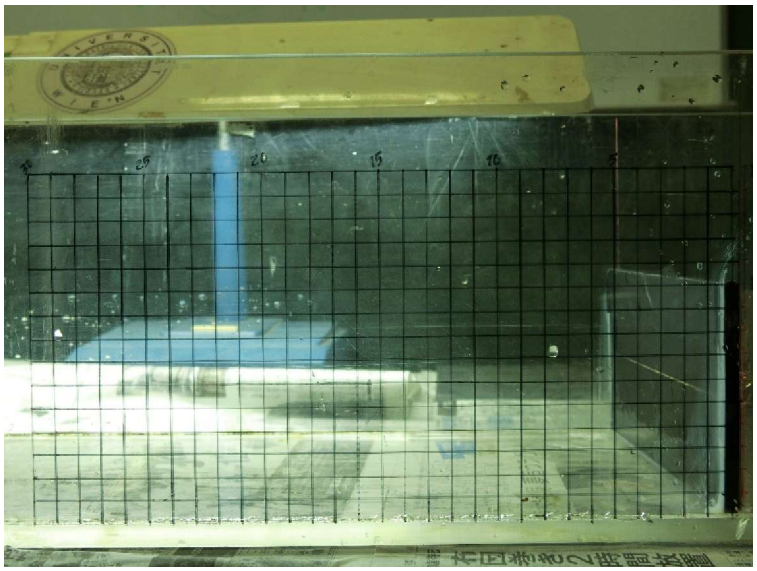

Fig. 3.2 The tank wall just before the oil reservoir was scaled finely with centimeter mesh

3.2 **Computational methodology and implementation to solve modelled phenomena**

The simulation was carried out using the same material properties and computational domain of the same size as the experiment. The implementation of the simulation was achieved by the use of OpenFOAM® CFD package (version 2.3.1) which provides a collection of libraries and utilities, which can be used to make custom CFD solver for various types of applications. The 'multiphaseEulerFoam' solver was used and it is developed by Wardle and Weller (2013).

The governing equations for the incompressible, isothermal flow for multifluid model was constructed by sets of mass and momentum equations for each phase *k*:

$$\frac{\partial \alpha_k}{\partial t} + \vec{u}_k \cdot \nabla \alpha_k = 0 \tag{3.1}$$

$$\begin{aligned} &\frac{\partial(\rho_k \alpha_k \vec{u}_k)}{\partial t} + (\rho_k \alpha_k \vec{u}_k \cdot \nabla)\vec{u}_k \\ &= -\alpha_k \nabla p + \nabla \cdot (\mu_k \alpha_k \nabla \vec{u}_k) + \rho_k \alpha_k \vec{g} + \vec{F}_{D,k} + \vec{F}_{S,k}, \end{aligned} \tag{3.2}$$

where the subscript *k* stands for each phase. α_k is the phase fraction of each phase so that the total summation of α_k of all phases is 1; $\alpha_k \leq 1$. ρ_k and $\vec{u}_k$ are the density, velocity for each phase, $\vec{g}$ is the acceleration due to gravity. The interface momentum transfer or drag force $\vec{F}_{D,k}$ and the surface tension force $\vec{F}_{S,k}$ are interfacial forces. But for current research, surface tension force was neglected as its contribution was very small as the flow was mainly advection dominant flow. However, the solver itself includes the surface tension capability (based on the continuum surface force model of Brackbill et al. (1992)) and surface contact angle effects are also included in the solver.

Hence, the drag force $\vec{F}_{D,K}$ is given by

$$\vec{F}_{D,k} = \frac{3}{4} \rho_c \alpha_c \alpha_d C_D \frac{|\vec{u}_d - \vec{u}_c|(\vec{u}_d - \vec{u}_c)}{d_d} \tag{3.3}$$

$$\vec{F}_{D,k} = \alpha_c \alpha_d K(\vec{u}_d - \vec{u}_c) \tag{3.4}$$

where K is

$$K = \frac{3}{4}\rho_c C_D \frac{|\vec{u}_d - \vec{u}_c|}{d_d} \tag{3.5}$$

where the subscript *c* stands for the continuous phase and *d* for the dispersed phase values.

The drag force is generically calculated inside the solver. A simple advantage in the drag force calculation is just to return the value of K. And, also, the value of the drag coefficient C_D, which is dominant in the equation of K, is also achieved by the various proposed model. In the literature, a variety models for the deduction of C_D were proposed. Consequently, several common models have been developed in the OpenFOAM®. In current case, the popular model of Schiller and Naumann (1935) was used. This model considers as C_D a function of the Reynolds number Re as shown below:

$$C_D = \begin{cases} \dfrac{24\left(1 + 0.15Re^{0.683}\right)}{Re}, Re \le 1000, \\ 0.44, Re > 1000, \end{cases} \tag{3.6}$$

Where

$$Re = \frac{|\vec{u}_d - \vec{u}_c| d_d}{\nu_c} \tag{3.7}$$

where ν is the kinematic viscosity of the continuous phase.

There are two ways to calculate the drag coefficient. The first method is to specify directly a dispersed phase in a continuous phase. The second method is independent calculation where each phase is considered as 'dispersed phase'. In the latter method, the overall drag coefficient for the momentum equations is taken as the volume fraction weighted average of the two values. This scheme is called blended scheme, and useful when solving the flow in the region in which either phase is primary phase. In current research, only constant droplet diameter size (defined independently for each phase) is assumed while models for variable droplet size can be implemented with this flexible framework.

3.3 **Interface capturing**

The interface compression method developed by Weller [5] is used to implement interface sharpening. The comparison of the methods used for interface sharpening and interface reconstruction algorithms for different CFD codes was done by Gopala and van Wachen (2008). This comparison is helpful in conducting trade-off methods between effectiveness and cost.

This scheme of interface compression developed by Weller (2008) adds an additional 'artificial' compression term to the left hand side of the volume fraction transport equation for each phase

$$\frac{\partial \alpha_k}{\partial t} + \vec{u}_k \cdot \nabla \alpha_k + \nabla \cdot \left(\vec{u}_c \alpha_k \left(1 - \alpha_k \right) \right) = 0 \tag{3.8}$$

The value of the artificial interface compression velocity $\vec{u}_c$ is given as

$$\vec{u}_c = \min\left(C_\alpha \vec{u}, \max\left(\vec{u}\right)\right) \frac{\nabla \alpha}{|\nabla \alpha|} \tag{3.9}$$

where $\vec{u}_c$ is the interface compression velocity to suppress the volume fraction field and keep a sharp interface. To activate this term only in the interface region, the term $\alpha_k \left(1 - \alpha_k\right)$ is added. And, in addition, $\frac{\nabla \alpha}{|\nabla \alpha|}$ ensures that the direction of the interface compression velocity is always towards the interface to compress against the surface.

Even in the worst case, dispersion of the interface can only occur as the same magnitude as the local velocity, so that the magnitude of velocity $\vec{u}_c$ is used in the interface compression equation. The solver has the option, to switch whether interface compression shall be used or not, by using the coefficient C_α . Although C_α can mathematically be any arbitrary value greater than 0, if one restricts $C_\alpha \leq 1$, equation (3.9) will reduce to

$$\vec{u}_c = C_\alpha \vec{u} \frac{\nabla \alpha}{|\nabla \alpha|} \tag{3.10}$$

Thus, C_α is considered as a binary coefficient switch which turns interface compression on (1) or off (0). For a given phase pair, when C_α is set to be 0, there will be no imposed interface

compression, which means that there is a phase dispersion according to the multifluid model. On the contrary, if C_α is set to be 1, VOF is applied across the interface to achieve interface capturing. In current simulation, C_α is defined and applied independently for all phase pairs in the implementation of the solver. For specific phase pair interface, C_α is set to 1 to keep a sharp interface throughout the whole simulation. (.i.e in air-oil and air-water interfaces). And conversely, C_α can be set to 0 for dispersed phase modeling in the other phase pair (water-oil interface) so that there is no interface compression.

Though interface reconstruction methods, for example Piecewise Linear Interface Construction (PLIC) are more accurate than current interface compression method, the development of Weller has the advantage of being easy to implement the solver and relatively faster than others. In addition, the most preferable advantage is that this method is mass conservative [6]. However on the other hand, the current method is not much desirable in small scale surface tension driven flow (capillary rise for the reason of the development of parasitic wavy current at the interface). However, for current case, the flow is mainly advective, and moreover, the undesirable interfacial currents can also be restricted by maintaining the Courant number Cr by means of sub time stepping and restricting $C_\alpha = 1$.

3.4 **Dynamic C_α switching**

As described in the above outline, the interface sharpening and dispersion can be manually controlled by presetting the C_α value. However, it is more convenient if C_α value can alternate dynamically as necessary, as the simulation process marches. This leads to the implementation of an upgraded solver, which enables simulation of complex flow which includes any combination of flow regimes ranging from fully dispersed to fully segregated. The drawback of this implementation is deciding by which method the switching between the dispersion and segregation of the interface form. This is the main controversial work dealt by various researchers who try to couple the multi-fluid and VOF methods. However, according to those outlined above, in this solver implementation, dynamic switching of the interface sharpening can only be occurred in the regions where the flow is segregated through implementation of spatially non uniform C_α field(s). There are also other proposals, and one of which is that this dynamic switching can be set according to predetermined flow regime map [7]. Yet, this approach is merely effective in the flow in simple

geometry; however, this current research is dealing with a relatively random nature of flow after the wave striking to the oil reservoir. Hence, current case asks for a more general physic based approach.

From a more general point of view, one of the switching methods is that the sharp interface capturing method should be applied where the droplet size is sufficient enough to be able to be captured the curvature by the local mesh size. On the other hand, when the droplet size is smaller than the local mesh size, the interface capturing method cannot catch the curvature of the droplet and the flow regime in that area is regarded as dispersive flow. This approach will surely need a method to predict the local droplet size (like population balanced method) and comparison of the droplet size with local mesh size to decide switching C_α on (1 VOF) or off (0 multi-fluid).

However, in the current solver implementation, the switching function based on the work by Cerne et al. (2001) is used. This switching relies on the magnitude of the gradient of the volume fraction, which assumes that if the gradient of the volume fraction is less than some cutoff value, there is only phase dispersion and the interface sharpening is deactivated. The gradient of volume fraction γ is the normalized magnitude of phase fraction as shown below:

$$\gamma = \frac{\nabla \alpha}{\max\left(\nabla \alpha\right)} \tag{3.11}$$

Hence, when $(\gamma > \gamma^*)$, there is no dispersion $(C_\alpha = 1)$, and interface sharpening is activated. A cutoff value of 0.4 is recommended: but, γ is the normalized value so the corresponding value may be somewhat different. The downside of this method is that it will apply interface compression to the already sharp interface if γ near that interface is high, and let the interface dispersion where dispersion is already happened if γ is low. Nonetheless it is an acceptable model for the coupling, and has been implemented in the solver.

In this research, two simulations were conducted: one in which dynamic C_α switching is on and other in which C_α values are fixed. In both cases, the entrainment of air into any liquid phases in neglected thus C_α is always 1, keeping a sharp interface for any air-liquid interfaces (interface sharpening is on) during the whole simulations. Conversely, only the C_α setting of liquid-liquid interface is different between these two simulations. In the first simulation, the liquid-

liquid phase is dispersed and segregated dynamically, while in the second simulation, the liquid-liquid interface will only be set to interdisperse and sharp interface will not be occurred.

Table 3.1 Parameters of the simulation

Geometry	
Length	1 m
Breadth	0.2 m
Height	0.2 m
Transport Properties	
Density of air	1.21 kg/m^3
Density of water	995 kg/m^3
Density of heavy oil	920 kg/m^3
Kinematic viscosity air	1.57E-05 m^2/s
Kinematic viscosity of water	1.02E-06 m^2/s
Kinematic viscosity of oil	5.904E-05 m^2/s
Turbulences Properties	
k	1.5E-04 m^2/s^{-2}
epsilon	$0.1 m^2/s^3$

3.5 **The solution procedure**

The procedure of calculation of the Multifluid-VOF coupling hybrid solver is as shown.

1. Update time step according to Courant number limit (ratio of time step to interface transit time in cell)
2. Solver coupled set of volume fraction equations with interface sharpening for selected phase pairs ((8) with multiple sub time steps);

3. Compute drag coefficients;
4. Construct equation set for phase velocities and solve for preliminary values;
5. Solve pressure-velocity coupling according to Pressure Implicit Splitting of Operators (PISO) algorithm:
6. Compute mass fluxes at cell faces;
7. Define and solve pressure equation (repeat multiple times for non-orthogonal mesh corrector steps);
8. Correct fluxes;
9. Correct velocities and apply BCs;
10. Repeat for number of PISO corrector steps;
11. Compute turbulence and correct velocities;
12. Repeat from 1 for next time step.

3.6 **Numerical considerations for stability of momentum coupling and phase conservation**

In maintaining a sharp interface, the velocities on either side of the interface must be equal to match the nonslip interface condition. This is easy in conventional VOF simulation as the phase velocities are equal everywhere in interface since all phases share a single momentum equation. For current method, where a sharp interface is created by the switching on the interface compression terms “on top” of a multifluid formulations, there are specific momentum equations for each phase to be solved, so that an additional virtual drag term is necessary to maintain the velocities at the interface to be equal. Hence, in the implementation of the solver, small residual drag and residual phase fraction constants were added for each phase pair (typically both equal to 1E-03) to stabilize the phase momentum coupling. These residual values were only added to the calculation of drag for momentum coupling stability and therefore did not have any effect on the actual phase fraction or overall phase conservation.

It is necessary to use limiters on the phase fraction and on the sum of the phase fractions before the explicit solution of the phase fraction equation system to ensure the phase conservation for the coupled phase fractions with added interface sharpening. These limiters setting are achieved in a new multiphase implementation of the Multidimensional Universal Limiter with Explicit Solution (MULES) solver framework within OpenFOAM®. The MULES algorithm implementation also improves the boundedness of the multiphase VOF-only solver

multiphaseInterFoam. The solution of volume fraction transport equation is stabilized by sub time stepping over several subintervals of the overall time step according to Courant number Cr limit. However, for this transient solver, the overall time step is maximized for decreasing the time to solution.

3.7 **Result and discussion**

At the end of the experiment, it was found that all the oil inside the reservoir was not spilled out though the reservoir was totally flooded after hitting by the wave. And, in addition, most of the oil was spilled out the reservoir from the portion close to the wall opposite to the incoming wave. But, this portion of oil spilled out may be occurred only in this particular case for this kind of model. However, this phenomenon was very effective to estimate the oil response to the incoming wave.

The results of the simulations proved relative agreement with the experimental outcomes. The critical period of both of experiment and simulations is between **t** (Time) =0.6**s**, the time at which the wave starts to hit the oil reservoir, and **t**=2**s**, when the back wash of the wave returns back. The overall profile snapshots of experiment in this period are shown in Fig. 3.3. And, the following visual demonstration shows the snapshots comparison of the experiment and two simulations cases: one with dynamic C_α switching (in Fig. 3.4) and one with fixed preset $C_\alpha = 0$ value in the oil-water phase pair (in Fig. 3.5). In both simulations, C_α is set to 1 (only VOF is activated) in the air-liquid (air-water and air-oil) phase pairs. Both simulations proved that not all oil was spilled out from the reservoir even though the reservoir was totally flooded. In Fig. 3.4, it was found that oil dispersion into the water between **t**=1.2s and **t**=2.0s shows a little closer representation to the experiment; unfortunately dispersion was not clearly seen in the experiment, due to oil sticking to transparent wall of the tank.

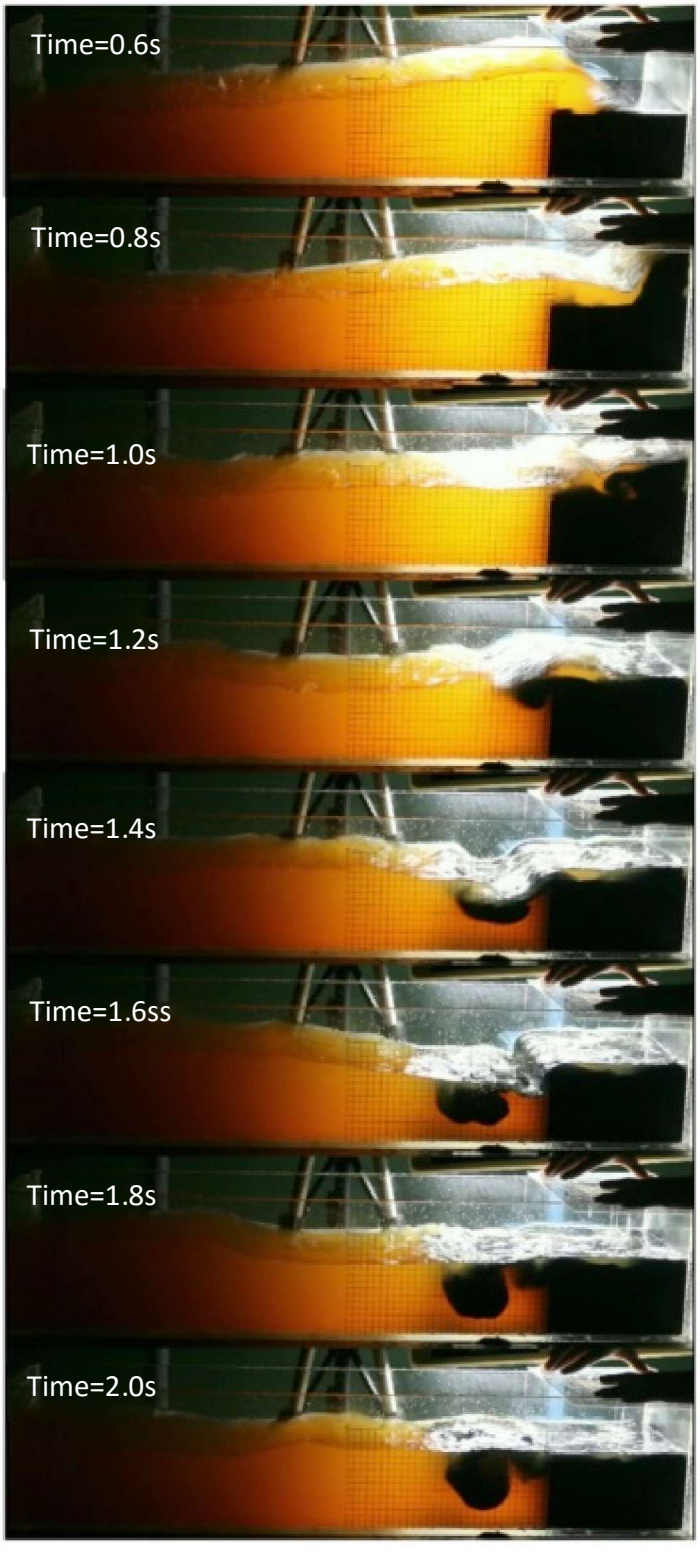

Fig. 3.3 Profile view of experiment between **t**=0.6**s** and **t**=2.0**s** with emphasizing the detail formation of oil ball phenomenon

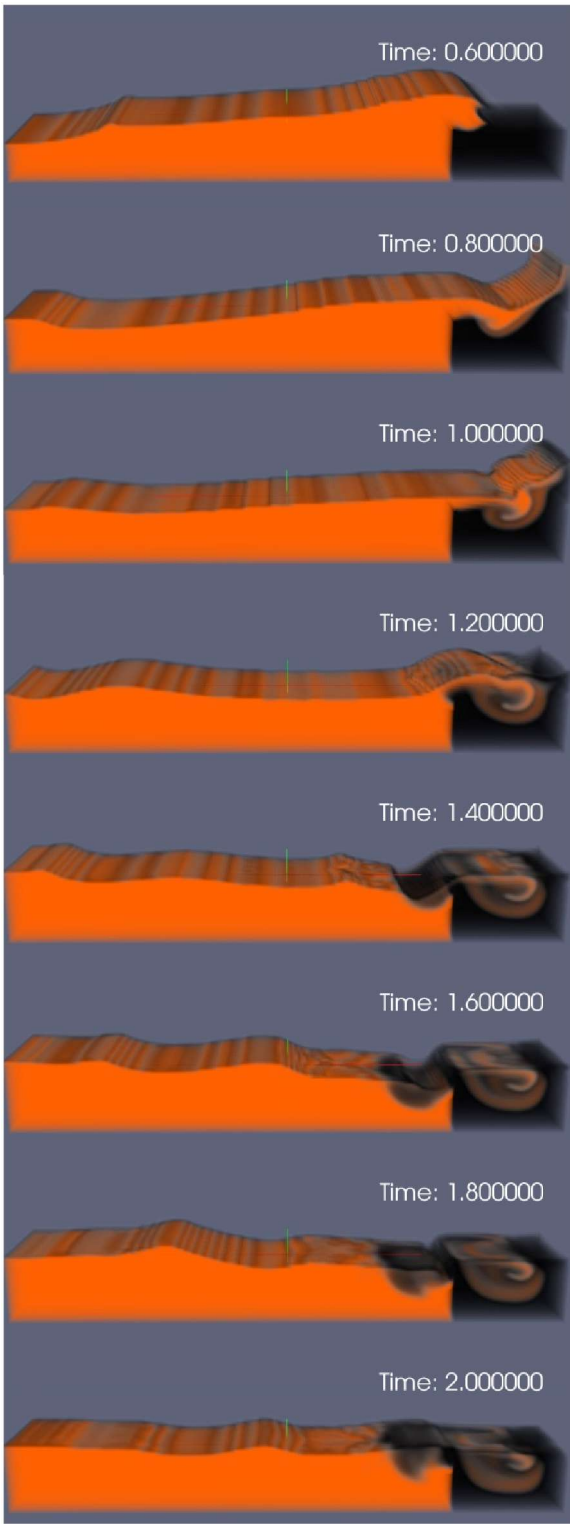

Fig. 3.4 Profile snapshots of simulation with dynamic C_α switching for oil-water phase pair between **t**=0.6**s** and **t**=2.0**s** with 0.2**s** time step

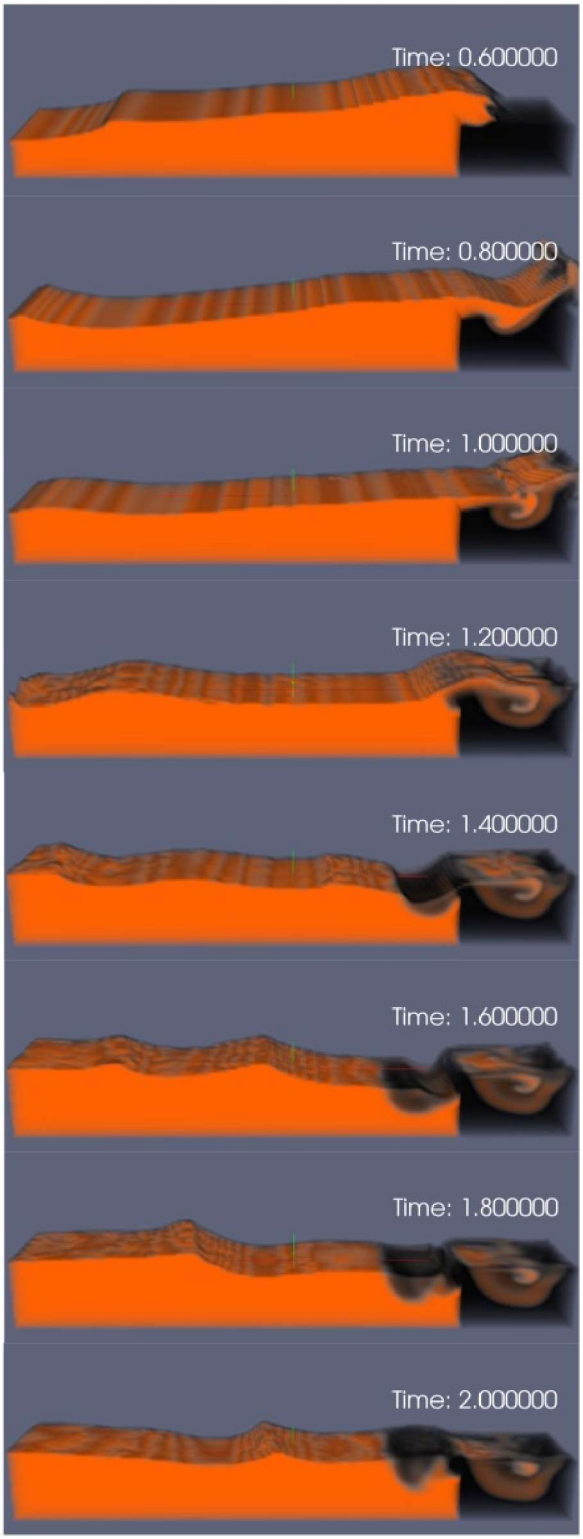

Fig. 3.5 Profile snapshots of simulation without dynamic C_α switching for oil-water phase pair between **t**=0.6**s** and **t**=2.0**s** with 0.2**s** time step

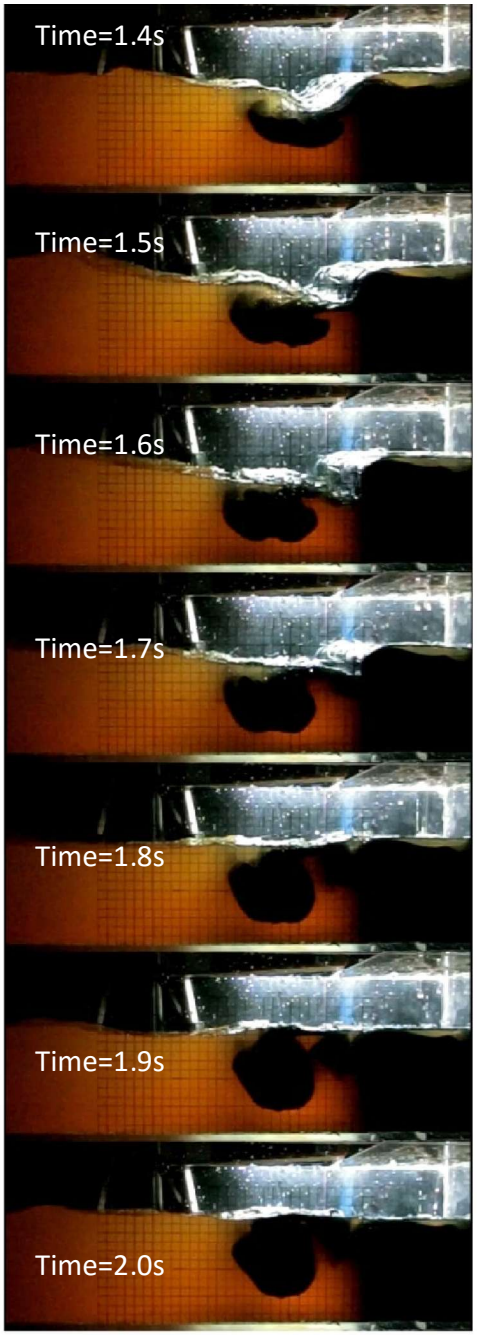

Fig. 3.6 Emphasizing the detail formation of oil ball phenomenon near the oil reservoir between **t**=1.4**s** and **t**=2.0**s** with 0.1**s** time step

In addition, the relatively significant oil ball formation phenomenon occurred between **t**=1.4**s** and **t**=2.0**s**. The magnified snapshots of this oil ball formation are reported in Fig. 3.6. This oil ball is considered to be important for the future research of submarine oil spill, which can be

occurred when the oil mixes with the soil particles of turbid water. All the visualization of the results is achieved by the help of post processing tool ParaView (version 4.1).

In the experiment, the maximum depth of the oil ball penetration below the normal water level after flooding was approximately 7.75 cm, and occurred at **t**=1.8**s**. However, the oil ball in both simulations could merely reach approximately 6 cm depth at **t**=1.8**s** as shown in Fig. 3.7. Moreover, the oil ball in experiment showed more segregated in nature than the dispersed oil balls in both simulations.

(a) (b)

Fig. 3.7 Simulations results of oil ball formation (a) with dynamic C_α switching for oil-water phase pair (b) without dynamic C_α switching for oil-water phase pair

In this analysis, the phenomenon of oil response to the incoming wave was observed experimentally. This resultant response of oil dispersed and segregated flow in water is simulated in both dynamic C_α switching (coupled VOF and multifluid) and method fixed $C_\alpha = 0$ value (only multifluid) method. The formation of oil ball after the oil reservoir being hit by the wave was observed, however this phenomenon of oil ball formation appeared in both simulations. Nonetheless, simulation with dynamic C_α switching has a slightly better representation of the phenomenon as the oil dispersion in water is shown a little closer to experiment in the post processing.

CHAPTER 4

ANALYSIS OF POTENTIAL TSUNAMI TRIGGERED OIL SPILL CASE FROM SAKAI SENBOKU INDUSTRIAL PARK IN OSAKA BAY

In this analysis, it is necessary to estimate the strength of the potential tsunami in the Osaka Bay area. Thus, combining of methods that includes the mass inflow of water representing the tsunami wave and the transport of oil spill is needed to simulate the whole scenario of tsunami-triggered oil spill. It is also necessary to implement the overflow of water over the dry land, where the primary source of oil spill existed.

First, the strength of the tsunami in Osaka Bay due to the movement of the Nankai fault was estimated by the Storm Surge and Tsunami Simulator in Oceans and Coastal Areas (STOC) developed by the Port and Airport Research Institute (PARI) of Japan (Kakinuma and Tomita, 2005; Tomita et al., 2006; Tomita and Yoem, 2012).

Then, using the resulting local wave information of STOC near the Sakai Senboku area, two types of oil spill simulations were conducted: a three dimensional simulation by an open-source computational fluid dynamics (CFD) code, OpenFOAM® and a two dimensional simulation by a STOC extension for oil spill simulation, STOC-OIL. The OpenFOAM® simulation can predict the oil spill in three-dimensions, including the vertical water column oil spill for a short time after the tsunami wave passes through the area, while the STOC-OIL simulation can estimate the distribution of the oil spill on the surface for several minutes after the tsunami attack.

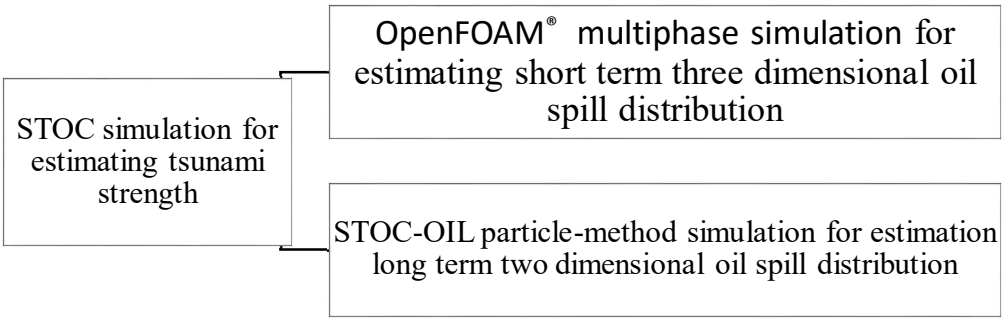

Fig. 4.1 General procedure of tsunami triggered oil spill simulation

4.1 STOC

STOC is mainly comprised of two sub programs: STOC-ML and STOC-IC.

4.1.1 STOC-ML

STOC-ML is a multi-layered static dynamics model. It uses hydrostatic approximation to calculate fluid dynamics resulted from a tsunami. It is a quasi-3-dimensional model, which originally is based on two dimensional model, where the water surface elevation is represented as a parameter, since the hydrostatic approximation can be applied for prediction of the tsunamis that occur offshore. In STOC-ML, the fluid body can be divided into multi layers along the depth of water; though usually, the single layer model is used in tsunami calculation.

4.1.2 STOC-IC

On the other hand, STOC-IC is a real three dimensional model for calculating the fluid dynamics resulting from a tsunami, based on the most fundamental equations in fluid dynamics. The model is employed for calculating changes in tsunamis resulting from structures found in coastal areas. In general STOC-IC is used in connection with STOC-ML. By coupling the two models, it is possible to calculate, with high accuracy, the behavior of tsunami that occur offshore and then propagate oceans and hit coastal areas, such as ports or harbors.

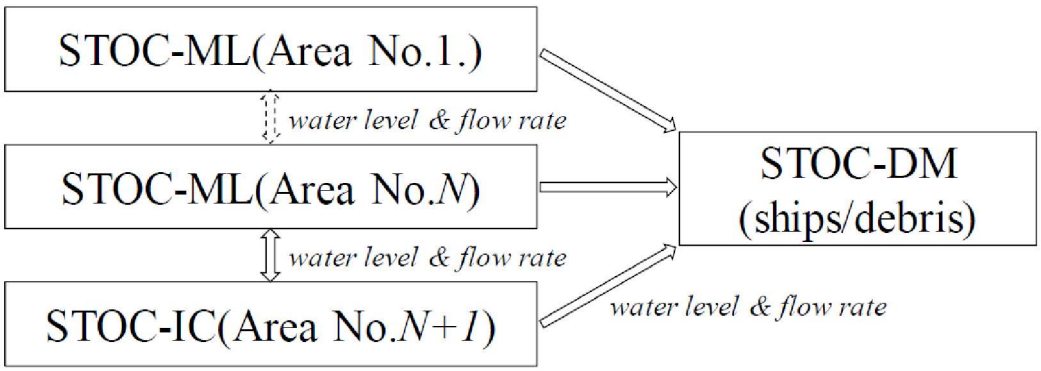

Fig. 4.2 Relationship among the Calculations Coupled in STOC

STOC-IC is used in connection with STOC-ML by means of a domain coupling technique called nesting. One or more STOC-ML domains can be coupled with one STOC-IC domain to calculate, high accuracy, the behavior of tsunamis that occur offshore and then propagate oceans

and hit coastal areas, such as ports or harbors, simultaneously shown in example of Fig. 4.3. This parallel calculation is achieved by the Message Passing Interface (MPI).

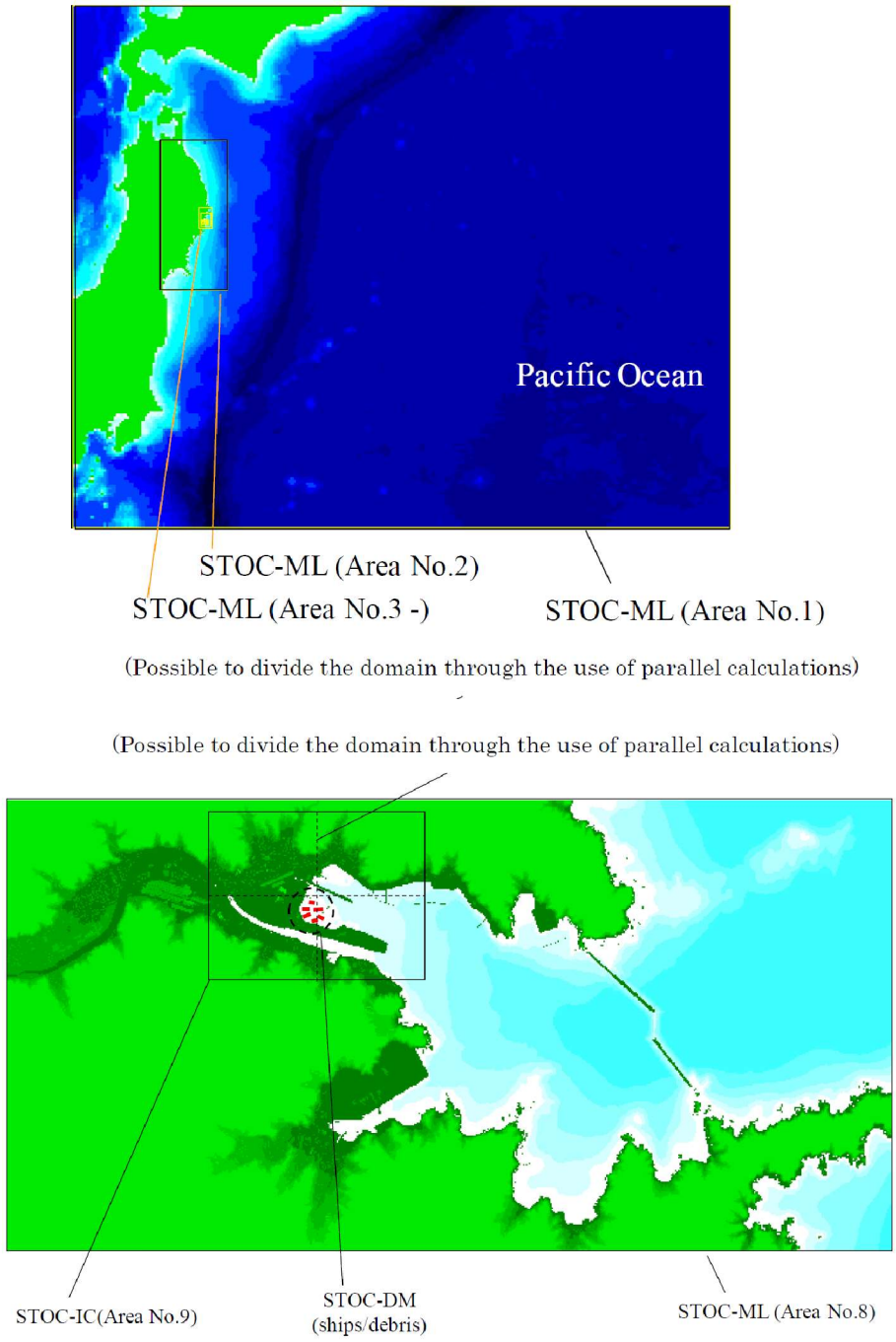

Fig. 4.3 Example of the Division of Domains in the Calculations Coupled by STOC

Table 4.1 STOC Functions

Item	Description
Analyzed	Storm surge and tsunami STOC-ML covers the propagation of waves over a wide range of sea bodies, from the open ocean to the coast. On the other hand, STOC-IC primarily covers the detailed calculation of the behavior of water streams in harbors.
Fundamental equation	An equation extended from the Navier-Stokes equation by using the Porous approximation for 3-dimensional incompressible viscous fluids. - Equation of continuity - Equation of momentum conservation - Equation for free surfaces - Hydrostatic conditions (STOC-ML)
Physical model	- Run-up tip model - Permeable structure model - Turbulent flow model (LES, k-ε) -Transparent boundary model - Dispersive wave model - Breaking wave model - Overflow model - Model for a change in water level due to an earthquake
Discretization	- Difference equations using staggered mesh - Shape approximation using the porous model
Advection term	- Second-order accurate central-differencing scheme - First-order accurate upwind scheme - Hybrid difference, weighted average of the above parameters
Time integration	- Leap-frog method - SMAC (Simplified Marker and Cell) method
Method to solve simultaneous linear equations	- MILU-BiCGStab method

The functions of STOC are listed in Table 4.1. STOC-ML and IC can also be couple with STOC-DM, which is for simulation of ships and debris drifting in tsunami, and STOC-OIL, which is two dimensional oil diffusion model, especially developed for tsunami triggered oil spill.

4.1.3 Fundamental Equations in a Plane coordinate system

Although STOC-ML is a hydrostatic model and STOC-IC a non-hydrostatic model, both models share a number of things in common. The following sections show all the fundamental equations and describe the differences between the two programs where there are any.

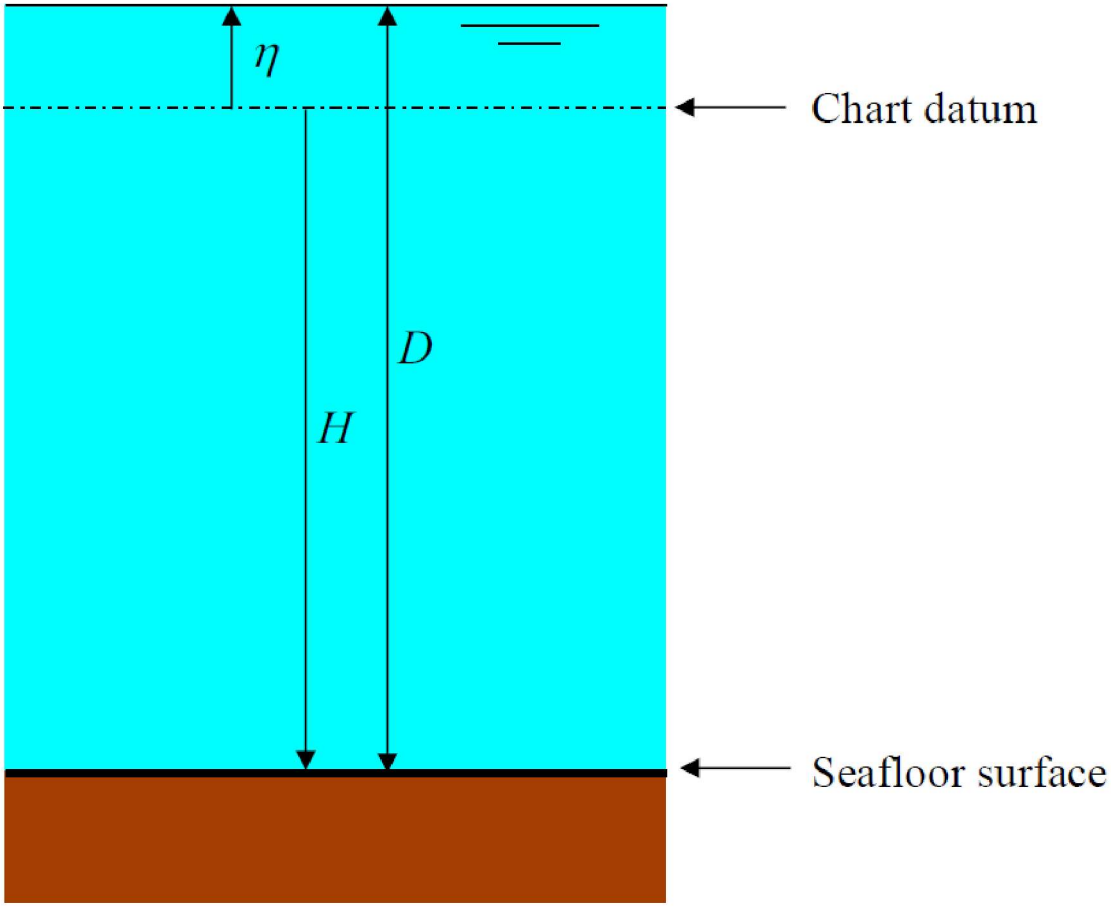

Fig. 4.4 Definitions of Water Level, Water Depth, and Total Water Depth

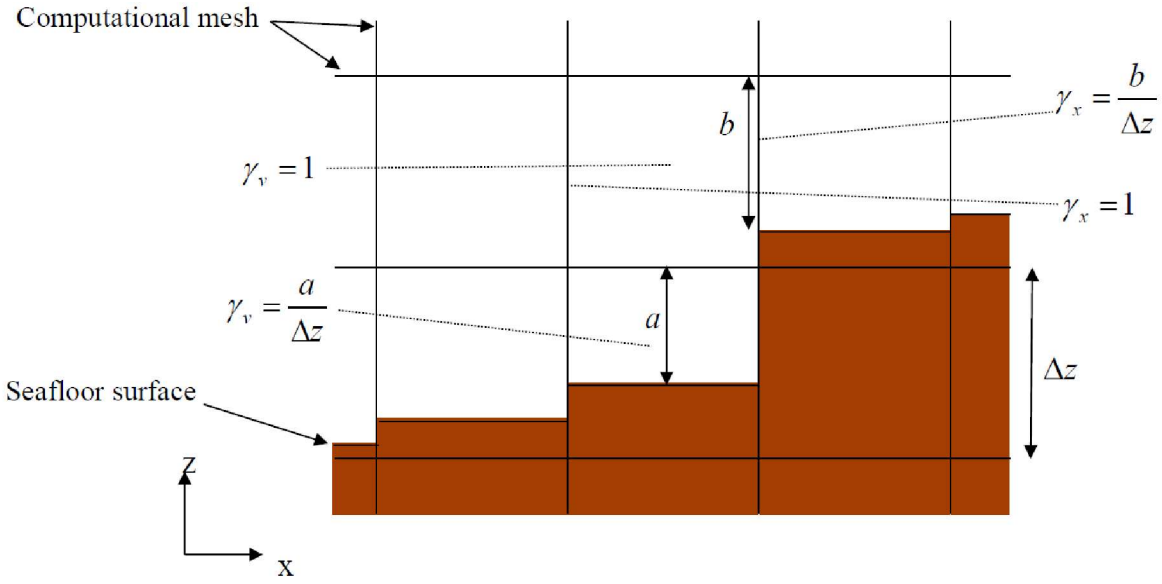

Fig. 4.5 Definition of Porous Values

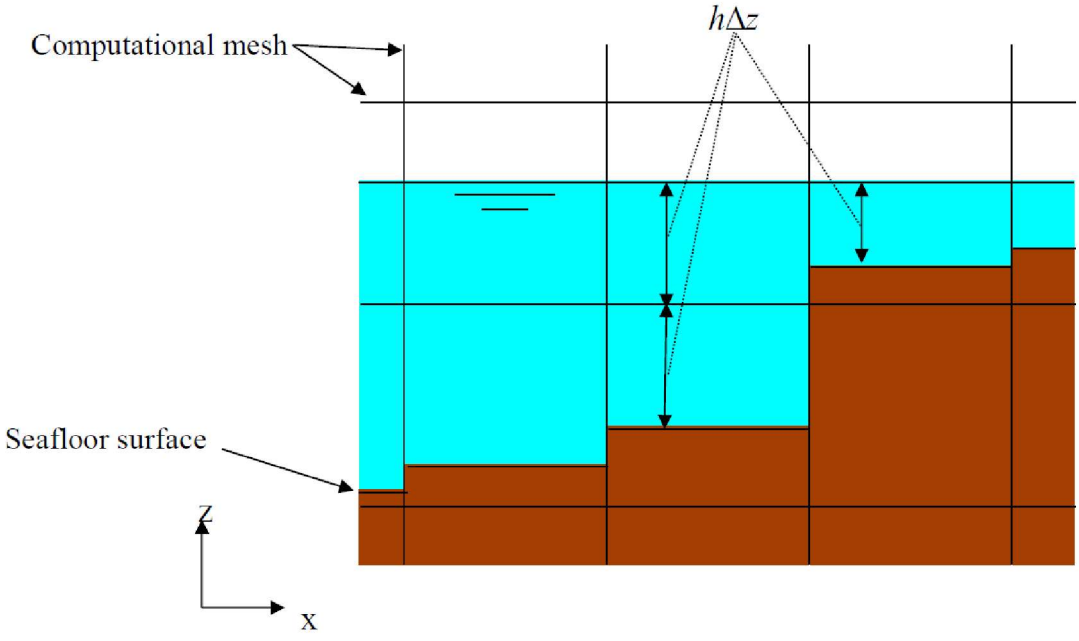

Fig. 4.6 Definition of Layer Thickness

Although STOC-ML is a hydrostatic model and STOC-IC is a non-hydrostatic model, both models share a number of things in common. The fundamental equations used in STOC-ML and STOC-IC are a 3-dimensional continuity equation and the momentum conservation equation. Fig. 4.4, Fig. 4.5 and Fig. 4.6 show the nomenclatures used in the fundamental equations.

Continuity Equation

$$\frac{\partial}{\partial x}(\gamma_x u)+\frac{\partial}{\partial y}(\gamma_y v)+\frac{\partial}{\partial z}(\gamma_z w)=0, \tag{4.1}$$

Momentum Conservation Equations

x direction

$$\begin{aligned}&\gamma_v \frac{\partial u}{\partial t}+\frac{\partial}{\partial x}(\gamma_x uu)+\frac{\partial}{\partial y}\left(\gamma_y uv\right)+\frac{\partial}{\partial z}(\gamma_z uw)-\gamma_v f_0 v\\&=-\gamma_v \frac{1}{\rho}\frac{\partial p}{\partial x}+\frac{\partial}{\partial x}\left(\gamma_x \nu_H 2\frac{\partial u}{\partial x}\right)+\frac{\partial}{\partial y}\left\{\gamma_y \nu_H\left(\frac{\partial u}{\partial y}+\frac{\partial v}{\partial x}\right)\right\},\\&+\frac{\partial}{\partial z}\left\{\gamma_z \nu_H\left(\frac{\partial u}{\partial z}+\frac{\partial w}{\partial x}\right)\right\}\end{aligned} \tag{4.2}$$

y direction

$$\begin{aligned}&\gamma_v \frac{\partial v}{\partial t}+\frac{\partial}{\partial x}(\gamma_x vu)+\frac{\partial}{\partial y}(\gamma_y vv)+\frac{\partial}{\partial z}(\gamma_z vw)-\gamma_v f_0 u\\&=-\gamma_v \frac{1}{\rho}\frac{\partial p}{\partial y}+\frac{\partial}{\partial x}\left(\gamma_x \nu_H\left(\frac{\partial v}{\partial x}+\frac{\partial u}{\partial y}\right)\right)+\frac{\partial}{\partial y}\left\{\gamma_y \nu_H 2\frac{\partial v}{\partial y}\right\},\\&+\frac{\partial}{\partial z}\left\{\gamma_z \nu_V\left(\frac{\partial v}{\partial z}+\frac{\partial w}{\partial y}\right)\right\}\end{aligned} \tag{4.3}$$

z direction (STOC-IC only)

$$\begin{aligned}&\gamma_v \frac{\partial w}{\partial t}+\frac{\partial}{\partial x}(\gamma_x wu)+\frac{\partial}{\partial y}(\gamma_y wv)+\frac{\partial}{\partial z}(\gamma_z ww)\\&=-\gamma_v \frac{1}{\rho}\frac{\partial p}{\partial z}+g+\frac{\partial}{\partial x}\left(\gamma_x \nu_H\left(\frac{\partial w}{\partial x}+\frac{\partial u}{\partial z}\right)\right)+\frac{\partial}{\partial y}\left\{\gamma_y \nu_H\left(\frac{\partial w}{\partial y}+\frac{\partial v}{\partial z}\right)\right\},\\&+\frac{\partial}{\partial z}\left\{\gamma_z \nu_V 2\frac{\partial w}{\partial z}\right\}\end{aligned} \tag{4.4}$$

where, u, v and w are the velocities in X, Y and Z-direction respectively, and p is the pressure (hydrostatic in case of STOC-ML), g is the acceleration due to gravity and ρ is the density of sea water. γ stands for the porous values according to Fig. 4.5.

In STOC-ML, w is calculated by performing the integrations upward from the sea floor to surface by assigning u and v to the continuity equation. Then, the continuity equation can be solved without solving the Z-direction momentum conservation equation.

Free Surface Equation

Only one water surface is defined at a certain point (x, y) in both STOC-ML and STOC-IC.

$$\gamma_z \frac{\partial \eta}{\partial t} + \frac{\partial}{\partial x}\int_{-H}^{\eta} \gamma_x u dz + \frac{\partial}{\partial y}\int_{-H}^{\eta} \gamma_y v dz = 0, \tag{4.5}$$

where η stands for water surface elevation.

Hydrostatic Pressure Equation (STOC -ML only)

$$p(z) = p_{atm} - \rho g(\eta - z), \tag{4.6}$$

In STOC-ML, the hydrostatic pressure calculation is implicit. The hydrostatic pressure is then calculated as a function of the vertical distance from the water surface as shown below. However, STOC-IC explicitly calculates the pressure by simultaneously solving the continuity and momentum conservation equations.

Based on the nonlinear dispersive wave theory a nonlinear dispersive wave model is implemented in STOC-ML to calculate the deformation behaviors of wave with good accuracy by adding dispersion terms.

4.1.4 Discretization Methods

A staggered grid as shown in Fig. 4.7 is used. u (i-1, j, k) is defined for the cell interface on the -x side of cell (i, j, k), and u (i, j, k) defined for the cell interface on the +x side. A rectangular grid is used. The mesh width is variable. Finite volume method is used for discretization. A hybrid scheme that combines the first-order upwind scheme and second-order central-differencing scheme is applied to discretize the advection term. The second-order central-differencing scheme

is applied to discretize other terms. The Leapfrog method is used to perform time integration. One layer of virtual cells outside of the computation area is deployed for processing boundary conditions as shown in Fig. 4.8. The 3-dimensional array size (MX, MY, MZ) is two meshes greater than the actual computation area size (MX-2, MY-2, MZ-2) for each direction, because this layer is necessary.

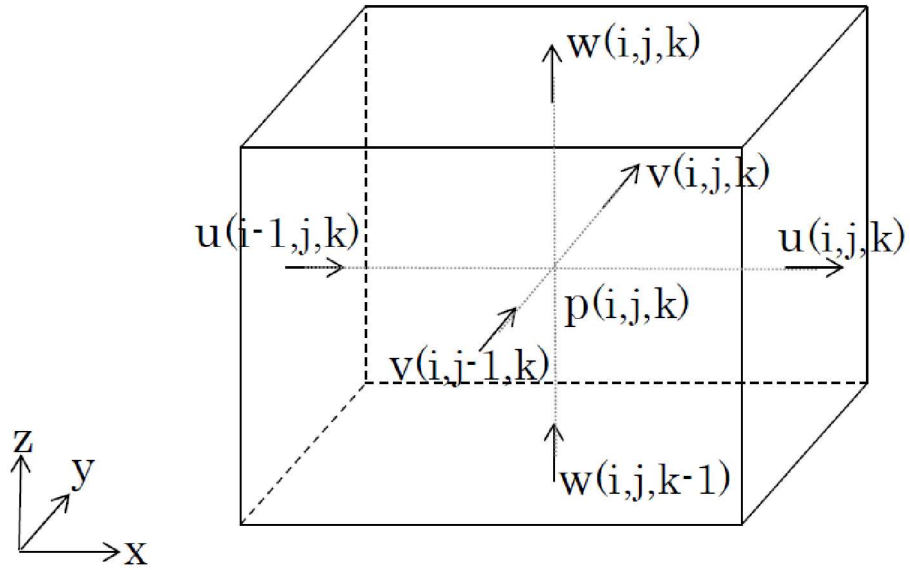

Fig. 4.7 Arrangement of Variables for Staggered Grid

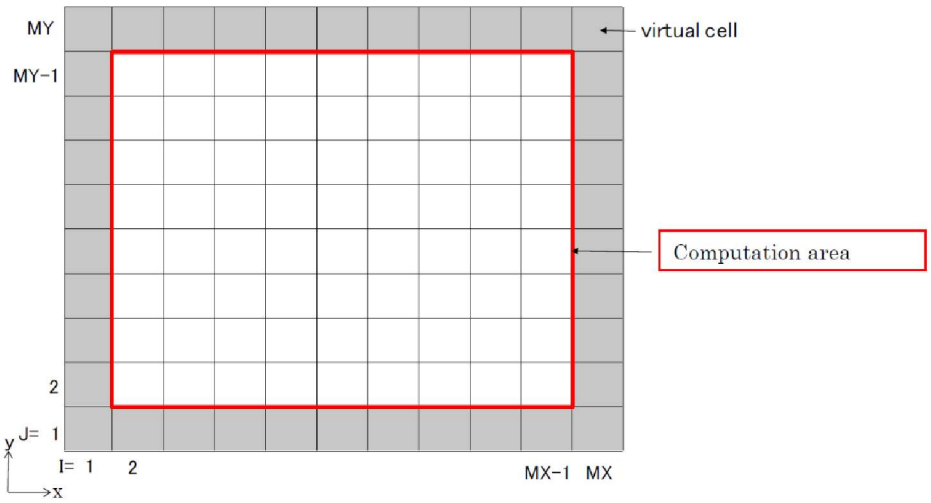

Fig. 4.8 Computational Area and Virtual Cells

4.1.5 Model Coupling with Nesting Function

The following combinations of simulations can perform coupled calculations by nesting calculation:

- STOC-ML and STOC-ML
- STOC-ML and STOC-IC

For example, they compute the outer wide regions with coarse meshes and compute the inner target points with fine meshes as shown in Fig. 4.8. Note that the time step should be the same for all the regions. A different process is used for each region for calculation, and data is exchanged between regions through Message Passing Interface (MPI).

4.1.6 Flow of Nesting Processing

The basic flow of processing for the nesting function is as follows.

(1)Calculate flow velocities “u” and “v” at the updated time.

(2) Transfer the “u” and “v” values, required for processing of the boundary conditions, between the parent and child.

(3) Calculate flow velocity “w” and the water level at the updated time.

(4) Transfer the “w” and water level values, required for processing of the boundary conditions, between the parent and child.

(5) If the current time is not yet the time to terminate the processing, return to step (1).

(6) Perform the termination processing.

4.1.7 Processing of the Boundary Conditions for the Nesting Section (Overlapped Area)

The area filled with grey in Fig. 4.8 is called an overlapped area for nesting. In this area, the flow velocity and water level values are transferred between the parent and child, and their boundary condition are set. Specify the width of this area as an input parameter. Typically, it should be equal to a single parent mesh. The boundary (- - - - -), which is called the connection boundary, is for transferring the boundary condition from the parent to the child, and the boundary (═══), which is called the child connection boundary, is for transferring the boundary conditions from the child to the parent.

The method of updating the values in an overlapping area is as follows.

4.1.8 Parent mesh calculation

In the parent mesh, the child connection boundary (- - - - -) is treated the same as a free inflow/outflow boundary, and the region within that boundary is not calculated.

The areas filled with slashes in Fig. 4.9 are processed as obstacles.

4.1.8.1 Flow velocity calculation

In the parent mesh, calculate the flow velocity (in the position indicated by ⟶ in Fig. 4.9) on both the connection boundary surface and overlapped area. Set the inner flow velocity (in the position indicated by ⟹) required for this calculation to the average value of flow velocities computed for the associated child meshes.

4.1.8.2 Water level calculation

In the parent mesh, set the water level (○) in the overlapped area and the inner water level (△) to the average value of water levels computed for the associated child meshes.

For nesting calculations, it is strongly recommended to match the water depth in both the overlapped area and the area immediately inside this overlapped area to the water depth for the child mesh.

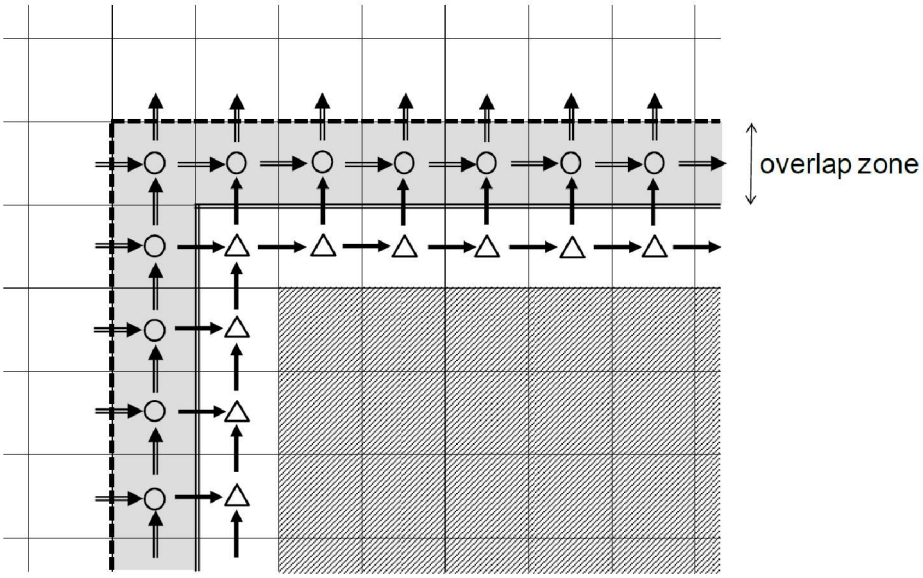

Fig. 4.9 Parent Mesh Calculation

4.1.9 Child mesh calculation

In the child mesh, the connection boundary (- - - - -) is treated the same as a fixed flow velocity boundary.

4.1.9.1 Flow velocity calculation

In the child mesh, calculate the flow velocity inside the connection boundary shown in Fig. 4.9. Set the flow velocity (in the position indicated by in Fig. 4.10) at the connection boundary to the value obtained by linear interpolation of the flow velocity for the parent mesh. Note that the data is corrected after linear interpolation so the flow rate at the connection boundary for the parent mesh and the outer boundary for the child mesh can match each other.

4.1.9.2 Water level calculation

The water levels for the child mesh are calculated in the regular way. For the overlapped area, the weighted average between the water levels calculated in the parent and child meshes is calculated. The weighting coefficients are configured to set the weight for the parent to 1 and that for the child to 0 at the connection boundary (- - - - -), as well as to set the weight for the parent to 0 and that for the child to 1 at the child connection boundary (═══).

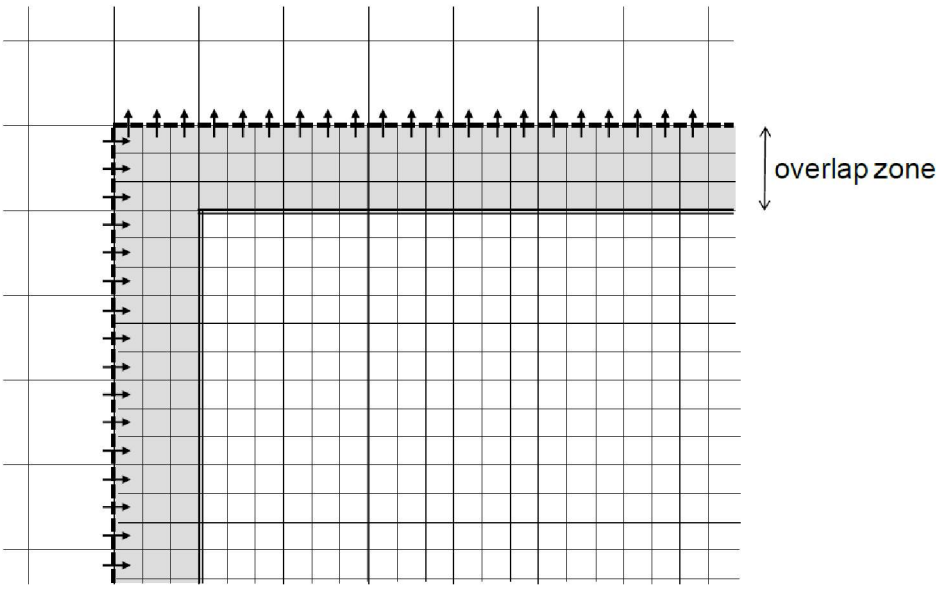

Fig. 4.10 Child Mesh Calculation

4.1.10 STOC System Configuration

Fig. 4.11 shows a typical I/O data flow in STOC (where the italic *Area* indicates the name of user-defined data; the other italic *NN* shows a processor number in parallel computations). "data.in" defines the relationship between connections across areas and exists solely on its own. On the other hand, there is as many of the other files as the number of areas to be computed. Table 4.2 shows a list of I/O data files used in STOC.

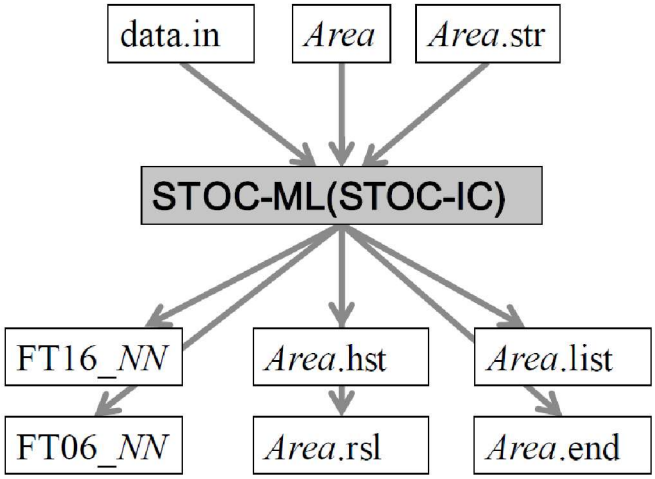

Fig. 4.11 I/O Correlation Diagram in STOC

Table 4.2 List of I/O Files in STOC

File	I/O	Contents	Remarks
data.in	I	Defines the relationship between connections across areas	Mandatory
area	I	Analysis condition	Mandatory
Area.str	I	Topography/geometry data	As required
Area.sbt	I	The amount of data for the time-dependent water level fluctuations by seismic action	As required
fault.txt	I	Seismic fault parameters	As required
Area.rsi	I	Data for restart (input)	As required

File	I/O	Contents	Remarks
Area.bci	I	Water level, flow velocity data at connection boundary (input)	As required
Area.tim	I	Flow velocity/ water level time-series input data	As required
Area.dpr	I	Permeable structure data	As required
Area.ofl	I	Data for specifying the location on which to apply the overflow model	As required
Area.fwc	I	Coefficient data for overflow model	As required
Area.ini	I	Initial distribution data of water temperature and chlorine level	As required
FT16_*NN*	O	Computation intermediate information	Output required
FT06_*NN*	O	Debugging information 1 (maximum velocity, etc.)	Output required
Area.hst	O	Time-series output data	As required
Area.lst	O	Spatial distribution data of water level/ flow velocity	As required
Area.end	O	Aggregate data, including the maximum water level, etc.	Output required
Area.rso	O	Data for restart (output)	As required
Area.bco	O	Water level, flow velocity data at connection boundary (output)	As required
data.in_debug	O	Debugging information 2 (relation between connections across areas, etc.)	Output required
Area.dbg	O	Debugging information 3 (value of common variables, etc.)	Output required
Area.ars	I/O	Data for automatic restart	As required

*The italic *Area* indicates the name of user defined data. The other italic *NN* shows a processor number in parallel computations.

4.1.11 Domain preparation

In STOC simulation to predict the behavior of tsunami, four domains were used. The largest and first domain has a mesh size of 1350km and encompasses an area of length 1215 km and width 742.5km, and it includes the Honshu, Shikoku and Kyushu of Japan, and is bounded between the latitude of 29° 25'16"N and 36° 6'23"N, and between the longitude of 128° 27' 40"E and 141° 26' 23"E, centering the Nankai fault in the middle of the domain to predict the tsunami waves effectively as shown in Fig. 4.12. Then, the second domain of mesh size 450m, enclosing an area of length 459 km and width 270km, is used inside the first domain as shown in Fig. 4.13. Again, inside the second domain, the third domain of mesh size 150m, enclosing an area of length 108km and 90km, is used as shown in Fig. 4.14. Meanwhile, the smallest and most precise fourth domain has a mesh size of 50m and a dimension of 70.5km by 64.5km bounding the entire Osaka Bay area as shown in Fig. 4.15.

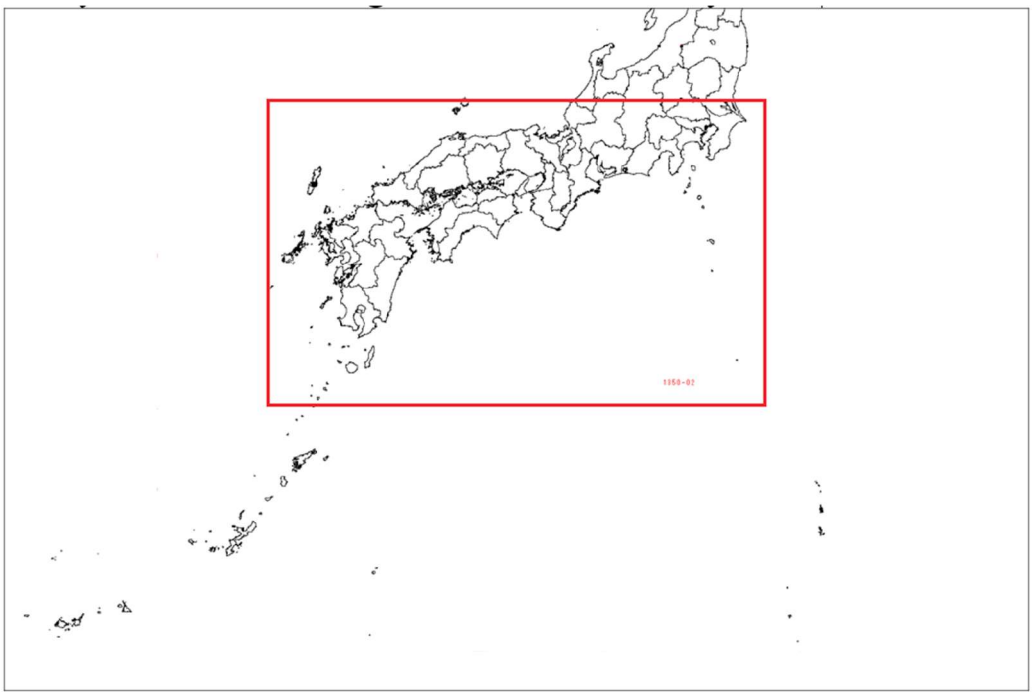

Fig. 4.12 First domain with 1350m mesh

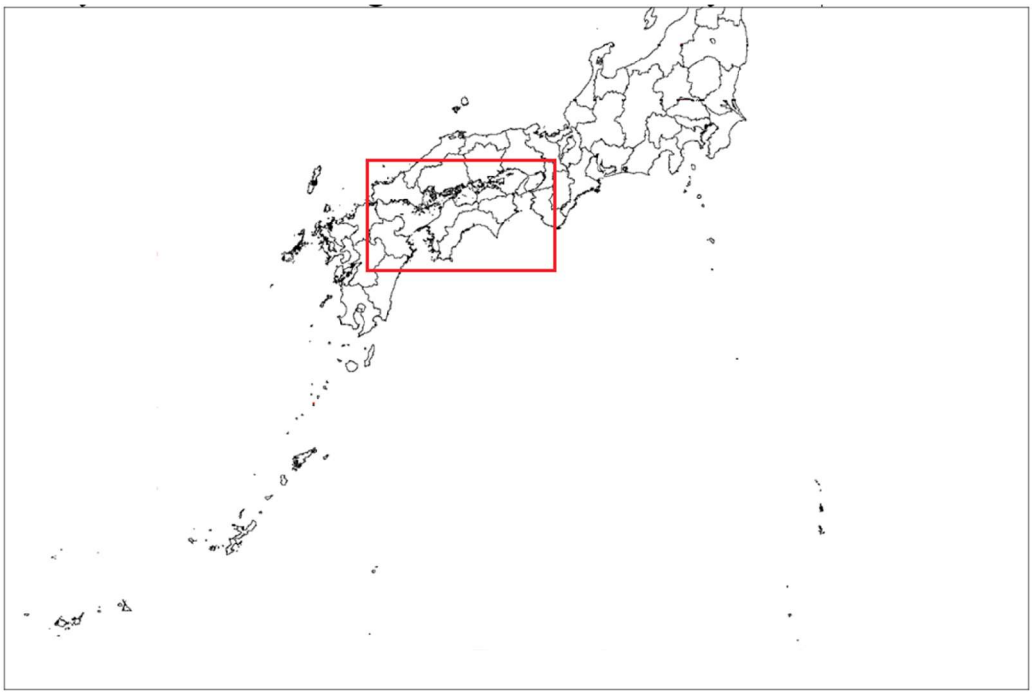

Fig. 4.13 Second domain with 450m mesh

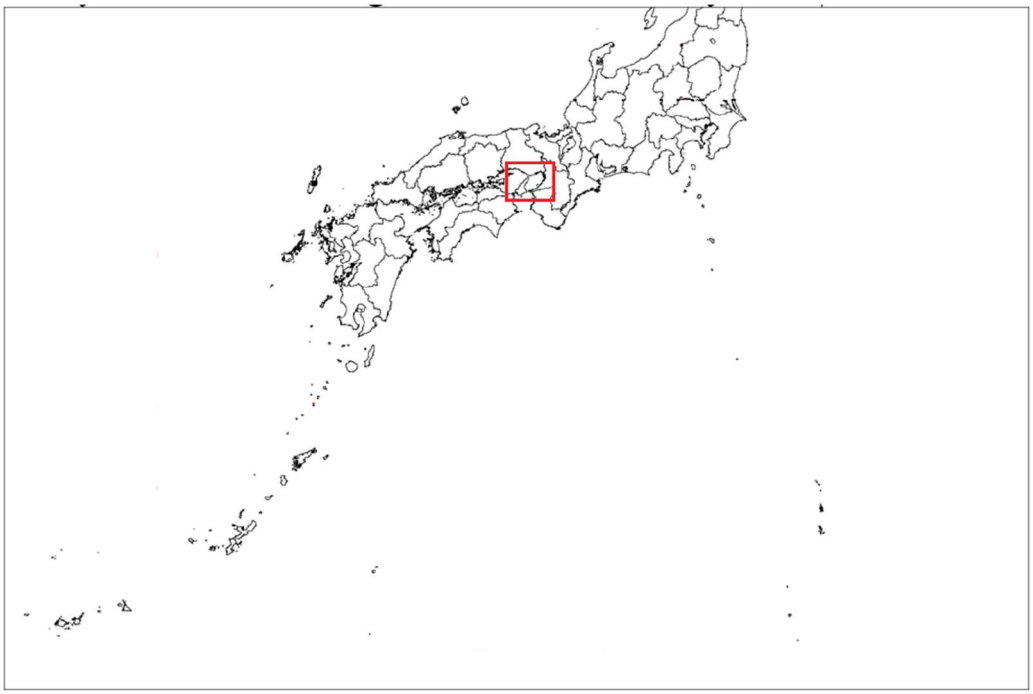

Fig. 4.14 Third domain with 150m mesh

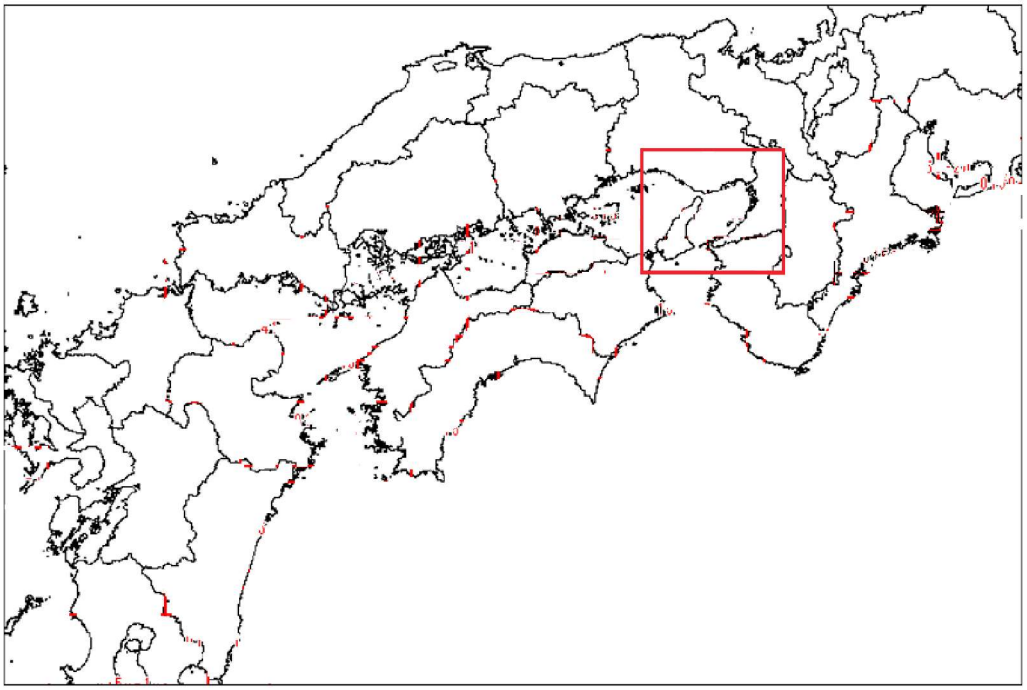

Fig. 4.15 Fourth domain with 50m mesh

Along the Nankai trough located south of the Japan main island, there are three main faults zones: Tokai fault, Tonankai fault and Nankai fault as shown in Fig. 4.1 6.

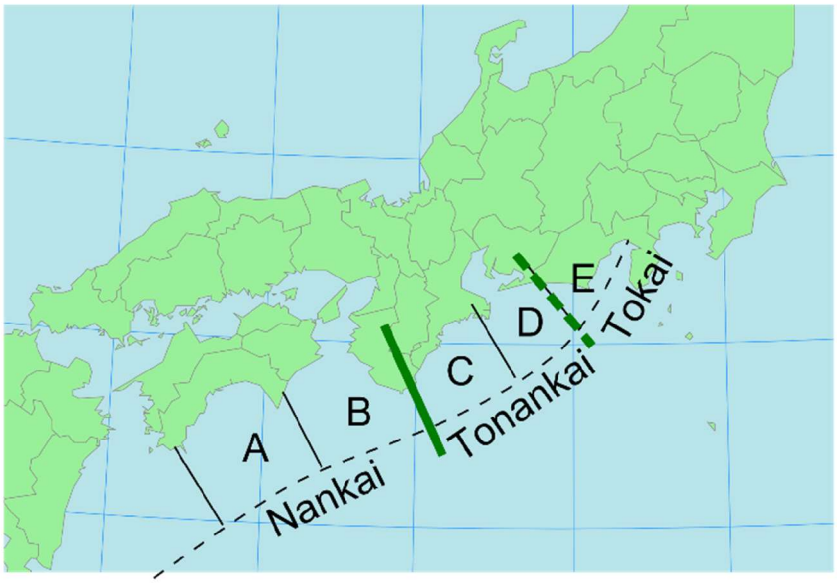

Fig. 4.16 Location of Nankai fault (Wikipedia)

Among these fault, only the Nankai fault zone is directly facing to the Osaka Bay area, and hence, it was used for initial water surface elevation. Previously, Nankai Megathrust Equake Investigation Commission of Osaka Prefecture had estimated that there were 11 fault models of Nankai fault movement, which can create a tsunami to Osaka Bay. In this study, the fault model of possible maximum damage to the Osaka Bay area was used. This fault model of Nankai is divided into 635 patches, STOC can generically generate the initial water surface elevation based on each patch of the fault movement. It was considered that all these 635 patches of the fault movement occur simultaneously to unleash the tsunami.

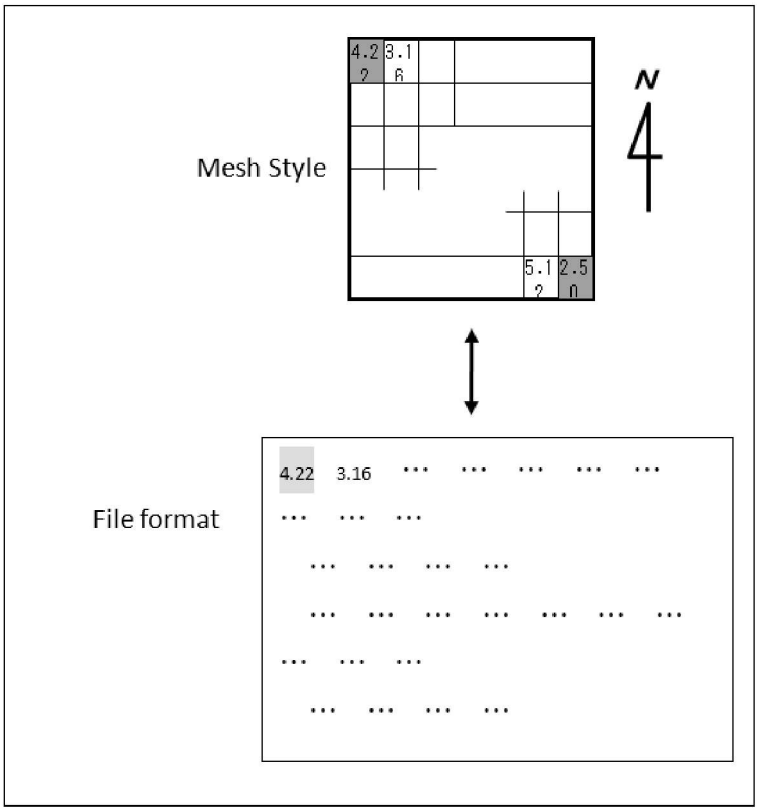

Fig. 4.17 Format of topology data

All the input data for STOC calculations and fault parameters were derived from the Publication of Tsunami and Earthquake Analysis Cabinet Office of Osaka prefecture, Japan. These data were arranged in the order as shown in Fig. 4.17.

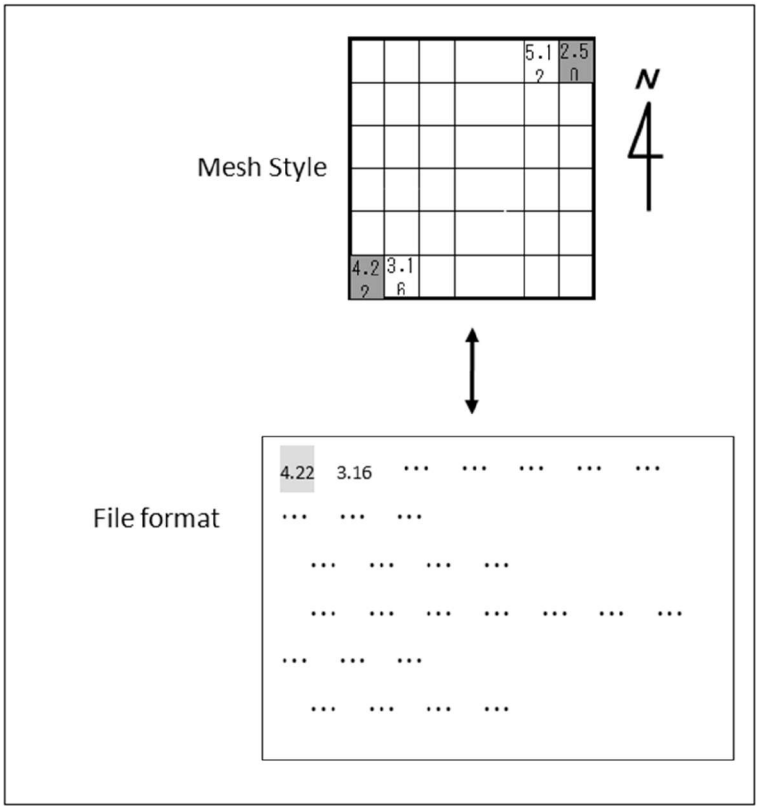

Fig. 4.18 Required input files' format for STOC calculation

However, the input files into STOC simulation had to be arranged in the opposite order as shown in Fig. 4.18. Hence, a new conversion Fortran code for the input of format of STOC simulation was created and used. The mean sea level is taken as 0.5 m above the 0 datum line according to tidal timetable. The simulation is carried out up to 14400s (240minutes) after the initial water surface elevation due to the fault movement. The output data were recorded every 60s (1minute). During the calculation, the domains were automatically decomposed for parallel computation by Massage Passing Interface. All the computations were conducted using the supercomputer of the Kyushu University.

4.1.12 Node points for catching flow wave height and velocity distribution

To couple with OpenFOAM®, it is only possible to perform manual coupling between STOC and OpenFOAM®, therefore it was necessary to predict the wave heights and wave velocity distribution around the Sakai Senboku area. Hence, STOC-ML is enough to achieve this goal. First, all four domains were dealt with only using STOC-ML calculations. During the simulation, 44

node points were distributed in the Osaka Bay around Sakai Senboku area to fetch the wave heights and wave velocity distribution. Fig. 4.19 indicates the location of the node points where the wave height and velocity distribution were recorded to input into OpenFOAM® oil spill simulation.

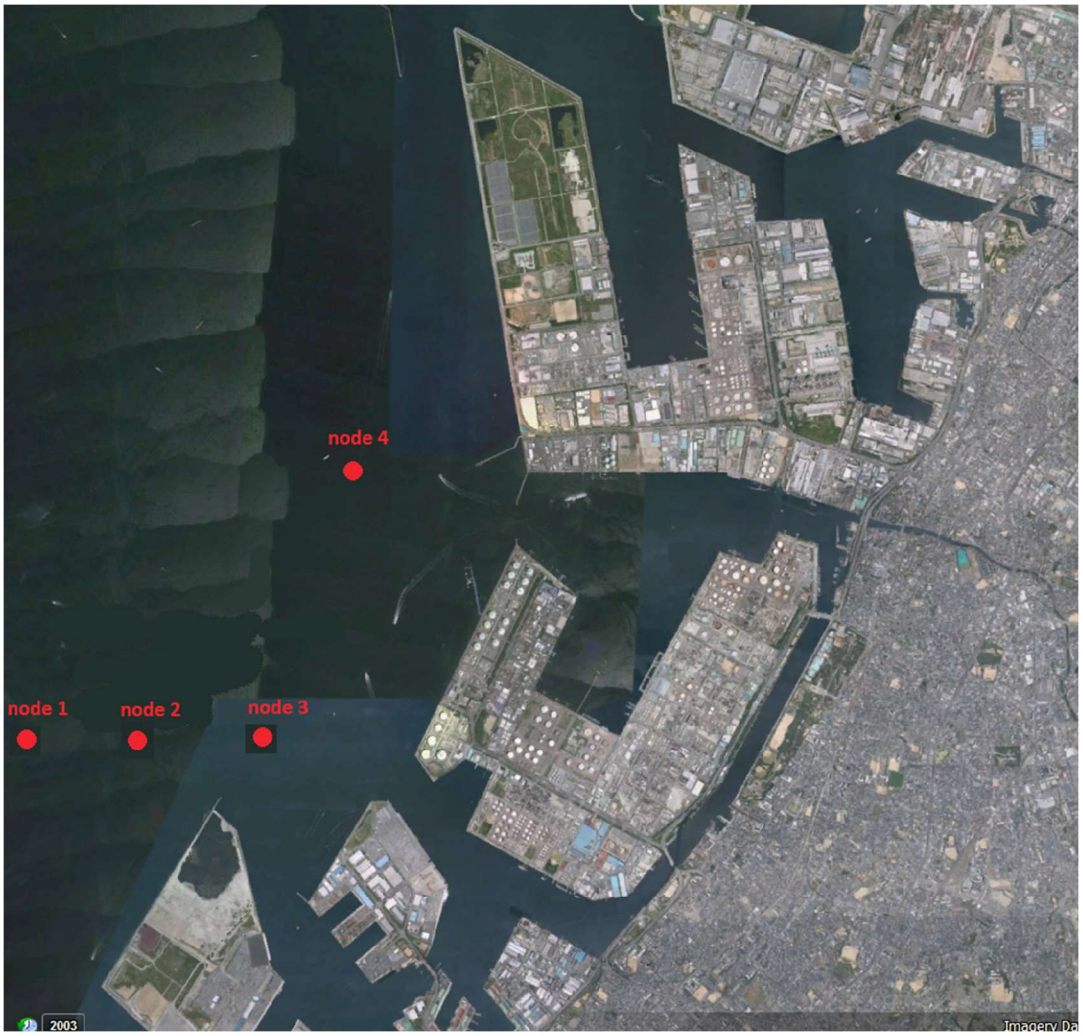

Fig. 4.19 Location of wave data sampling node points near Sakai Senboku area

4.1.13 Visualization

In addition to the wave height and velocity distribution at specific points, it is also effective to see the complete visualization of the tsunami generation and approaching to the shore. However, there is no specific post processing visualization tool for STOC output. Hence, a new Fortran conversion code was developed to change the STOC output into the predefined format of the visualization tool called PARAVIEW, which is usually used with OpenFOAM ®.

4.1.14 Osaka Bay geometry nature

In Osaka Bay, there were two specific oil storage tanks concentrated areas: Osaka North Port and Sakai Senboku Industrial Zones as shown in Fig. 4.20. And, Fig. 4.21 depict the aerial view of the locations of oil storage tanks on Sakai Senboku Industrial Zones. In 2014, Osaka Prefecture Petrochemical Disaster Prevention Cabinet Headquarters (2014) reported the estimated amount of potential oil spill according to tsunami inundation into the industrial parks and oil storage area.

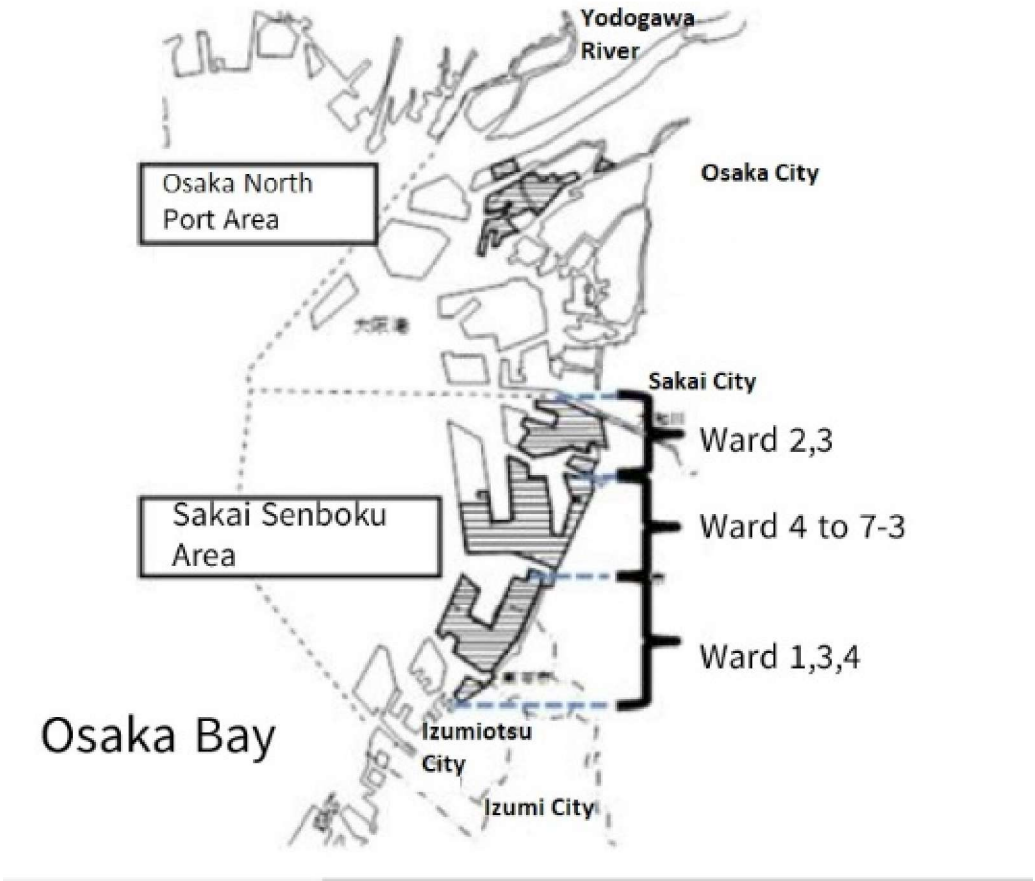

Fig. 4.20 Industrial zones in Osaka Bay and Sakai Senboku Industrial Zones

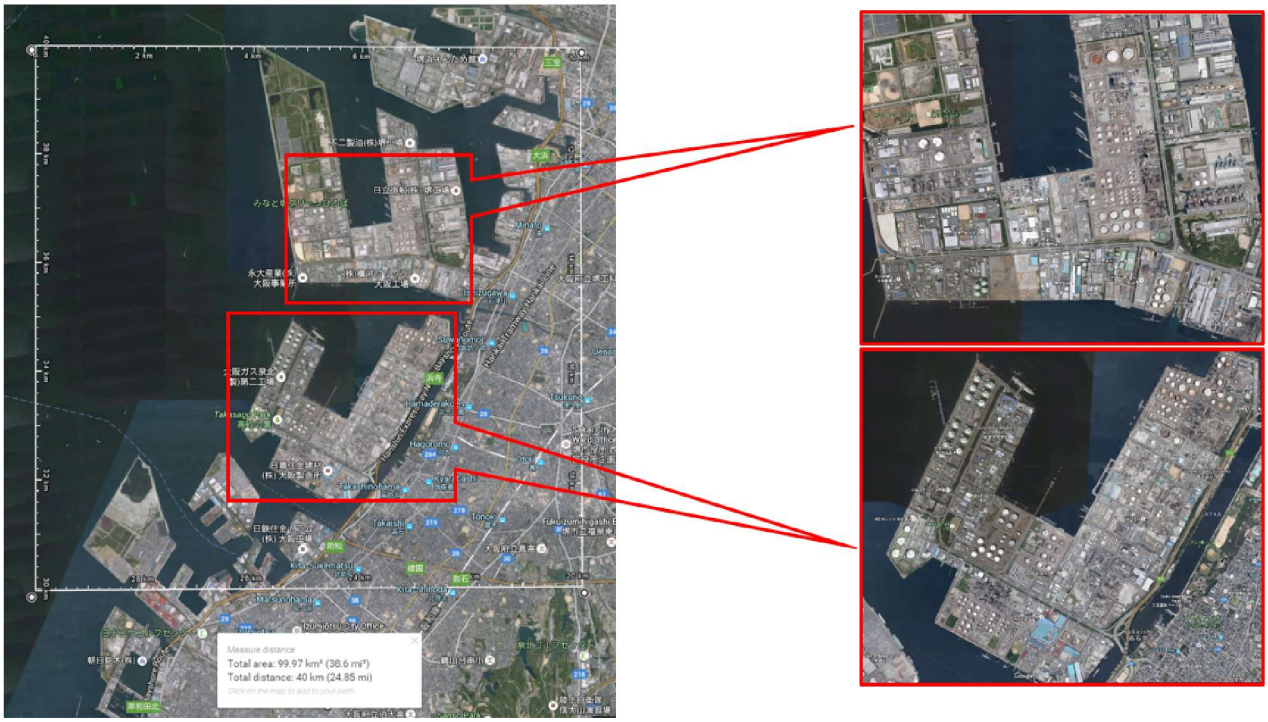

Fig. 4.21 Ariel view of oil storage tanks in Sakai Senboku Industrial Zones

4.1.15 Result of STOC simulation

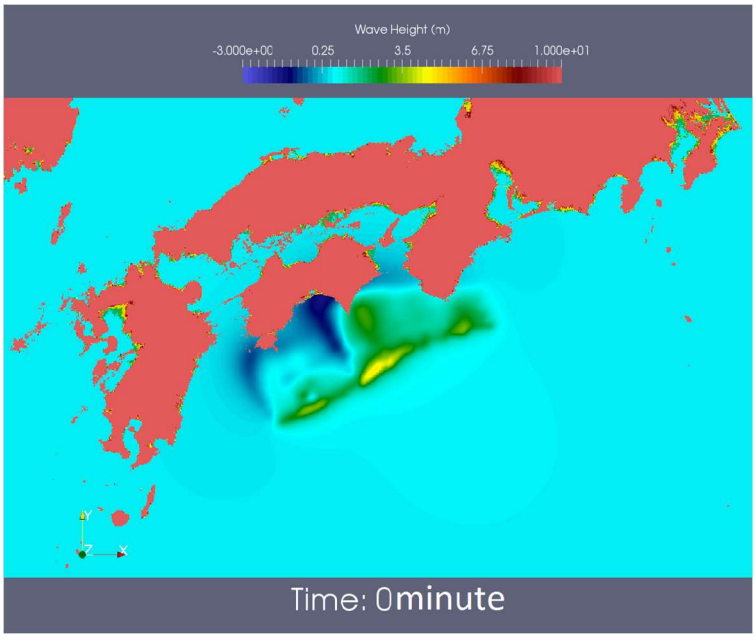

Fig. 4.22 STOC simulation of initial water surface elevation due to Nankai fault movement

Fig. 4.22 shows the initial water surface elevation due to Nankai fault together with the largest domain. The other three domains are embedded inside this domain for fine calculation of wave distribution in Osaka bay area. The maximum wave height contribution in the fourth domain up to 14400s (240 minutes) is as shown in Fig. 4.23.

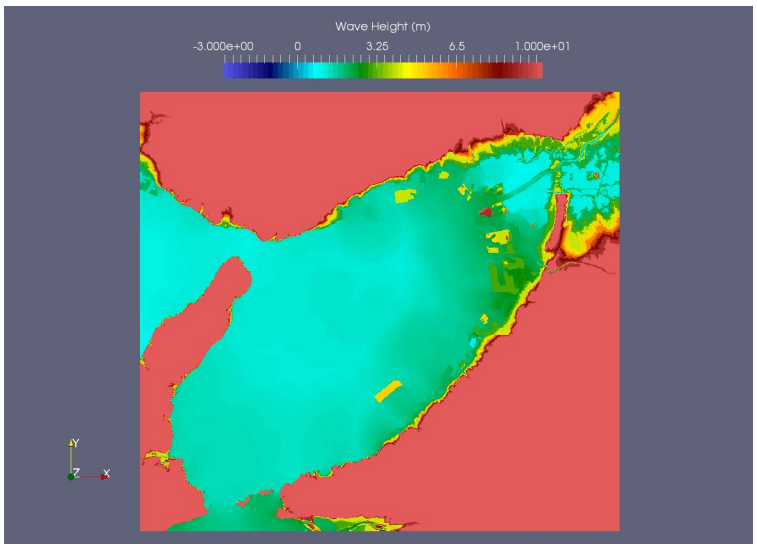

Fig. 4.23 maximum wave height contribution in the fourth domain up to 14400s (240 minutes)

The sample water surface elevation at node 1, node 2 and node 3 (as in Fig. 4.18) with time progression is as shown in Fig. 4.24.

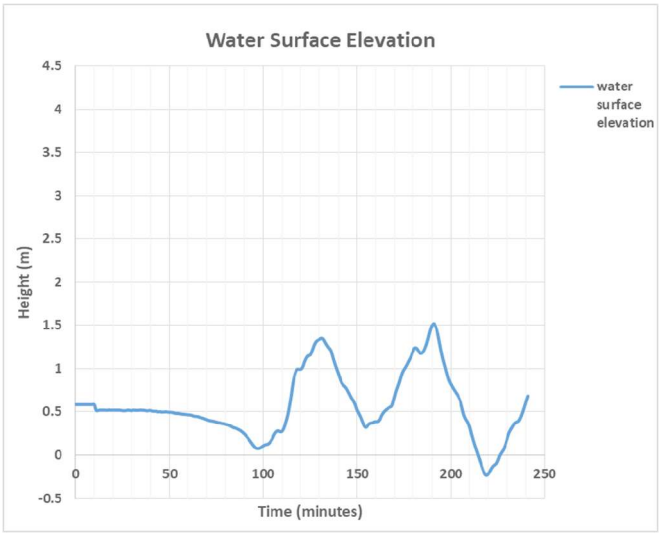

(a)

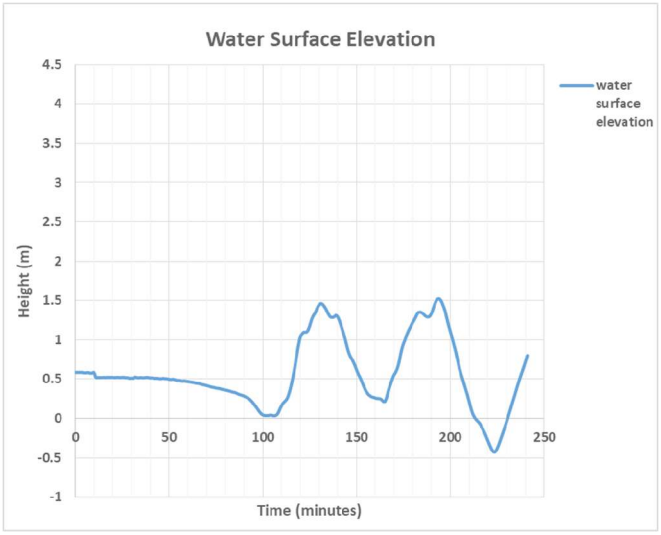

(b)

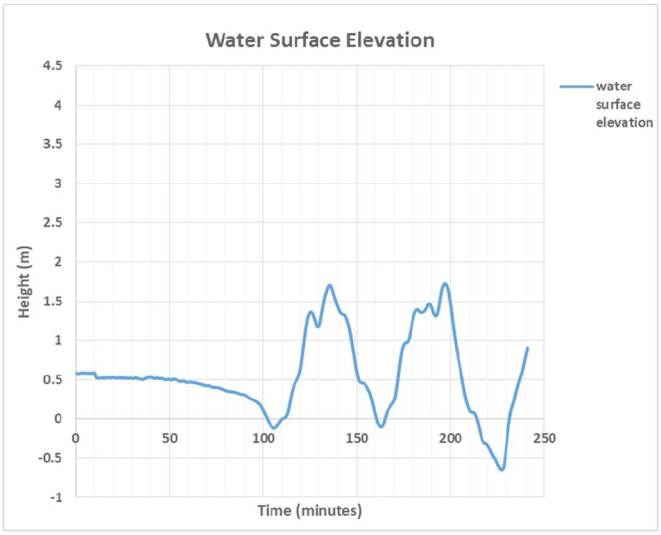

(c)

Fig. 4.24 Water surface elevation at (a) node 1, (b) node 2 and (c) node 3 (as in Fig. 4.18) with time progression

Fig. 4.25 depicts the time progression of tsunami wave after the fault movement. Before the arrival of tsunami wave, a significant drop in sea level is found at 110 minutes according to Fig. 4.26(a). Then, the sea level suddenly rise up.

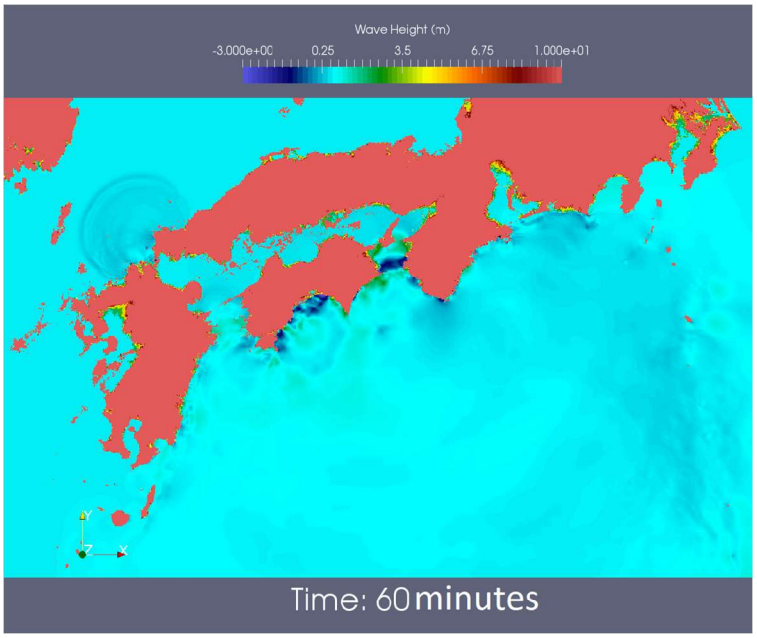
Wave Height (m)
-3.000e+00
0.25
3.5
6.75
1.000e+01
Time: 60 minutes

(a)

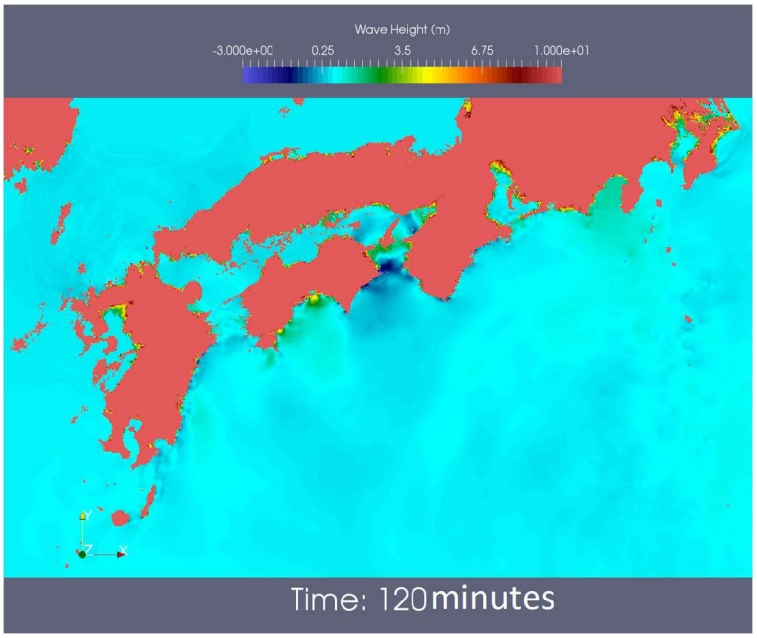
Wave Height (m)
-3.000e+00
0.25
3.5
6.75
1.000e+01
Time: 120 minutes

(b)

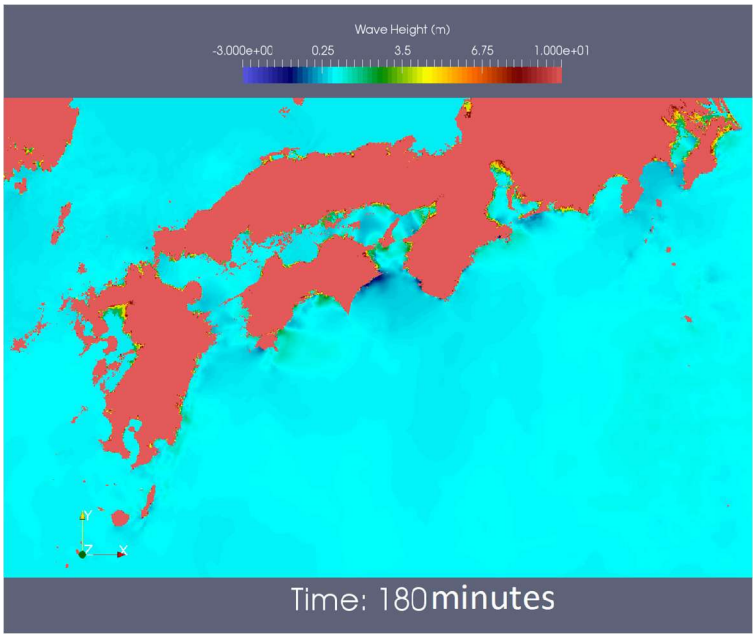

(c)

Fig. 4.25 Time progression of tsunami wave (a) 60 minutes (b) 120 minutes and (c) 180 minutes after the fault movement.

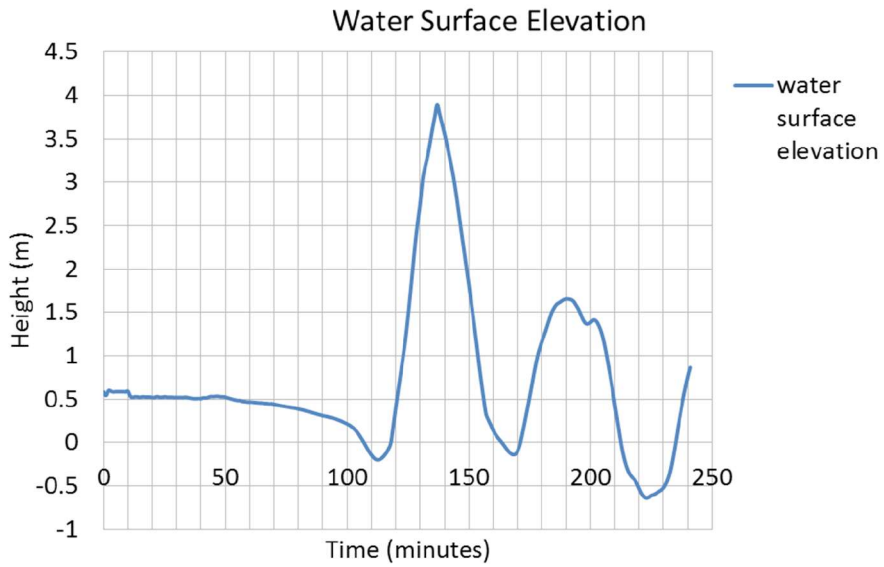

(a)

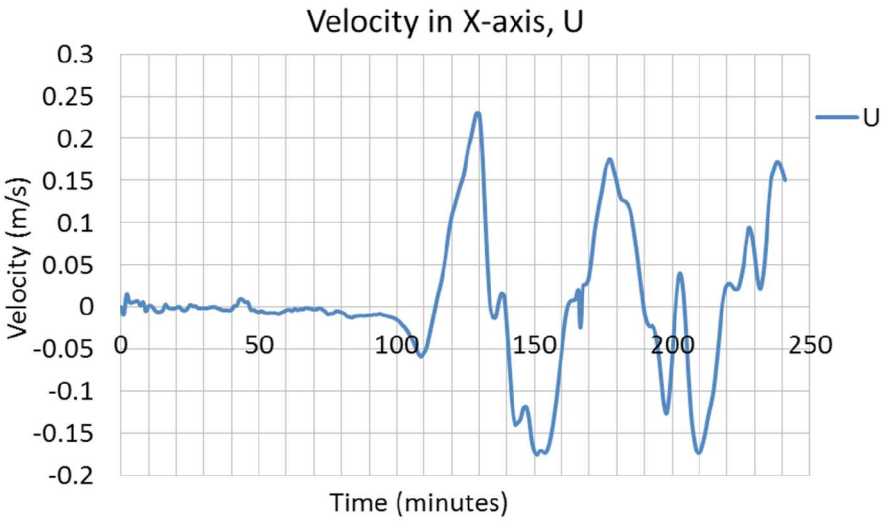

(b)

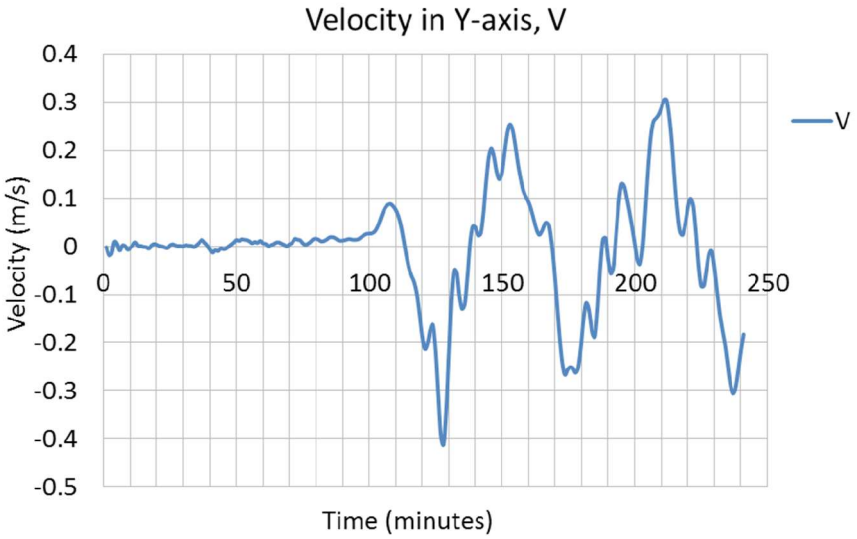

(c)

Fig. 4.26 Calculated results at the node 4 (as in Fig. 4.18) near Sakai Senboku area (a) Water surface elevation, (b) Velocity in X-axis, U, and (c) Velocity in Y-axis,V

The maximum wave height at the node near the Sakai Senboku area occurs at 137 minutes after the fault movement. The sample result of wave height and velocity distribution at node 1, which is 2km from the Sakai Senboku area are shown Fig. 4.26 assuming the standard of tide height of 0.5m.

4.2 STOC-OpenFOAM® coupling simulation

Table 4.3 summarized the Osaka Prefecture Petrochemical Disaster Prevention Cabinet Headquarters' report. The oil tanks are categorized according to their storage capacity. The table shows number of oil storage tanks, total amount of oil and the potential amount of oil spill due to tsunami inundation in respective areas. It was reported that 210 tanks out of total 237 tanks have the potential to be drifted away by inundation in the Osaka North Port area. From these tanks, the possible maximum oil spill is estimated as 27227 kiloliters. Meanwhile in Sakai Senboku area, there are total 818 tanks, and 230 tanks are vulnerable to drifting away by inundation. However, the possible maximum oil spill out in Sakai Senboku area is estimated as 4838 kiloliters.

The oil storage tanks which have potentials to be attacked by tsunami in each area are also analyzed and checked using Google Earth as shown in Fig. 4.27. Each oil tank was analyzed according to its capacity and its location which has tendency to be attacked by tsunami wave to estimate the initial location of potential oil spill for oil spill simulation.

Using the amount of potential oil spill out prediction of the cabinet, numerical simulation is carried out for the distribution of oil spill around Sakai Senboku area in case of the tsunami inundation at the potential Nankai Trough earthquake.

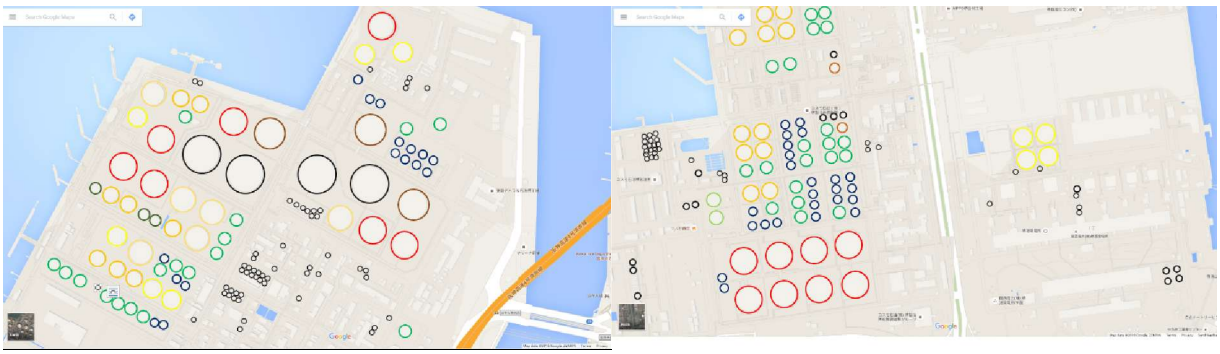

Fig. 4.27 Example of Google Earth analysis for estimating the location of potential oil spill

Table 4.3 Oil storage tanks distribution and potential oil spill amount in Osaka North Port and Sakai Senboku Area

Area	Location	Capacity	Number of tanks	Number of possible drifting tanks	Total capacity	Potential amount of spill
Osaka North Port Area	Total number of oil tanks in Northern Osaka Port Area	More than 10000 kL	0	0	0	0
		1000–10000 kL	31	31	125297	15797
		500–1000 kL	62	52	48849	5169
		100–500 kL	71	63	23159	4454
		Less than 100 kL	73	64	2599	1807
		Total	237	210	199904	27227
Sakai Senboku Area	Wards 2, 3	More than 10000 kL	0	0	0	0
		1000–10000 kL	0	0	0	0
		500–1000 kL	2	0	1795	0
		100–500 kL	0	0	0	0
		Less than 100 kL	19	2	828	23
		Total	21	2	2623	23
	Wards 4 to 7-3	More than 10000 kL	53	0	1782120	0
		1000–10000 kL	55	4	26826	436
		500–1000 kL	39	13	29581	555
		100–500 kL	53	23	15929	472
		Less than 100 kL	84	26	2942	168
		Total	284	66	2099398	1631
	Wards 1, 3, 4	More than 10000 kL	74	0	2538650	0
		1000–10000 kL	122	10	559660	1127
		500–1000 kL	45	15	35130	554
		100–500 kL	116	55	24108	957
		Less than 100 kL	156	82	5463	546
		Total	513	162	3163011	3184
	Total number of oil tanks in Sakai Senboku Area	More than 10000 kL	127	0	4320770	0
		1000–10000 kL	177	14	828486	1563
		500–1000 kL	86	28	66506	1109
		100–500 kL	169	78	40037	1429
		Less than 100 kL	259	110	9233	737
		Total	818	230	5265032	4838

4.2.1 OpenFOAM® for multiphase oil spill simulation

The implementation of the three-dimensional oil spill simulation was achieved by the use of OpenFOAM® CFD package. As validated in chapter 3, the ‘multiphaseEulerFoam’ solver was used. Here, sea water is treated as the continuous phase and oil is treated as the dispersed phase.

4.2.2 Domain creation

The nature of domain required by OpenFOAM® simulation needs a base mesh and geometry of the Osaka Bay. The base mesh is a rectangular domain of 6.05 km by 3.4 km, have a horizontal mesh size of 0.5 m. However, the geometry of Osaka Bay is derived from the data of Publication of Tsunami and Earthquake Analysis Cabinet Office of Japan.

4.2.3 Domain decomposition

The base mesh is vertically divided into three parts. The domain is vertically 60m, with 30m above and below the sea level. 0.5 m mesh is used between 15 m above and below the sea level. The rest is divided using with a mesh of 1m.

During the computation, the whole domain is decomposed into 128 parts for parallel computation.

4.2.4 Mesh production

Firstly, the point data of topology of the Osaka Bay is created as point cloud geometry as shown in Fig. 4.28. Then, using the point cloud data, a surface mesh is created using MeshLab® as shown in Fig. 4.29.

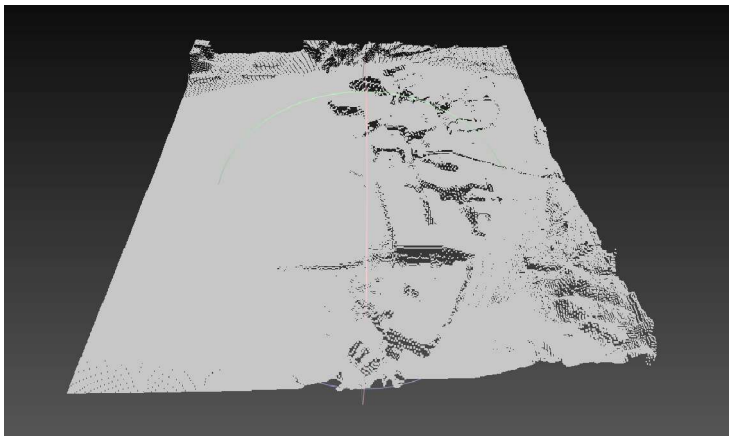

Fig. 4.28 Point cloud data for Sakai Senboku area

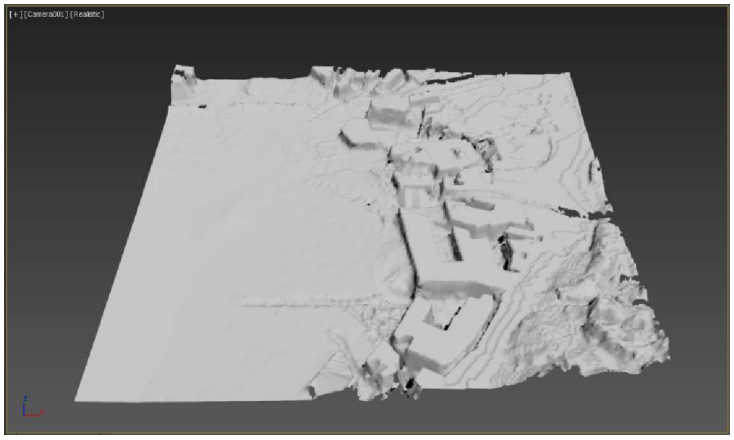

Fig. 4.29 Surface mesh for Sakai Senboku area

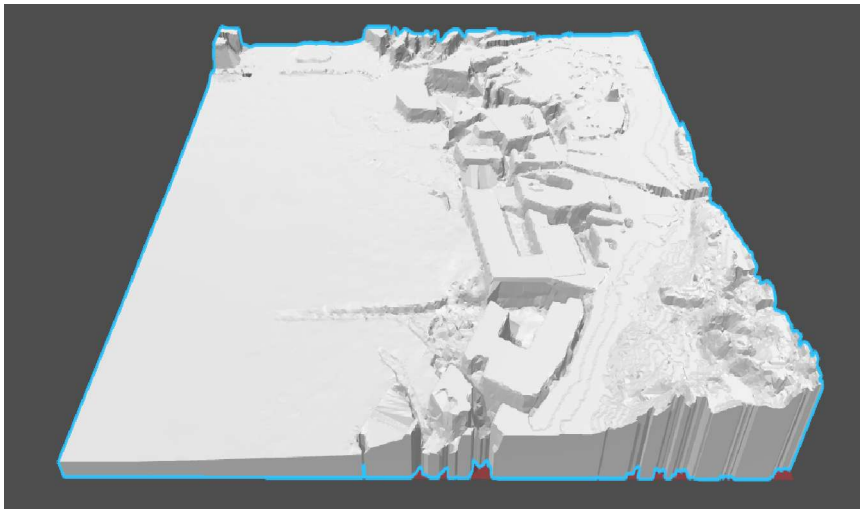

Fig. 4.30 Extruded geometry for Sakai Senboku area

The surface mesh cannot be used directly to extract the mesh domain. Hence, the surface mesh is extruded vertically to make the volume geometry as shown in Fig. 4.30. The extruded geometry can be readily used to create the domain required for the oil spill simulation around Sakai Senboku area.

4.2.5 The initial location and amount of oil

According to Table 1, the potential amount of oil spill on Sakai Senboku area in case of tsunami is 4838kL. The initial amount of oil spill was distributed on with respect to the distribution of tank size on each area according to Google Earth analysis. Hence, the amount of potential oil spill on Ward 4 to 7-3 area, as shown in Fig. 4.20, became 1638kL, while that of Ward 1, 3, 4 area was 3200kL. Initially, the oil was assumed to be concentrated on the refineries plant storage area of Sakai Senboku area.

4.2.6 IHFOAM®

The implementation of wave inside the computational domain was achieved by the use of open-source boundary condition IHFOAM®, developed by the Environmental Hydraulics Institute "IH Cantabria" of Spain as demonstrated (Maza et al., 2015; Higuera et al, 2014a, 2014b, 2013a, 2013b; Iturrioz et al. 2015). IHFOAM® is a 3-dimensional numerical two-phase flow solver specially designed to simulate coastal, offshore and hydraulic engineering processes. Its core is based on OpenFOAM®.

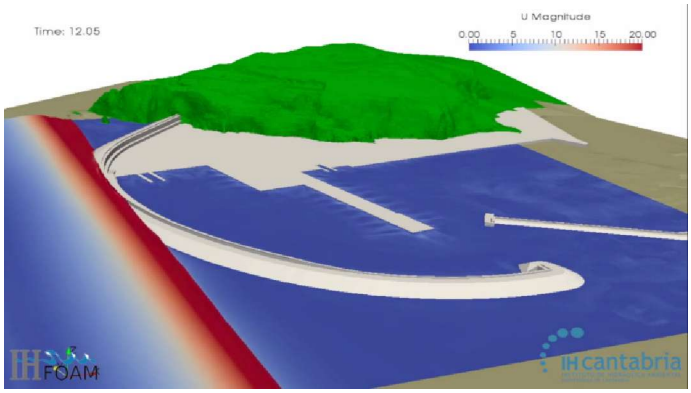

Fig. 4.30 Example IHFOAM tsunami simulation

4.2.7 Solitary wave by Boussinesq approximation

Due to the long period nature of tsunami wave, it is numerically very expensive to simulate the whole wave train, which usually last several minutes up to hours. The solutions is the solitary wave, which is not an oscillatory wave, but a translational wave. What that means is that all the particles of the wave move in the direction of propagation, because its shape is always over the still water level, without evident wave troughs.

There are a number of solitary wave theories. Some of them are reviewed in Lee et al. (1982), from which the expressions for velocities and free surface can been taken. Boussinesq theory is the chosen one, but any of them would be easily implemented and added.

The free surface expression is as follows:

$$\eta = H \sec h^2\left[\sqrt{\frac{3H}{4h^3}}X\right], \tag{4.7}$$

in which $X = (x - ct)$, and the wave speed c is $\sqrt{g(h+H)}$

The velocity components are straightforward, although they involve derivatives in η. They are presented in equations 4.8 and 4.9.

$$\frac{u}{\sqrt{gh}} = \frac{\eta}{h}\left[1 - \frac{1}{4}\frac{\eta}{h} + \frac{h}{3}\frac{h}{\eta}\left(1 - \frac{3}{2}\frac{z^2}{h^2}\right)\frac{d^2h}{dX^2}\right], \tag{4.8}$$

$$\frac{w}{\sqrt{gh}} = \frac{-z}{h}\left[\left(1 - \frac{1}{2}\frac{\eta}{h}\right)\frac{d\eta}{dX} - \frac{1}{3}\eta^2 + \frac{1}{3}h^2\left(1 - \frac{1}{2}\frac{z^2}{h^2}\right)\frac{d^3h}{dX^3}\right] \tag{4.9}$$

Using the presented equations and assuming the boundary to be at $x = 0$, the free surface will start at the highest point of the solitary wave. In order to generate the full wave, an artificial lag in space has to be added. There is an obvious problem with this, as a solitary wave theoretical wave length is infinite. This lag in space is directly translated in a lag in time, therefore there is a need to keep it as low as possible to reduce the simulation (and computational) time. Nevertheless, the free surface decreases rapidly and an effective wave length can easily be defined. The usual criterion to calculate it is to set a percentage of the maximum wave height in which the simulation will start. For example, if 1% is fine, the lag will be $l = \frac{3.5}{\sqrt{\frac{H}{h}}}$. Sometimes 5% is preferred, in this case the lag will be $l = \frac{2.5}{\sqrt{\frac{H}{h}}}$. Here the 1% criterion is used because the other one would involve half a cell of error in the case in which wave height is discretized using 10 cells.

4.2.8 The result of OpenFOAM® simulation

Fig 4.31(a) reveals that the maximum wave at the point 2km near Sakai Senboku area occurred at 137 minutes after the Nankai fault movement. Hence, these wave data were taken and set as boundary conditions for the OpenFOAM® simulation.

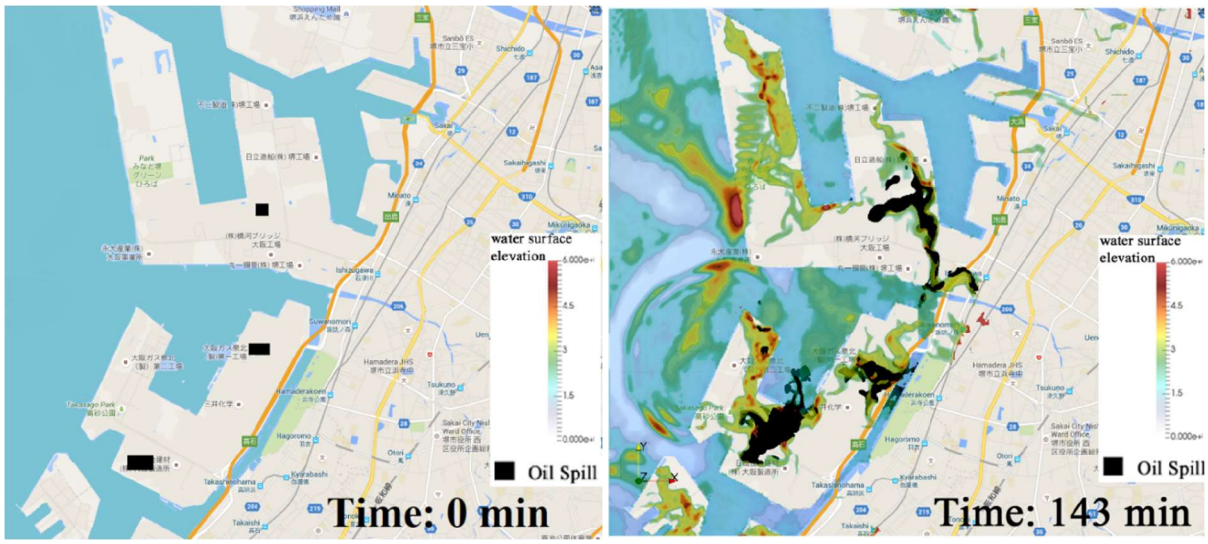

(a) (b)

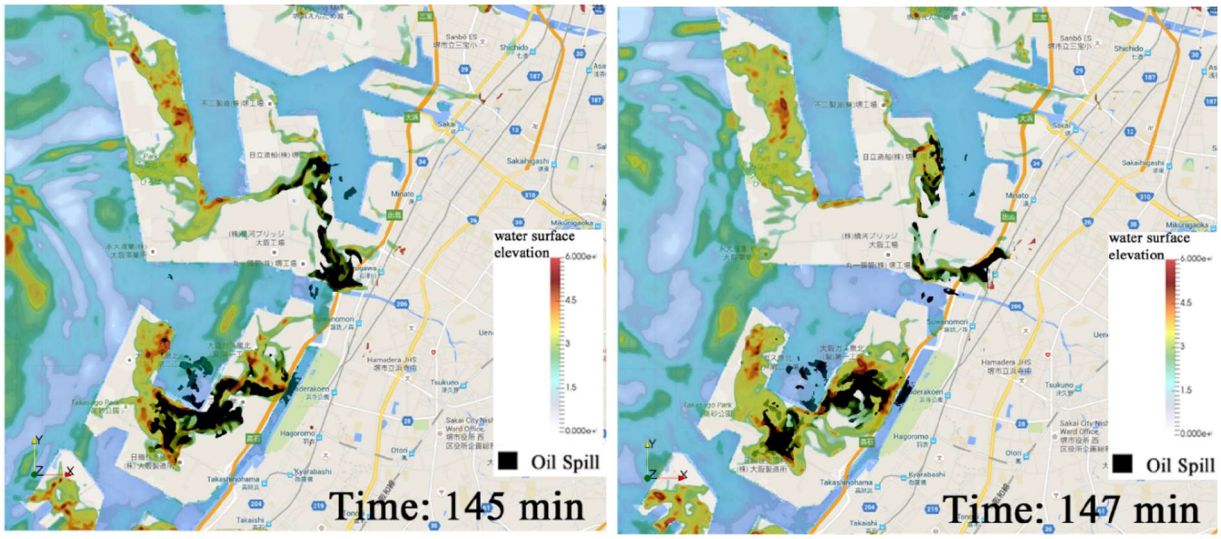

(c) (d)

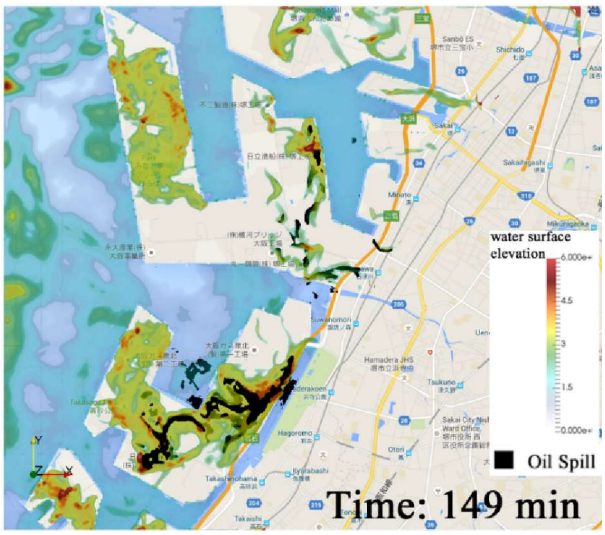

(e)

Fig. 4.31 Oil spill pattern around Sakai Senboku area at (a) 0 minute (initial oil position) (b) 143 minutes (c) 145 minutes (d) 147 minutes (e) 149 minutes after the Nankai fault movement

Fig. 4.31 shows the precise wave and oil spill distribution on and near the Sakai Senboku area at 143 minutes, 145minutes, 147 minutes and 149minutes after the Nankai fault movement. The range of water surface elevation is shown in color pattern, while the black color represents the oil spill. Fortunately, major oil refinery plants on Sakai Senboku area are not situated on the area directly opened to the sea, hence there is less chance for the oil storage tanks to face the direct

impact by the tsunami. Nevertheless, these oil storage tanks still suffer the effect the tsunami inundation. At time 143 minutes, the main wave hit the sea front region of Sakai Senboku area and some part of the wave reflects back into the sea. However, there is still tsunami inundation to the oil storage tanks. Later, the inundation mixes with oil and washes some of the oil into the sea. The inundation height decreases and covers much wider over the Sakai Senboku area with time, while the visible amount of oil spill on the surface decreases showing that the oil spill intrusion vertically into the water column.

Fig. 4.33 illustrates the oil spill distribution after 149 minutes after the Nankai fault movement and it reveals that spilled oil spreads into the residential area near the Sakai Senboku area and penetrates into the sea. Fig. 4.34 shows the variations of the percentages of oil concentration along the water columns at four points in Sakai Senboku area at time 149 minutes after the Nankai fault movement.

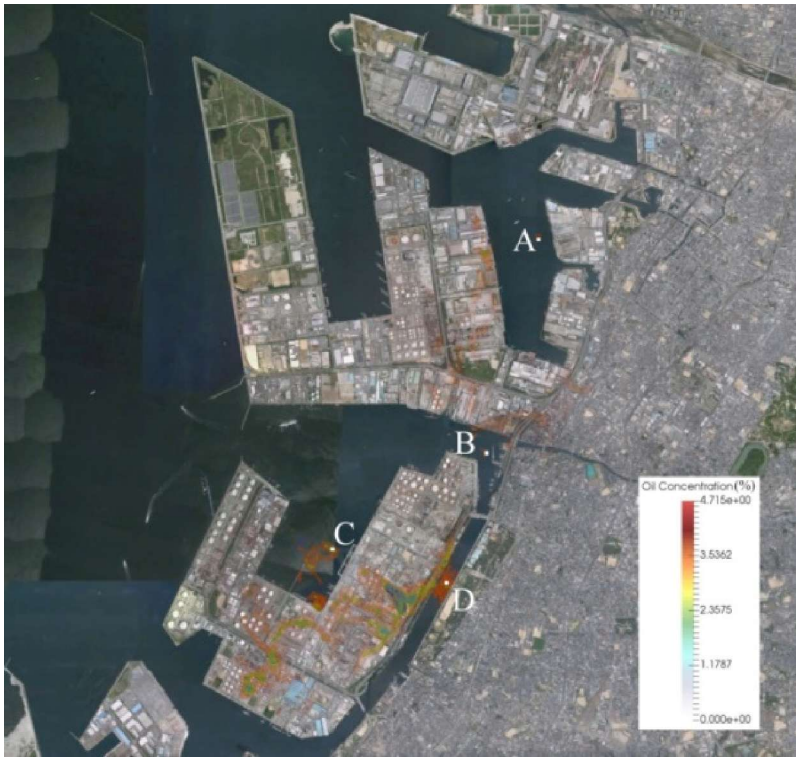

Fig. 4.33 Oil spill pattern predicted around Sakai Senboku area at 149minutes after Nankai fault movement

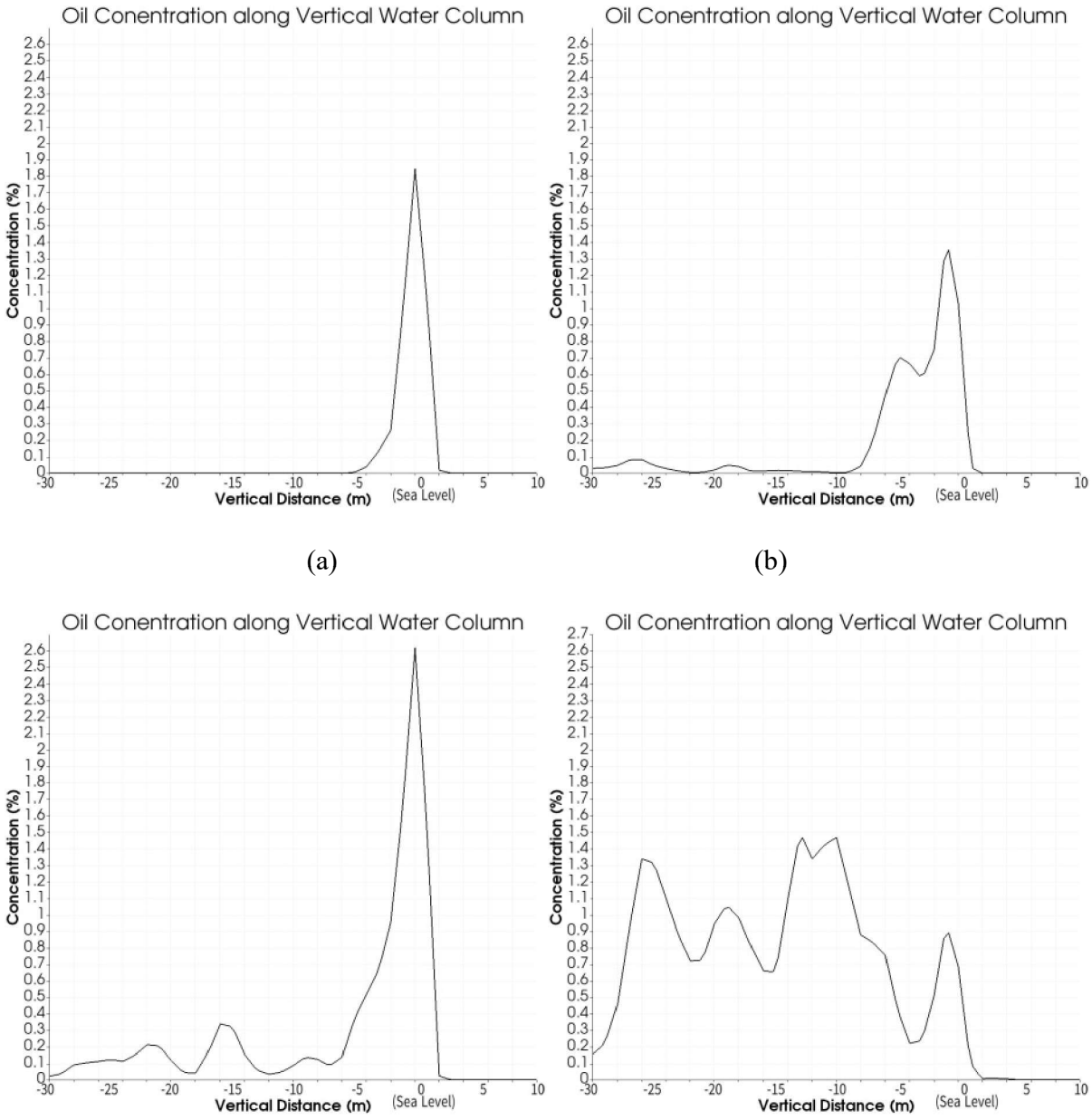

Fig. 4.34 Variations of the percentages of oil concentration along the water columns; (a) at point A, (b) at point B, (c) at point C, (d) at point D

Fig. 4.34(c) shows the highest possible contamination of oil spill with a concentration of oil 2.6%. Generally, most oil spill is believed to float on the surface, hence the oil spill concentration decreases with increase in depth. However, there is an exception case of abnormal oil spill concentration distribution along the water column at point D (in Fig. 4.34 (d)), where the

oil concentration around 14meter depth is higher than the sea level. This may be attributed to the narrow channel at point D. The area around point D has a high risk of underwater oil contamination as the case of Kessenuma Bay.

4.3 STOC-OIL simulation

STOC-OIL program uses the output velocity distribution of STOC to calculate the oil drifting on the sea surface. The calculation of the movement of oil, OIL program, was also developed by PARI to work in connection with both STOC-ML and STOC-IC without affecting their basic functions. The nesting domain coupling method allowed two or more of these different programs at the same time; the coupling of OIL with STOC-ML, the coupling of OIL with STOC-IC, and the coupling of OIL with both STOC-ML and STOC-IC. In this research, STOC-ML is used to couple with OIL to save the numerical simulation time for long-term prediction.

4.3.1 Fundamental Equations of STOC-OIL

In STOC-OIL, the movement of the oil is modelled by using Lagragian approach which considers oil as discrete particles. The relation of position of each particle x_i and the velocity of each particle $\boldsymbol{U}_i$ is described by the equation.

$$\frac{d\boldsymbol{x}_i}{dt} = \boldsymbol{U}_i, \tag{4.10}$$

and time integration was done by Euler explicit method.

$$\boldsymbol{x}_i^{n+1} = \boldsymbol{x}_i^{n+1} + \boldsymbol{U}_i \Delta t, \tag{4.11}$$

STOC-OIL is only 2-dimension calculation, hence the velocity $\boldsymbol{U}_i$ is considered only on the sea surface. In the calculation of $\boldsymbol{U}_i$, the effect of wind velocity $\boldsymbol{W}$ and ocean current velocity $\boldsymbol{U}_0$, are added into the equation as follow.

$$\boldsymbol{U}_i = C_{w0}\left(C_{W1}(n)\begin{bmatrix}\cos\theta & -\sin\theta \\ \sin\theta & \cos\theta\end{bmatrix} + C_{W2}\right)\boldsymbol{W} + C_{c0}(C_{c1}+C_{c2})\boldsymbol{U}_c + C_{s0}(C_{s1}+C_{s2})\boldsymbol{U} \tag{4.12}$$

All the values of the coefficient C s are calculated generically according to predefined formulae. There are two ways of STOC-OIL calculation: online STOC-OIL calculation and offline STOC-OIL calculation. In online STOC-OIL calculation, $\boldsymbol{U}_c$ in STOC and $\boldsymbol{U}_i$ in STOC-OIL were calculated by MPI simultaneously. However, in offline STOC-OIL calculation, $\boldsymbol{U}_c$ was firstly

calculated by STOC, then calculation of $\boldsymbol{U}_i$ by STOC-OIL was coupled by reading the velocity file from STOC at the specific time step.

In either method, STOC calculates the surface velocity at the node of the mesh. Adjusting the surface velocity values at the particle positions in STOC-OIL was achieved by using the linear interpolation of the respective velocity values on staggered coordinate of STOC.

Similar to the simulation of the STOC, the result output of STOC-OIL simulation cannot be directly visualized with specific post processing tool. Therefore, a new conversion FORTRAN code is created to make the output file into the specific format of PARAVIEW visualization tool.

In the STOC-OIL calculation, the offline STOC-OIL simulation was conducted with 5000 oil particles; each occupies a volume of 0.963 kiloliters. Using the potential oil spill amount predicted by the Headquarters' report and specific location previously analyzed by Google Earth, the oil particles are initially distributed on the Sakai Senboku area.

4.3.2 The result of STOC-OIL simulation

Offline STOC-OIL simulation was also coupled with STOC wave data at 137 minutes after the fault movement. Similar to OpenFOAM® simulation, all four domains were dealt with STOC-ML to couple with 2-dimensional STOC-OIL simulation. However, unlike 3-dimensional OpenFOAM® simulation, this relatively faster STOC-OIL simulation estimated the distribution of oil spill up to 230 minutes after the Nankai fault movement.

Fig. 4.35 shows the oil spill distribution pattern around Sakai Senboku area by STOC-OIL simulation at every 10 minutes, between 150 minutes and 230 minutes, after the Nankai fault movement. The distribution of oil spill at 150 minutes of STOC-OIL had a slightly different distribution of oil spill at 149 minutes of OpenFOAM® simulation as shown in Fig. 4.30, though these two figures can be considered as the oil spill distribution at the same time. This is because STOC-OIL overestimates the oil spill on the sea surface, and there is no vertical instrusion of oil into water column. Although STOC-OIL simulation is not as precise as OpenFOAM® simulation, it is still one of the useful methods to estimate the oil spill distribution roughly. The oil spill pattern at 150minutes shows that oil spill is only at the beginning state, and still on and near the Sakai Senboku area. However, the oil spill dispersion increases with time and finally reaches far inland to the residential area and off into the bay after 230minutes (2hours 50minutes). This proves that

the oil spill can reach residential areas and disturb the ship navigation routes nearly at 3 hours after the Nankai fault movement.

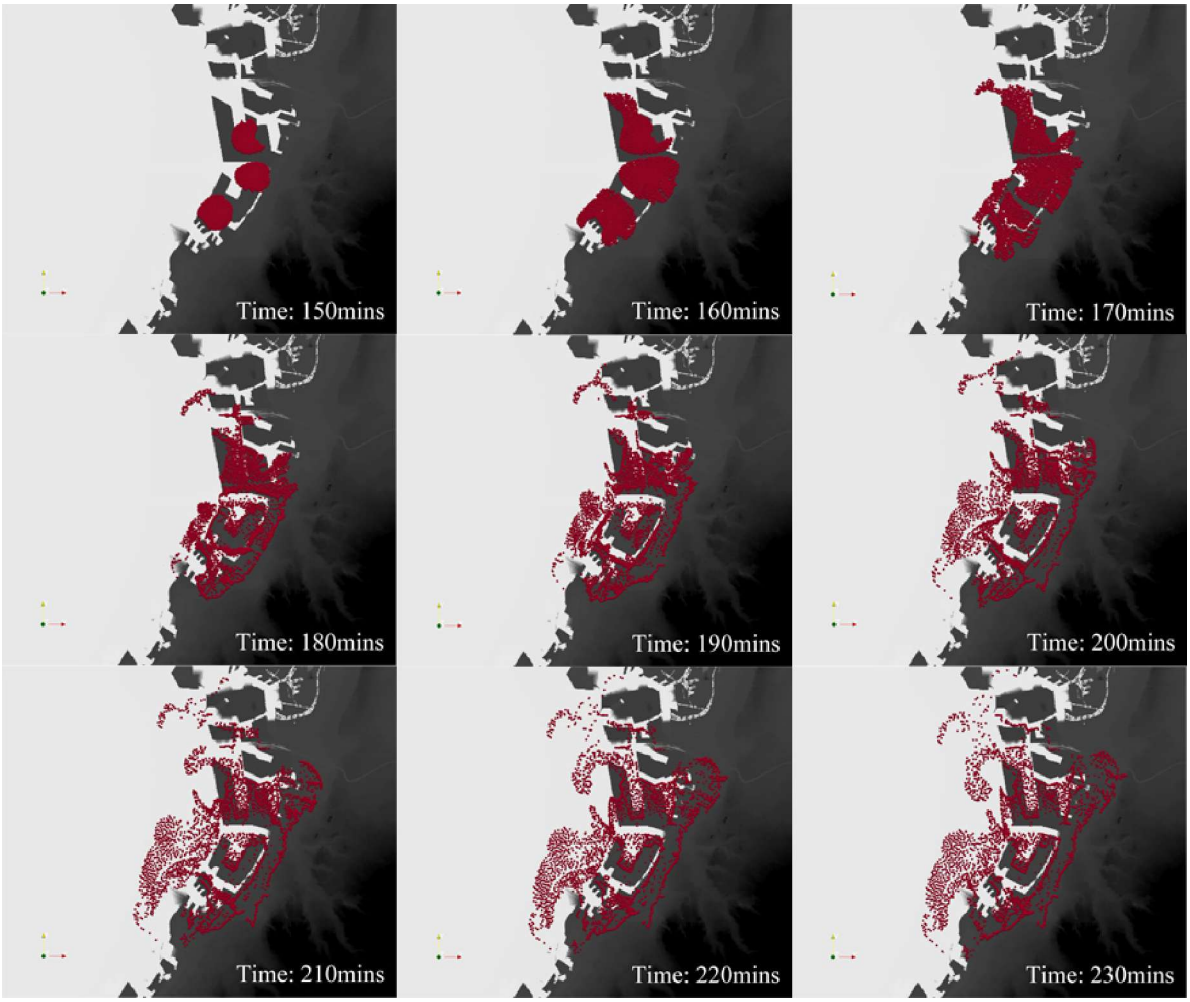

Fig. 4.35 Oil spill pattern around Sakai Senboku area with time (a) 143 minutes (b) 145 minutes (c) 147 minutes (d) 149 minutes after the Nankai fault movement

CHAPTER 5

ANALYSIS OF THE TENDENCY OF TANK DRIFTING IN TSUNAMI WAVE

In both 2011 Great East Japan Earthquake and 2004 Indian Ocean tsunami caused by the Sumatra earthquake, oil storage tanks in port and industrial complexes were drifted and damaged by tsunami inundation. Although there was no tsunami-triggered oil spill case reported after the Indian Ocean tsunami, there was major oil spills from the damaged oil storage tanks in the case of Japan.

As mentioned in chapter 3, 22 out of 23 oil storage tanks were broken and drifted in Kesennuma bay as shown in Fig. 5.1(a) and Fig. 5.1(b). 11523 m^3 of oil, mainly heavy oil as well as gasoline and light oil, was released through the way in 2011 Great East Japan Earthquake. Storage tanks from an oil tank farm in Banda Acech city were also displaced a considerable distance from their base 2004 Indian Ocean tsunami as seen in Fig. 5.1(c) (Reconnaissance Team of JSCE, 2005).

As introduced in Chapter 3, it can generally be concluded that the tendency of tank drifting by the tsunami is inversely proportional to its capacity and size. Based on the investigation carried out by the Japan Association of Fire Science and Engineering (Hokugo, 2013), there are three main tsunami-induced fire breakout patterns. One of the patterns is tsunami-induced fire related to leak from oil storage tanks, which is the case found in Kesennuma Bay. Kesennuma city suffered from fire during the disaster due to tsunami triggered oil spill. Tsunami-induced fire is generally expanded due to the presence of petroleum facilities and storage tanks which have a potential of discharging combustible gases and liquids.

(a)

(b)

(c)

Fig. 5.1 (a) Oil spill in dike due to failure in pipes in the Great East Japan earthquake (National Research Institute of Fire and Disaster, FDMA) and (b) Displaced oil tanks in Banda Aceh city due to the Indian Ocean tsunami (Reconnaissance Team of JSCE, 2005)

5.1 **Countermeasures For The Disaster After Tsunami -Triggered Oil Spill And Fire**

The potential risk of damage to oil storage tanks in coastal industrial zones by tsunami waves was known of and analyzed before the Great East Japan Earthquake, however, virtually no

countermeasures were taken. After the 2011 Great East Japan Earthquake, the FDMA carried out investigation and had published that the pipes and other oil conveying facilities between the tanks start to burst out if the height of the tsunami inundation is between 2.5 to 5m, and the main body of tank suffers damage if the tsunami is above 5m. Based on the result of investigation, the tendency of tank movement was checked considering the effect of intrusion of tsunami water into the gap between the tank bottom plate and foundation, and the effect of anchor bolts. Damage to storage tanks is also analyzed by smoothed particle hydrodynamics methods and structural assessment methods for cylindrical storage tanks were proposed (Ibata et al., 2013). Since the tsunami-induced fire in Kesennuma Bay revealed the increment in the disaster risks in the coastal industrial zones with oil storage tanks, 33 prefectures in Japan, where petrochemical complexes exist, were called to review their disaster prevention plans.

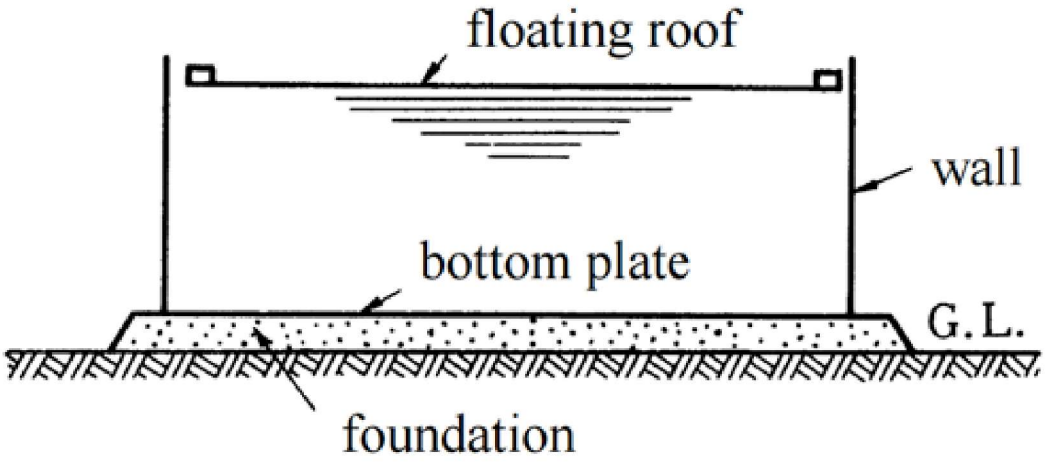

Fig. 5.2 Typical Oil Storage Tank Configuration

5.2 **Objectives**

This analysis has the objectives to review the applicability of the guidelines of FDMA for safety criteria and oil storage tank drifting and lifting, and to revise the guidelines of FDMA and propose its modification. This study mainly focus on the oil storage tank located in the industrial parks in the Osaka Bay area. By aiming at predicting the possibility of drifting of these oil storage tanks in case of tsunami attack, accurate estimation of the oil spill distribution in Osaka Bay and nearby coastal line in case of tsunami attack can be performed. For these objectives, this study

carried out experiments of behaviors of drifting of oil tank models in incoming tsunami wave in experimental tsunami tank, and numerical simulations of drifting of oil tank models.

Fig. 5.3 and Fig. 5.4 shows the distribution of oil storage tanks in Osaka North Port and Sakai Senboku area. According to the report, 210 tanks out of 237 tanks could be drifted and damaged by tsunami inundation in Osaka North Port area, and 230 tanks out of 818 tanks, in Sakai Senboku area. The total amount of potential oil spill in Osaka North Port was estimated to be 27227m^3, while the amount was estimated to be 4838m^3 in Sakai Senboku area where major oil refineries are operating. Although there are oil refineries which consist of more than 10000m^3capacity oil storage tanks in Sakai Senboku area, the amount of potential oil spill in Osaka North Port is larger due to the small and vulnerable oil storage tanks used in the logistic services. In addition, there are also gas and chemical storage tanks, which can release combustibles to the nearest residential area to start fire in case of tsunami attack.

Fig. 5.3 Distribution of oil storage tanks in Osaka North Port area

Fig. 5.4 Distribution of oil storage tanks in Sakai Senboku area

However, this estimation is based on theoretical safety criteria of the tank drifting and tank lifting by FDMA. Moreover, to get precise prediction of the oil spill distribution in case of tsunami, it is necessary to know the specific locations of initial oil spill, which was not reported in the publication of Headquarters. Hence, to get the specific location of the oil storage tanks in each industrial zones, the areas, prone to be attacked by tsunami, are analyzed and the oil storage tanks are counted according to their size by using Google Earth.

5.3 **Guidelines Of Fire And Disaster Management Agency (F DMA)**

FDMA considers six possible damage patterns of oil storage tank during tsunami attack as shown in Fig. 5.5.

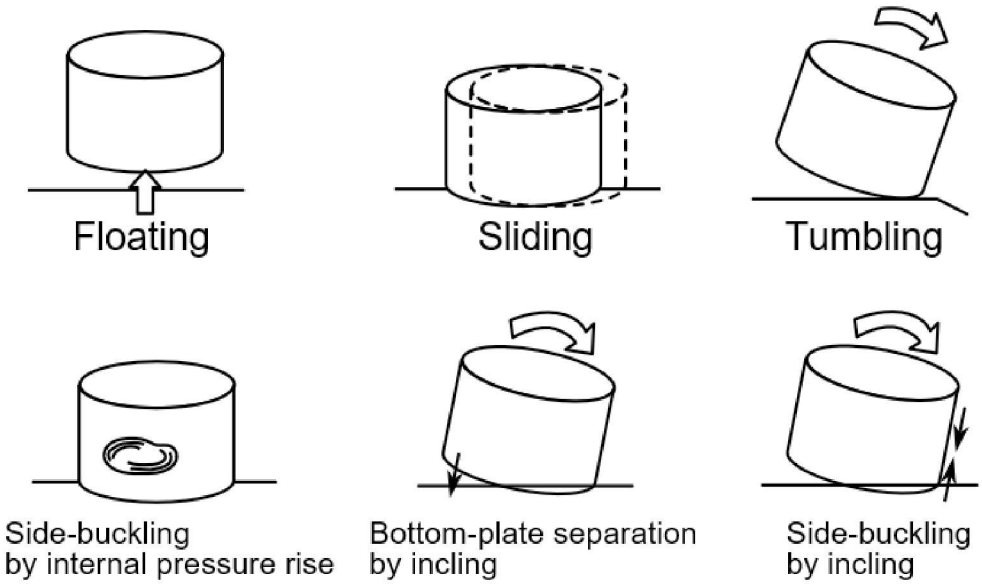

Fig. 5.5 Possible damage pattern of oil storage tank during tsunami attack (FDMA)

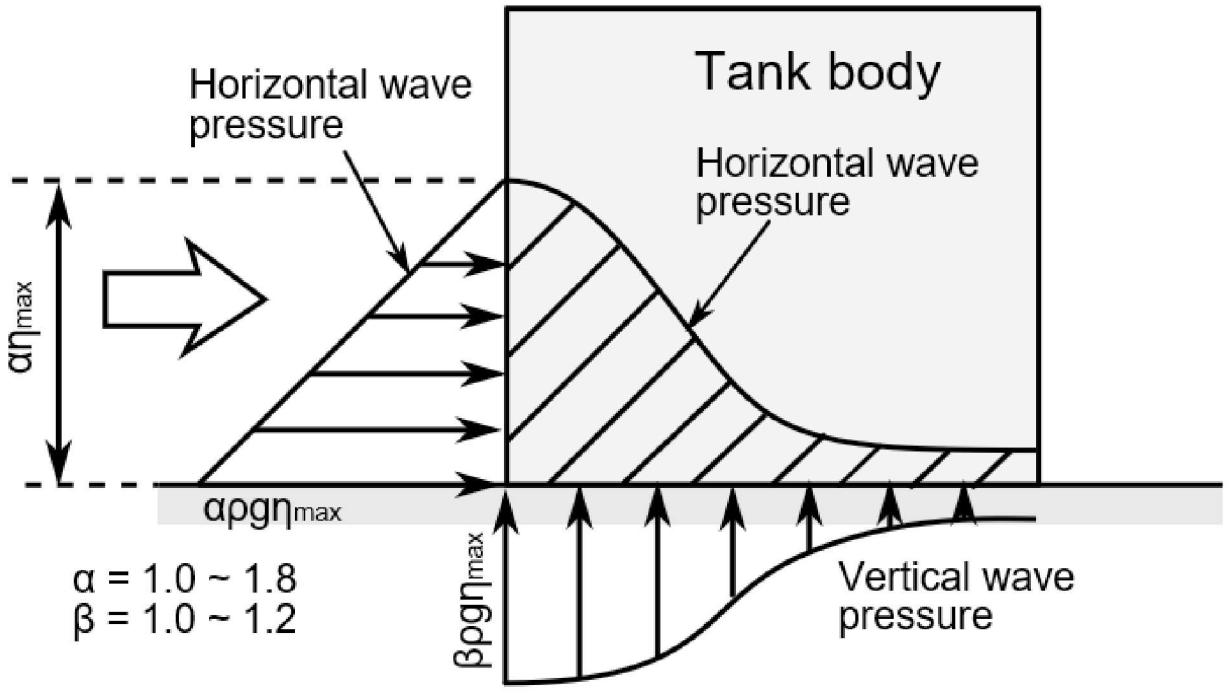

Fig. 5.6 Wave pressure distribution on tank by FDMA (FDMA)

A simple theoretical wave profile is assumed as shown in Fig. 5.6. Then, the incoming wave pressure forces on the tank are calculated by equations (5.1) and (5.2).

$$F_{tH} = \frac{1}{2}\int_{-\pi}^{\pi} \rho g \left[\alpha \eta_{\max} \sum_{m=0}^{3} p_m \cos(m\theta)\right]^2 R\cos\theta d\theta, \quad (5.1)$$

$$(p_0 = 0.680,\ p_1 = 0.340,\ p_2 = 0.015,\ p_3 = -0.035)$$

$$F_{tV} = 2\int_{0}^{\pi} \rho g \left[\beta \eta_{\max} \sum_{m=0}^{3} q_m \cos(m\theta)\right] R^2 \sin^2\theta d\theta, \quad (5.2)$$

$$(q_0 = 0.720,\ q_1 = 0.308,\ q_2 = 0.014,\ q_3 = -0.042)$$

where F_{tH} = horizontal hydrodynamic force on the tank

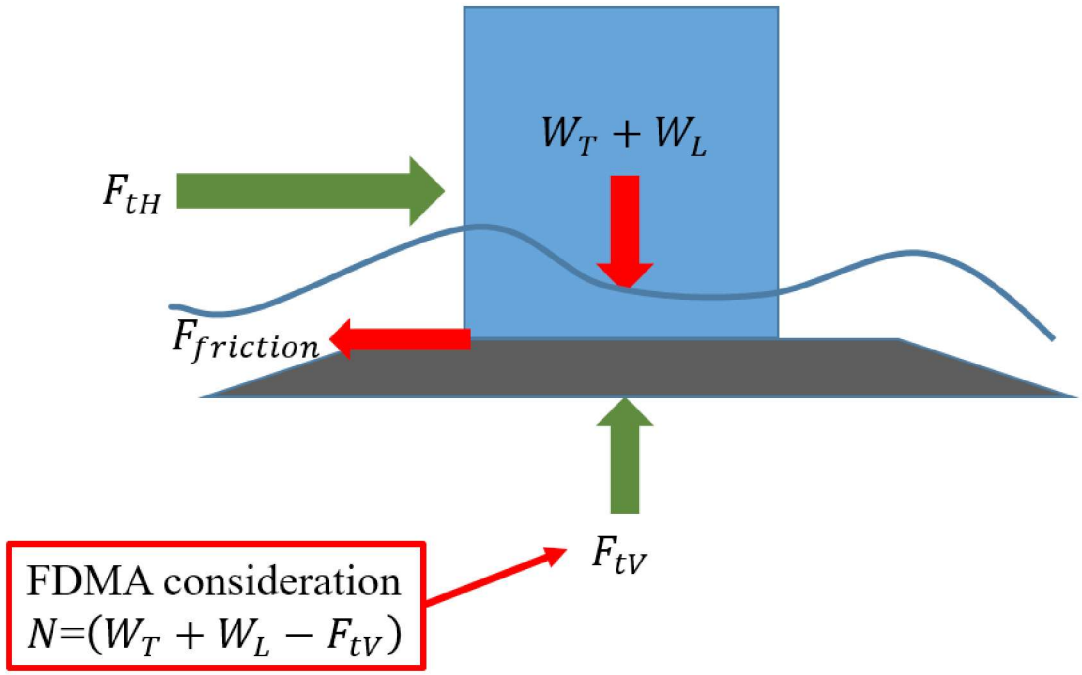

Fig. 5.7 Forces on the oil storage tank according to the assumption of FDMA guidelines

Typical forces on oil storage tank according to FDMA is depicted in Fig. 5.7. Among the possible damage patterns of oil storage tank, for drifting of the tank in tsunami wave, the FDMA safety factor is defined as

$$F_{Sb} = \frac{\mu(W_T + W_L - F_{tV})}{F_{tH}}, \tag{5.3}$$

if $F_{Sb} \leq 1.0$: the tank will drift with the wave,

if $F_{Sb} > 1.0$: the tank will remain stable,

where μ = mechanical friction between the tank bottom plate and tank base

W_T = weight of the storage tank

W_L = weight of the internal fluid

5.4 **Experiments**

In this analysis, the oil storage tanks are divided in five categories in the same way as the report of Headquarters. The category of oil storage tank with less than 100m^3 is considered to be certainly drifted and damaged due to the relatively small size and light inner liquid. On the other hand, the category of oil storage tank with more than 10000m^3 is assumed to be able to withstand the tsunami run up due to their relatively larger structure and heavier inner liquid than other categories. The remaining three categories of oil storage tank are chosen to conduct specific analysis to check their potential to be drifted along with tsunami inundation. Table 5.1 shows the representative tanks and their model dimension for each category that will be used in the experiments. The representative tanks are scaled down with 1:100 ratio to conduct experiments.

Table 5.1 Dimensions of representative tanks and their model tanks for analysis

	Representative tank			Model tank		
Capacity	Diameter (m)	Height (m)	Volume (kL)	Diameter (m)	Height (m)	Volume (L)
100~500kL	7.5	7.5	331.340	0.075	0.075	0.331
500~1000kL	10	10	785.398	0.1	0.1	0.785
1000~10000kL	16.5	16.5	3528.107	0.165	0.165	3.528

In chapter 4, simulation of tsunami due to the movement of Nankai Fault was conducted by using the STOC. The result showed that possible maximum wave height around Sakai Senboku area is estimated to be 3.9 m and that around Osaka North Port area is around 5 m. Hence, the possible maximum height of tsunami on oil storage tanks in Osaka Bay is assumed to be 5 m.

Experiments of tank drifting in incoming tsunami wave were conducted in tsunami wave tank at Osaka University. Since the inflammable petroleum based oil is dangerous and difficult to remove after experiment, the tanks were filled with olive oil, which has nearly the same density as heavy oil, as internal fluid. For each tank, three cases of experiment were carried out by varying the volume rate of internal fluid: 0%, 50% and 100%. First, the hydrodynamic forces of incoming wave on the tanks were measured for each case. Then, the tanks were again allowed to move freely along with the incoming wave for each case. According to the predicted 5 m high tsunami, the wave forces on the tanks needed to be analyzed by the guidelines of FDMA, and checked by experiment. The height of incoming wave before the tank was scaled down to be 5 cm using the same ratio as in modeling the tanks.

Unlike the case of waves hitting on an ordinary floating object, it is necessary in current analysis to consider the effect of mechanical friction in addition to ordinary effects of hydrodynamic pressure and drag. Usually the oil storage tanks are sat on the cement slabs as the tank bases, the phenomena of tank drifting along with the incoming wave is restraint by the effect of mechanical friction between the tank bottom plate and tank base.

Table 5.2 Dimensions of model oil storage tank and respective dike

Model Tank		Model Dike		
Diameter (m)	Height (m)	Height (m)	Length (m)	Breadth (m)
0.075	0.075	0.01	0.19	0.19
0.1	0.1	0.01	0.29	0.29
0.165	0.165	0.02	0.44	0.44

Also the oil storage tanks are usually surrounded by dike, the effect of these dikes are also considered in the experiment. The square shaped dikes for each tank were designed according to the regulation of dike for oil storage tanks, and were scaled down with respect to their model tanks. The dimensions of model dikes are shown in table 5.2.

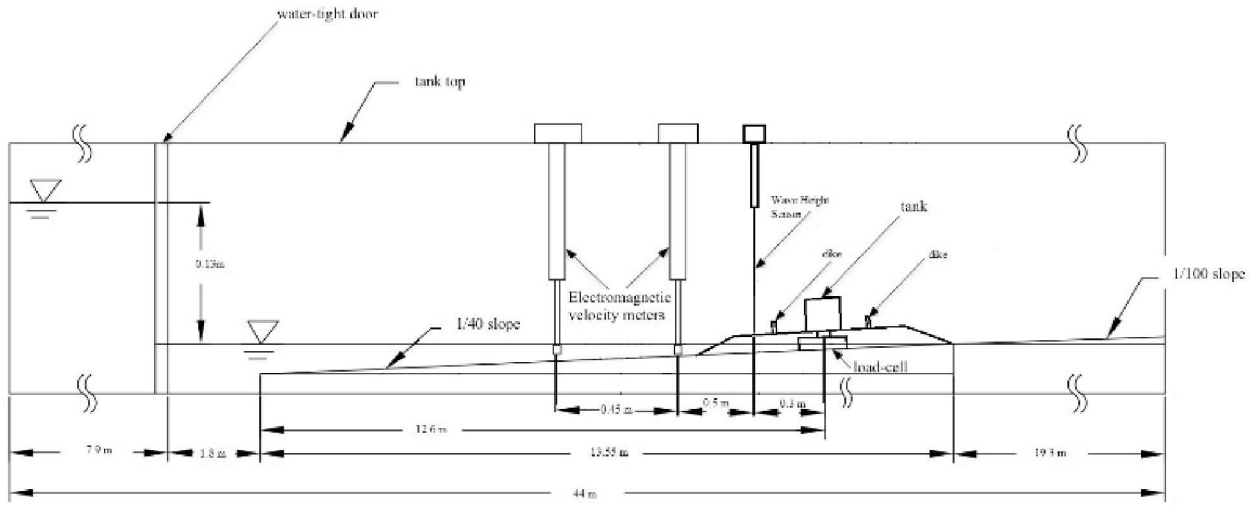

Fig. 5.8 Dimension of experimental tsunami tank with the position of oil storage tank and sensors

Table 5.3 Tank weight according to internal amount of oil

	Weight, W_T+W_L (N)		
Tank(cm)	empty	50% Oil	100% oil
7.5	0.458127	1.770705	3.100941
10	0.793629	4.194756	7.170129
16.5	1.774629	15.55474	30.28739

Fig. 5.8 shows the sketch of the experimental setup. Table 5.3 shows the weight of each tank for different internal amount of oil. The two electromagnetic velocity meters before the tank were used to check the velocity of the flow during the experiment. The wave height sensor is placed 0.3m before the tank to make sure the incoming wave to the tank will have a mean height 0.05m. This capacitive wave height sensors can measure from 10 to 100mm of wave height with 0.3% error. To measure the forces, underwater load cell was used, which has a broad range of

measurement up to 500N with an accuracy of 0.05%. Each sensor was calibrated before experiments, and Fig. 5.9 shows the calibration of underwater load cell. The water level in the dam before the water-tight door was adjusted to get the desired wave height at the wave height sensor position before the tank. The experiments for each case was conducted at least three times.

The incoming wave to the tanks was created by dam break method, in which the water-tight door was opened to release the reserved water, to mimic the flow nature of tsunami wave. However, since the wave length of tsunami wave is relatively long, the nonlinear tsunami wave is difficult to be reproduced exactly in small scale experimental tsunami tank. In current analysis, the nonlinear wave transformation near the tank due to change of water depth was neglected as the tank behavior in the wave was the only concern.

Fig. 5.9 Calibration of underwater load cell (load cell is attached below the tank)

5.5 **Simulation**

The tank drifting in incoming wave is also analyzed by numerical simulation method. This is achieved by the use of OpenFOAM® computational fluid dynamic CFD package (version 3.0.0). OpenFOAM® allows users to customize the required CFD solvers. And the package itself comes with variety of libraries and utilities to apply in various types of applications. For current analysis, the transient 'multiphaseInterFoam' solver is used to estimate the hydrodynamic forces of incoming wave on tanks, and the 'multiphaseInterDyMFoam' dynamic motion solver is applied to check the tank drifting with the incoming wave.

The 'multiphaseInterFoam' solver are based on transport and momentum equations of each n phase as shown in equation (5.4) and equation (5.5).

$$\frac{\partial u}{\partial t} + \nabla \cdot \left(\alpha_{phase} u\right) = 0, \tag{5.4}$$

$$\frac{\partial u}{\partial t} + u \cdot \nabla u = -\nabla p + \upsilon \nabla^2 u + F_\sigma + \rho g, \tag{5.5}$$

ρ and u are the density, velocity for each phase, respectively, and g is the acceleration due to gravity.

The 'multiphase' solvers are used to contribute the dynamic pressure distribution of internal fluid on the tank when the wave force exerts on the tank. Like the sloshing of the tank due to the ground movement in the earthquake, it was found that the sloshing phenomena of the internal oil even though the tank was not drifted in experiment. This change in shape of internal fluid create changes in pressure distribution on the internal wall of the tank, and hence it is considered in the simulation. For the movement of the tank, OpenFOAM® generically allows mesh motion by the use of 'sixDofRigidBodyMotion' solver to work together with any dynamic motion solver.

Due to the strong turbulent nature of tsunami wave, both simulation cases were conducted using RAS incompressible turbulence model, k-epsilon, which is generic inside the solver.

5.6 **Implementation Of Restraint Force Due To Mechanical Friction**

However, the physics behind the scenario consists of the effect of mechanical friction between the tank bottom plate and tank base. The 'sixDofRigidBodyMotion' solver originally provides restraint types of springs and dampers to control the mesh motion. Hence, it is necessary to implement a restraint type of friction inside the code. The algorithm of implementing the

restraint force, $F_{restrain}$ due to mechanical frictional force, F_{fr} is as shown in Fig. 5.10. The restraint force is applied to the mesh motion equation during the calculation.

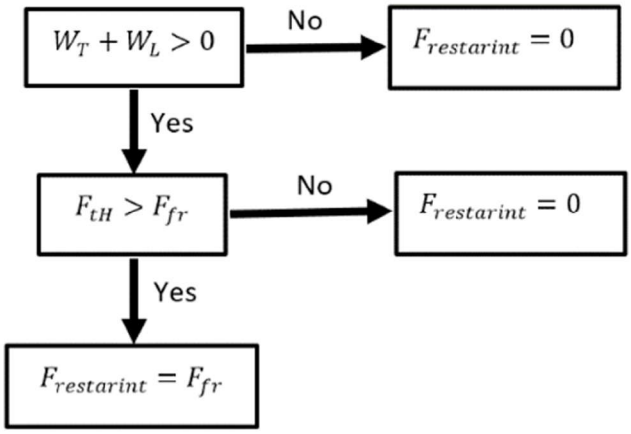

Fig. 5.10 algorithm of implementation friction

Fig. 5.11 shows the sample simulation domain which is set up according to the experimental setup in Fig. 9. However, to avoid the unnecessary calculation on the empty space, the domain is only considered up to 5.95m behind the tank. Hence, the total length of the domain became 26.45m.

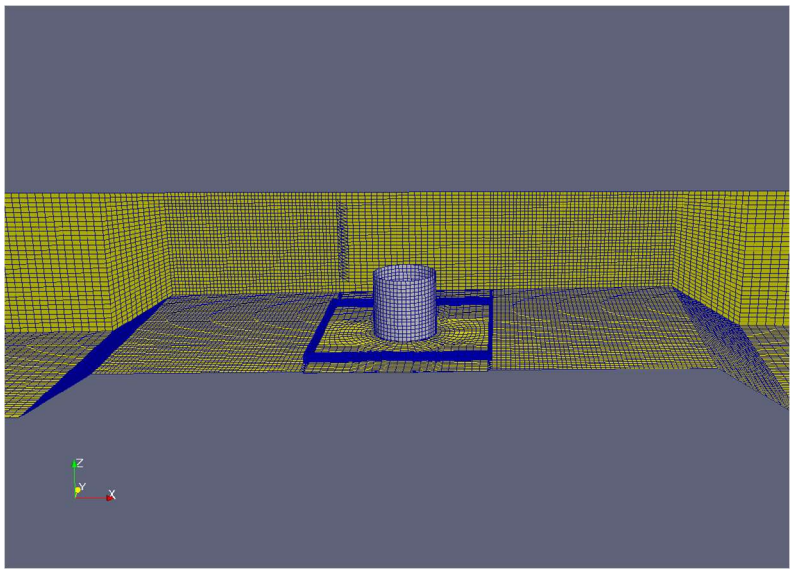

Fig. 5.11 Simulation domain showing the 16.5cm diameter tank surrounded by dike

The simulations are conducted with an average 2 million cells. In the far field, the grid resolution is 0.01m which is refined up to 0.00075m near the tank to ensure the accuracy. The watertight door is opened at 0s of simulation. The average time taken for the first wave to reach the tank is 6.9s after breaking the dam. Hence, each simulation is carried out up to 15s for all the waves to pass the tank. Table 5.4 shows the parameters of the simulation.

Table 5.4 Parameters of the simulation

Geometry	
Length	26.45m
Breadth	0.75m
Height	0.65m
Transport Properties	
Density of water	995 kg/m^3
Density of oil	920 kg/m^3
Kinematic viscosity of water	1.02E-06 m^2/s
Kinematic viscosity of oil	5.904E-05 m^2/s
Turbulences Properties	
k	1.5E-04 m^2/s^{-2}
epsilon	0.1m^2/s^3
Dynamic Mesh Properties	
Coefficient of friction	0.5178

5.7 **Result And Discussion**

The measured horizontal wave force on each tank is as shown in Fig. 5.12. Fig. 5.14 to 5.19 show the different behaviors of model tanks when subjected to wave. According to

experiments, lighter tanks with empty or small oil capacity drifted with the incoming wave as shown in Fig. 5.14 and Fig. 5.16. But the heavier tank, as in Fig. 5.19, remained stable in the wave. In most cases of tank drifting, the tanks stayed upright without tumbling ash shown in Fig. 5.13. However, in some cases of the smallest 7.5cm tank, the tank tumbled by hitting its own dike as shown in Fig. 5.14.

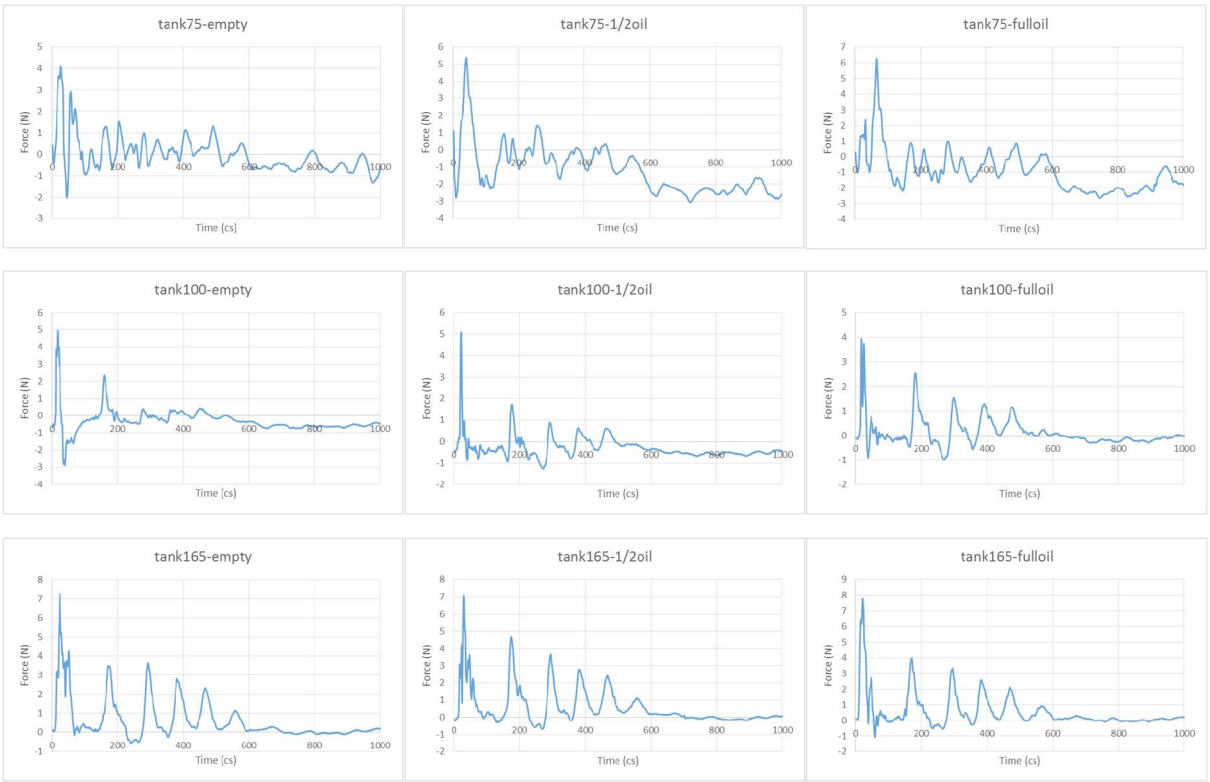

Fig. 5.12 Measured horizontal wave force on each tank

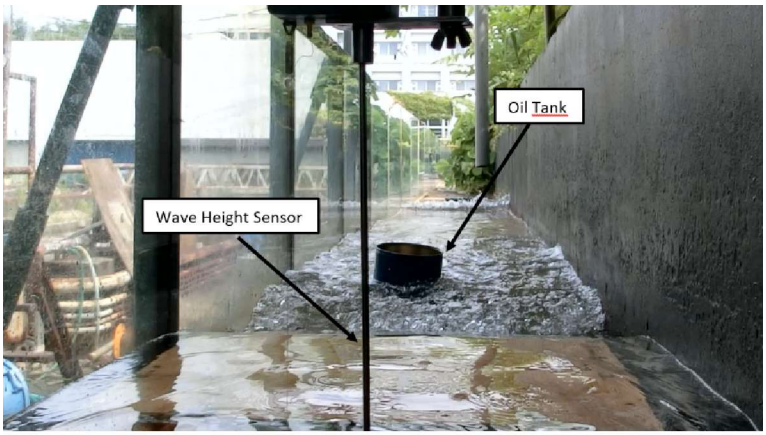

Fig. 5.13 model oil tank remain stable while drifting in the wave

Fig. 5.14 7.5cm diameter tank with 50% oil tumbles by the dike before drifting

Fig. 5.15 7.5cm diameter tank with 100% oil drift and stops at the dike

Fig. 5.16 10cm diameter tank with 50% oil drift and stops at the dike

Fig. 5.17 10cm diameter tank with 100% oil drift and stops at the dike

Fig. 5.18 16.5cm diameter tank with 50% oil drift and stops before reaching the dike

Fig. 5.19 16.5cm diameter tank with 100% oil remains stable in the wave

In the FDMA safety criteria of tank movement, the buoyant force of the tsunami run up is considered to be on the tank, when the wave hit the tank. However, in the experiments, only the sliding action occurred in most cases, especially in the case of heavier tanks. Since the incoming wave did not build enough pressure under the tank, the tanks were not lifted easily. These phenomena were prominent in the cases of heavy tanks with internal fluid. The hydrostatic pressure under the tank corresponding to the buoyant force was built up only when the water totally surrounded the tank after all the waves had passed.

These phenomena were not clearly visible in the cases of light tanks. The restraint moment of the light tank was not enough to withstand the moment due to the horizontal force of incoming wave and tumble of the tank occurred. As a consequence, pressure was readily built up under the tank in the space between the tank bottom plate and tank base, and vertical uplifting force on the tank appeared. Hence, the cases of light tanks were in line with the former FDMA safety criteria. However, in the case of heavier tanks, the horizontal forces of incoming wave and vertical uplifting buoyant forces did not exert simultaneously on the tank.

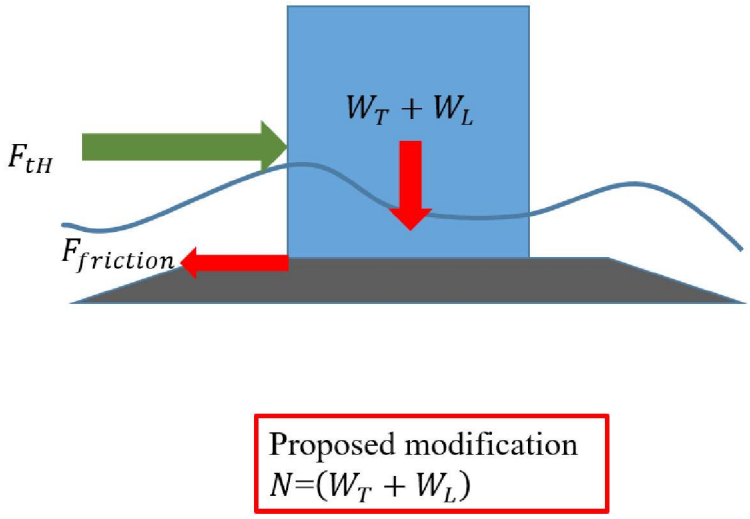

Fig. 5.20 Forces on the oil storage tank according to the modified assumption

For example, in the case of 16.5cm tank with full oil, the tank did not float up at all even after all the waves passed through it. And, it could be said that there was apparently zero net vertical uplifting force in that case. Hence, the possibility of drifting for large and heavier tanks

might be overestimated by applying the FDMA safety criteria. This result is also agree with the probabilistic simulation of the risk of tank failure carried out by Mebarki et al. (2016).Therefore, after analyzing the measured hydrodynamic forces, removing the buoyant term in the previous FDMA safety criteria are proposed for deciding the drifting of the tank.

Modified assumption of forces on the oil storage tank is as shown in Fig. 5.20. The proposed safety factor for tank movement becomes

$$F_{Sb} = \frac{\mu(W_T + W_L)}{F_{tH}}, \tag{5.6}$$

if $F_{Sb} \leq 1.0$: the tank will drift with the wave,

if $F_{Sb} > 1.0$: the tank will remain stable,

Simulation for each case of experiment can estimate the possibility of tank drifting. Although the simulation can predict the tendency of the tank movement, it cannot represent the whole scenario of tank drifting or tank tumble phenomena, due to limitation of mesh dependency. In the case of small tanks and light tanks, the velocity of the tank is relatively high, the mesh cannot coordinate the new position of the tank within specific time step. Since the RAS turbulence model used simulation represents fully turbulent flow of the wave, some of coefficients turbulence model are estimated based on assumption. There is undesired reduction drag force on the tanks in simulation, which lead to lower F_{tH} values than the experiment. Fig. 5.21 shows the example of simulation case of 16.5cm diameter tank with 100% oil.

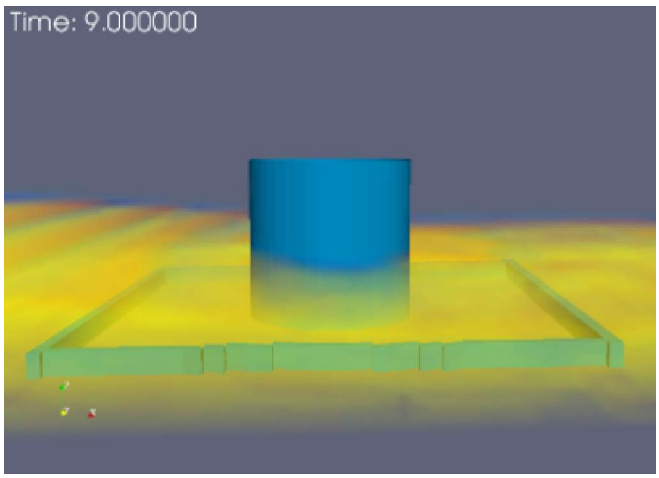

Fig. 5.21 Simulation of 16.5cm diameter tank with 100% oil remains stable in the wave

Table 5.5 Summary of experimental results with former FDMA safety factor and proposed safety factor

Diameter of the tank (m)	Internal Volume (L)	Volume rate (%)	Wave Height (m)	F_{tH} (N)	F_{tV} (N)	W_T+W_L (N)	μ	F_{Sb} (FDMA guidline)	F_{Sb} (Proposed)	Tank Movement Behavior
0.075	331	0	0.0481	4.089	3.250	0.458	0.518	-0.354	0.058	drift
		50	0.0470	5.381	3.250	1.771	0.515	-0.142	0.169	drift
		100	0.0487	6.276	3.250	3.101	0.517	-0.012	0.255	drift, stop at dike
0.1	785	0	0.0506	4.947	6.934	0.794	0.529	-0.657	0.085	drift
		50	0.0522	5.079	6.934	4.195	0.586	-0.316	0.484	drift, stop at dike
		100	0.0529	4.921	7.705	7.170	0.562	-0.061	0.819	move slightly
0.165	3528	0	0.0483	7.247	18.879	1.775	0.514	-1.212	0.126	drift
		50	0.0491	7.079	19.927	15.555	0.518	-0.320	1.138	almost stable
		100	0.0495	7.796	20.557	30.287	0.459	0.573	1.783	stable

Table 5.5 tabulates the summary of experimental results, comparing the values of F_{Sb} for the former FDMA safety criteria with those for newly proposed safety criteria. It is obvious the former FDMA safety criteria do not comply with the tank movement behavior, whereas the proposed safety criteria showed a good agreement with the result.

Sliding of tanks in the simulation case of 7.5cm diameter tank with 50% oil in the tank is as shown in Fig. 5.22. The tank slides significantly in 1.2 sec, between 6.9 sec, when the first wave reaches the tank, and 8.1 sec, when the tank is totally surrounded by water.

In the simulation case of 10cm diameter tank with 50% oil in the tank, the tank relatively resists the sliding, though it still move in the same period of time as the above case of 7.5cm tank as shown in Fig. 5.23.

However, the tank does not move totally in the case of 16.5cm tank, unlike the case of its experiment. In the experiment for the case with 16.5cm diameter tank with 50% oil, the tank moved a few centimeters within the dike, from its original position. However, in the simulation of this case, the tank stands still as shown Fig. 5.24 in contrast to its slight movement in experiment.

Nevertheless, when the simulation of the case with 40% oil in the tank was tested, the tank showed the slight movement. Therefore, simulation method can be applied to estimate oil spill from full scale oil storage tanks in the industrial zones.

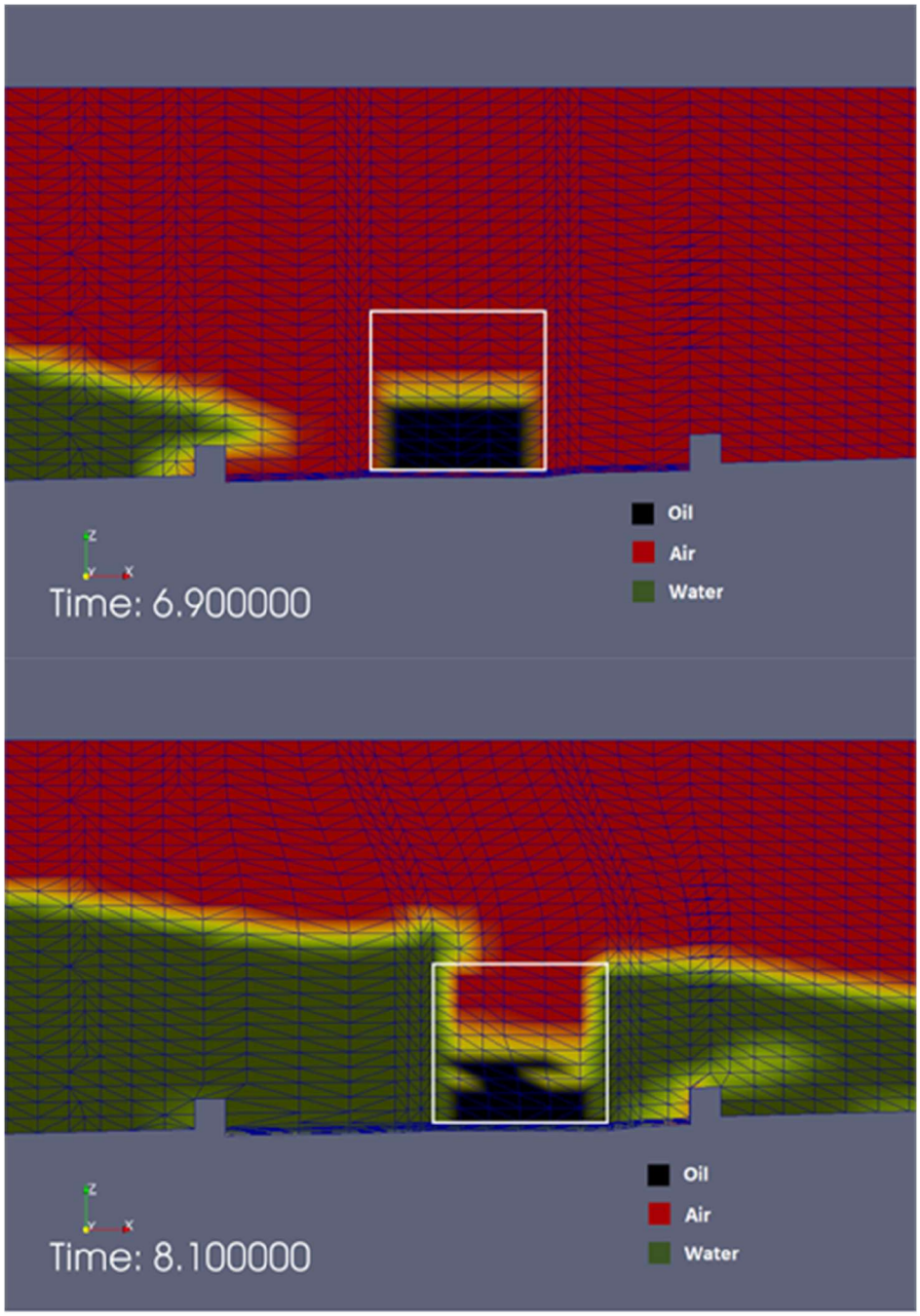

Fig. 5.22 simulation showing the sliding of 7.5cm tank with 50% oil in the tank between 6.9 sec and 8.1 sec after breaking the dam

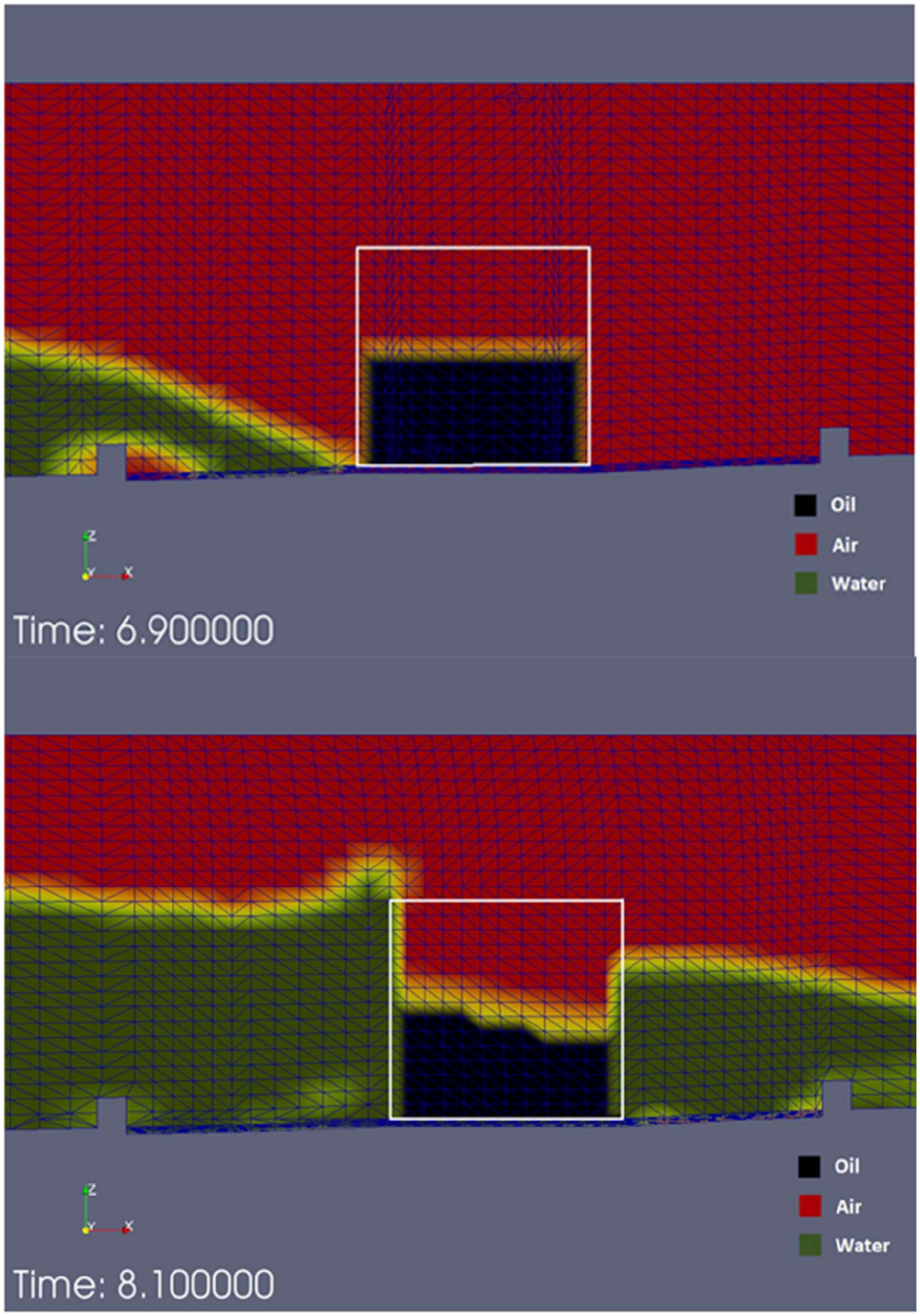

Fig. 5.23 simulation showing the sliding of 10cm tank with 50% oil in the tank between 6.9 sec and 8.1 sec after breaking the dam

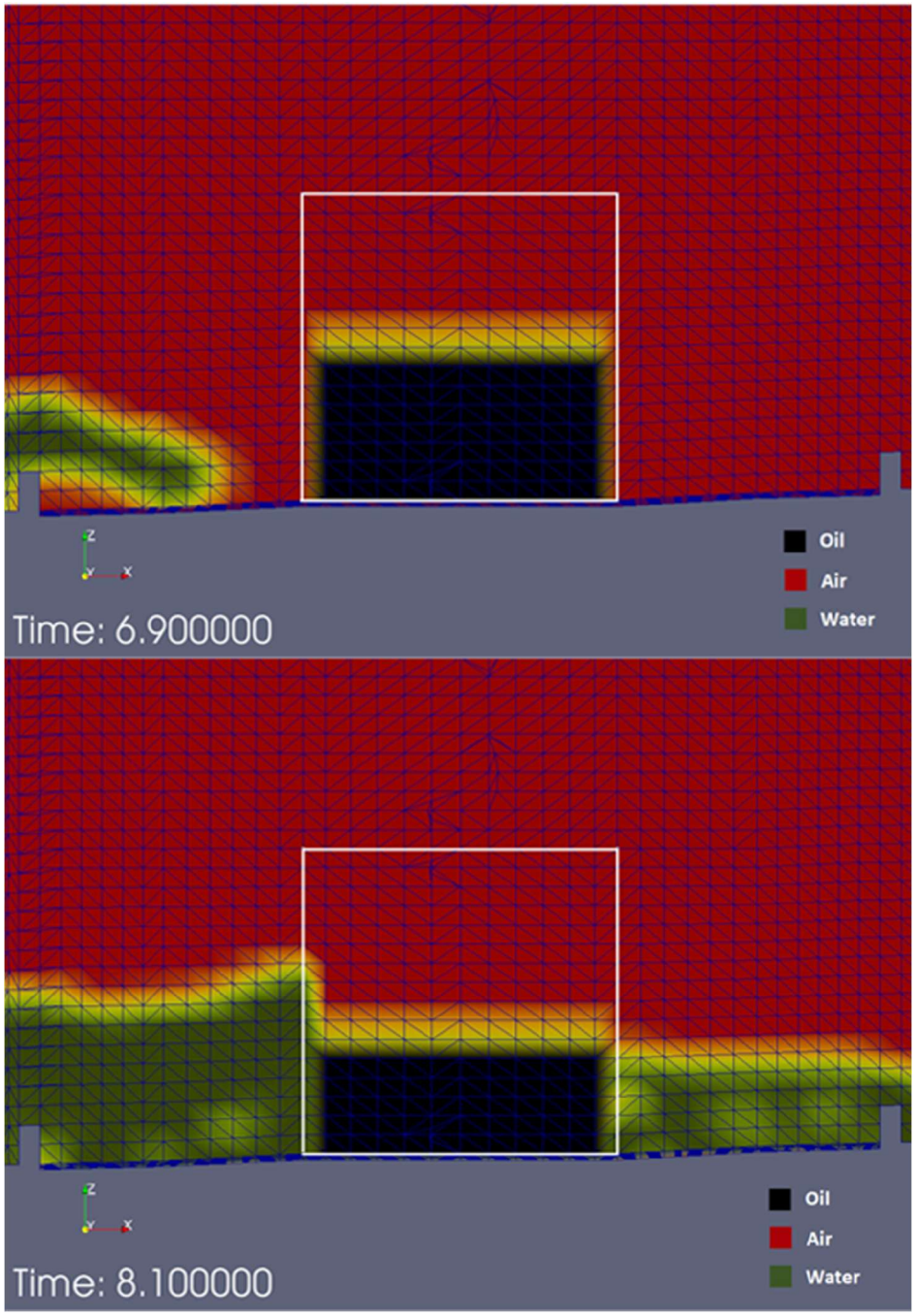

Fig. 5.24 simulation showing the stable 16.5cm tank with 50% oil in the tank between 6.9 sec and 8.1 sec after breaking the dam

Summary of the results of simulation in Table 5.6 also compares the values of F_{Sb} for two safety criteria. The value of F_{Sb} by the former FDMA safety factor is merely in line with the last case of 16.5cm diameter tank with full oil, nevertheless the value of F_{Sb} by the proposed safety criteria are consistent with the observed tank movement behavior.

To calculate the values of F_{Sb} by the former FDMA safety criteria, it is necessary to assume that the vertical uplifting force by the wave is obtained at the same time with horizontal hydrodynamic force. However, as described above, F_{tV} rarely occurred in both experiment and simulation. Hence, in Table 5.5 and Table 5.6, F_{tV} is assumed from the theoretical calculation of buoyant force, based on the water level that surrounds the tank at the time of peak F_{tH} on the tank.

Table 5.6 Summary of the results of simulation with former FDMA safety factor and proposed safety factor

Diameter of the tank (m)	Internal Volume (L)	Volume rate (%)	Wave Height (m)	F_{tH} (N)	F_{tV} (N)	W_T+W_L (N)	μ	F_{Sb} (FDMA guidline)	F_{Sb} (Proposed)	Tank Movement Behavior
0.075	331	0	0.048	2.715	3.250	0.458	0.518	-0.532	0.087	drift
		50	0.047	2.501	3.250	1.771	0.518	-0.306	0.367	drift
		100	0.049	2.378	3.250	3.101	0.518	-0.033	0.675	drift
0.1	785	0	0.051	3.814	7.705	0.794	0.518	-0.938	0.108	drift
		50	0.052	3.792	7.705	4.195	0.518	-0.479	0.573	drift
		100	0.053	3.744	7.705	7.170	0.518	-0.074	0.992	drift
0.165	3528	0	0.048	4.768	20.976	1.775	0.518	-2.085	0.193	drift
		50	0.049	4.749	20.976	15.555	0.518	-0.591	1.696	stand
		100	0.050	4.765	20.976	30.287	0.518	1.012	3.291	stand

5.8 **Conclusions**

In both experiment and simulation, the tank usually stayed upright even when it was drifted with the incoming wave. But, in some cases, the tank tumbled when it collided with its own dike.

The cylindrical shape and low center of gravity of the tanks contribute to a good stability when they float on water.

Generally, the tendency of tank drifting with the incoming wave depends on the weight of the tank and the amount of internal fluid. However, the amount of oil inside each storage tank is varied from time to time. In addition, the attachments of the storage tank to the tank base, oil conveying pipes and assembly can also deter the motion of tank.

Although the capsizing of tank and spill out of oil in this analysis, both experiments and simulations, is rare, there is a high chance of spilling out all the oil from the storage tank in real incident, if the tank is drifted in tsunami inundation. As there can be certain obstacles (buildings, fences or even its own dike) on the way of drifting with the tsunami inundation, the drifting tanks may tumble and spill out oil. Also, the oil conveying facilities connecting to the tank may easily be broken when the tank drifts or by the tsunami wave force, oil spill from these pipes and mechanism is also needed to be considered.

CHAPTER 6

CONCLUSION

In the preliminary analysis of the behavior of oil movement in the incoming wave, the phenomenon of oil response to the incoming wave was observed experimentally. Then, the multiphase solver of OpenFOAM® was applied for the simulation of experiments. The simulations could not only show good agreement with the experiment but also mimic the formation of oil ball after the oil reservoir being hit by the wave. In this way, the multiphase solver was validated for the further use of full scale estimation of potential tsunami triggered oil spill.

Then, the potential tsunami triggered oil spill from industrial parks in Osaka Bay was estimated by combining numerical analysis methods of tsunami simulation, STOC, multiphase oil spill simulation using OpenFOAM® and STOC-OIL program. The results of this study can help the risk assessment of Sakai Senboku industrial park area for the worst scenario of oil spill in case of tsunamis. The results of 3-dimensional OpenFOAM® simulation would help the analysis of submarine oil pollution as the tsunami-triggered, high turbid seawater has a potential to mix with oil spill. Also, the results of STOC-OIL would help to point out the oil spill in the residential and the bay areas for evacuation of residences and arrangement of safe navigation routes for vessels.

Also, the analysis of the tendency of tank drifting in tsunami wave showed the guidelines of former FDMA overestimated the tendency of the tank drifting with tsunami. Hence, a new safety factor for tank drifting with tsunami was proposed. This modification to the guidelines would help to revise the previous estimation of the amount of potential oil spill in the industrial zones and oil storage area in Osaka Bay.

REFERENCES

Arakawa, H., Nakamura M., 2016. Monitoring of oil spill pollution on seabed of the Kesennuma Bay in the wake of the Great East Japan Earthquake. Journal of Japan Institute of Marine Engineering, vol. 51(6), pp. 83-86.

Brackbill, J. U., Kothe, D. B., Zemach, C., 1992. A continuum method for modeling surface tension. Journal of Computational Physics, vol. 100(2), pp. 335-354.

Cerne, G., Petelin, S. and Tiselj I., 2001. "Coupling of the interface tracking and thee two-fluid models for the simulation of incompressible two-phase flow," Journal of Computational Physics, vol.171, no.2, pp.776-804

Chao, X., Shankar, N. J., Cheong, H. F., 2001. Two - and three-dimensional oil spill model for coastal waters. Ocean Engineering, 28(12), pp. 1557-1573.

Chen, H. Z., Li, D. M., Xiao, L., 2007. Mathematical modeling of oil spill on the sea and application of the modeling in Daya Bay. Journal of Hydrodynamics, ser. B, 19(3), pp. 282-291.

Daily Mail, (2012, February 14). http://www.dailymail.co.uk/news/article-2100784/Map-25million-tons-tsunami-debris-hit-California.html (accessed 20.12.2016)

FDMA survey report on the damage of firefighting activities on 2011 Great East Japan Earthquake, (2011, December) http://nrifd.fdma.go.jp/publication/gijutsushiryo/gijutsushiryo_81_120/files/shiryo_no82.pdf (accessed 25.12.2016)

Gisler, G, Weaver, R, and Gittings, M L, 2006, "Sage Calculatio ns of The Tsunami Threat From La Palma", Science of Tsunami Hazards, Vol. 24, No. 4, pp. 288 -301.

Gopala, V. R., and van Wachem, B. G. M., 2008. "Volume of fluid methods for immisible-fluid and free-surface flows," Chemical Engineering Journal, vol. 141. No.1-3, pp. 204-221

Guo, W. J., Wang, Y. X., 2009. A numerical oil spill model based on a hybrid method. Marine Pollution Bulletin, 58(5), pp. 726-734.

Hatayama, K (2014). "Damage to Oil Storage Tanks due to Tsunami of the Mw9. 0 2011 off the Pacific Coast of Tohoku, Japan," Proc 10th US National Conference on Earthquake Engineering Frontiers of Earthquake Eng, pp 21-25.

Higuera, P., Lara, J. L., Losada, I. J., 2013a. *Realistic wave generation and active wave absorption for Navier–Stokes models: Application to OpenFOAM®*. Journal of Coastal Engineering, vol. 71, pp. 102-118.

Higuera, P., Lara, J. L., Losada, I. J., 2013b. *Simulating coastal engineering processes with OpenFOAM®*. Journal of Coastal Engineering, vol. 71, pp. 119-134.

Higuera, P., Lara, J. *L., Losada, I. J., 2014a.* Three-dimensional interaction of waves and porous coastal structures using OpenFOAM®. Part I: Formulation and validation. Journal of Coastal Engineering, vol. 83, pp. 243-258.

Higuera, P., Lara, J. L., Losada, I. J., 2014b. *Three-dimensional interaction of waves and porous coastal structures using OpenFOAM®. Part II: Application.* Journal of Coastal Engineering, vol. 83, pp. 259-270.

Hokugo, A (2013). "Mechanism of tsunami fires after the Great East Japan Earthquake 2011 and evacuation from the tsunami fires," The 9th Asia-Oceania Symposium on Fire Science and Technology, Procedia Engineering, 62, 140 -153.

Ibata, T, Nakchi, I, Ishida, K, and Yo kozawa, J (2013). "Damage to storage tanks caused by the 20114 Tohoku earthquake and tsunami and proposal for structural assessment method for cylindrical storage tanks. Proceedings of the 17th International Conference and Exhibition on Liquefied Natural Gas, Texas, LNG17.

Iturrioz, A., Guanche, R., Lara, J. L., Vidal, C., Losada, I. J., 2015. Validation of OpenFOAM® for oscillating water column three-dimensional modeling. Journal of Ocean Engineering. vol. 107, pp. 222-237.

Iwasaki S. 1987, "On the estimation of a tsunami generated by underwater landslide", Proc., Int. Tsunami Symp., Vancouver, B. C., pp. 134 -138.

Kahoku Shimpo Publishing Co, 2014. Wagakoto: disaster prevention and reduc tion, Part 10: Tsunami Fires (3 -End) Fragility / Major Oil Spill, a Sea of Flames. http://www.kahoku.co.jp/special/spe1151/20150309_08.html (accessed 08.06.2016).

Kakinuma, T., Tomit a, T., 2005. Storm surge and tsunami simulator in oceans and coastal areas. Proceeding of International Conference on Monitoring, Prediction and Mitigation of Water-Related Disasters, Disaster Prevention Research Institute, Kyoto Univ.

Kirby, J., 1996, "Nonlinear, dispersive long waves in water of variable depth." Research Report No. CACR-96-02.

Kowalik, Z., 2001, "Basic Relations between tsunami calculations and their physics", Sci. *Tsunami Hazards* , 19(2), pp. 99–115.

Madsen, 0. S. and Mei, C. C., 1969, "The Transformation of a Solitary Wave Over an Uneven Bottom", Journal of Fluid Mechanics, Vol. 39, pp. 781 -791.

Matsuzaki, Y., Fujita, I., 2012. Development of a simulation model for oil transport resulting from a tsunami. Technical Note of the Port and Airport Research Institute, no.1255.

Matsuzaki, Y., Fujita, I., 2014. A numerical simulation method of oil transport at sea surface and hindcast simulation of oil spill incidents. Journal of Japan Society of Civil Engineers, Ser. B2 (Coastal Engineering) vol. 70(1), pp. 15-30.

Maza, M., Lara, J. L., Losada, I. J., 2015. *Tsunami wave interaction with mangrove forests: A 3-D numerical approach*. Journal of Coastal Engineering, vol. 98, pp. 33-54.

Mebarki, A., Barbosa, S. J., Prodhomme, G., and Reimeringer, M., 2016. Natural hazards, vulnerability and structural resilience: tsunamis and industrial tanks. Taylor and Francis Group.

Nishi, H (2012), "Damage On Hazardous Materials Facilities," Proc Int Symp on Engineering Lessons Learned from the 2011 Great East Japan Earthquake, Tokyo.
Niu, H., Li, S., King, T., Lee, K., 2016. Stochastic modeling of oil spill in the Salish Sea. The 26th Int. Ocean and Polar Engineering Conf. Int. Society of Offshore and Polar Engineers.

Osaka Prefecture Petrochemical Disaster Prevention Cabinet Headquarters, (2014). "Report of the investigation on the possible damage of earthquake and tsunami in Osaka Prefecture,"
http://www.pref.osaka.lg.jp/attach/6693/00150913/06%20sankou%20bukaihokoku%20.pdf (accessed 08.06.2016).

Overview of the industrial accidents caused by the great Tohoku earthquake and tsunami, (2013, March), analysis, research and information on accident database operated by French Ministry of Ecology, Sustainable Development and Energy.
http://www.aria.developpement-durable.gouv.fr/wp-content/files_mf/Overview_japan_mars_2013_GB.pdf (accessed 08.06.2016).

Reconnaissance Team of Japan Society of Civil Engineer (2005). "The Damage Induced by Sumatra Earthquake and Associated Tsunami of December 26, 2004," A Report of the Reconnaissance Team of Japan Society of Civil Engineer,
http://www.jsce.or.jp/committee/2004sumatra/report.htm (accessed 08.06.2016).

Saatcioglu, M, Ghobarah, A, and Nistor, I (2006). "Performance of Structures in Indonesia during the December 2004 Great Sumatra Earthquake and Indian Ocean Tsunami," Earthquake Spectra, 22(S3), 295-319.

Schiller. L., and Nauman, Z., 1935. "A drag coefficient correlation," Zeitschrift des Vereins Deutscher Ingenieure, vol.77, pp. 318

Strubelj L. and Tiselj, I., 2011. “Two -fluid model with interface sharpening,” International Journal for Numerical Methods in Engineering, vol.85, pp. 575-590

The Mainichi Newspaper, (2012, April 11). http://www.ne.jp/asahi/kibono/sumika/kibo/kinkyo1204.htm (accessed 08.06.2016).

Titov, V.V. and Gonza´ Lez, F.I., 1997, “Implementation and testing of the Method of Splitting Tsunami (MOST) model”, NOAA Tech. Mem. ERL PMEL -112

Tomita, T., Honda, K., Kakinuma, T., 2006. Application of storm surge and tsunami simulator in oceans and coastal areas (STOC) to tsunami analysis. Technical Memorandum of Public Works Research Institute, vol. 4022, pp. 90-96.

Tomita, T., Yoem, G. S., 2012. Tsunami damage in ports by the 2011 off Pacific coast of Tohuku Earthquake. Proc. Int. Sym. on Engineering Lessons Learned from the 2011 Great East Japan Earthquake.

Wang, S. D., Shen, Y. M., Guo, Y. K., Tang, J., 2008. Three -dimensional numerical simulation for transport of oil spills in seas. Ocean Engineering, 35(5), pp. 503-510.

Wardle, K. E., Weller, H. G., 2013. Hybrid multiphase CFD solver for coupled dispersed/segregated flows in liquid–liquid extraction. International Journal of Chemical Engineering, 2013.

Weller, H. G., 2008. “A new approach to VOF -based interface capturing methods for incompressible and compressible flow,” Tech. Rep., OpenCFD

Zama, S, Nishi, H, Hatayama, K, Yam ada, M, Yoshihara, H and Ogawa, Y (2012). “On Damage of Oil Storage Tanks due to the 2011 off the Pacific Coast of Tohoku Earthquake (Mw9.0, Japan,” 15th World Conference on Earthquake Engineering, Lisbon.

Zhang, C, Knepley, M G, Yuen, D A, Shi, Y, 2007, “Two New Approaches in Solving the Nonlinear Shallow Water Equations for Tsunamis”, Preprint ANL/MCS -P1459-0907, ANL, September 2007.